Deciding where to verify the fatigue resistance of an orthotropic steel bridge deck

C.M. Stellinga

Understanding today.
Improving tomorrow.

Deciding where to verify the fatigue resistance of an orthotropic steel bridge deck

by:
C.M. Stellinga, 4974174

to obtain the degree of Master of Science
at the Delft University of Technology,
to be defended publicly on April 24, 2023 at 3:00 PM.

Graduation committee:	Dr. Ir. Cicirello, A. (Alice)	Delft University of Technology (Chair)
	Prof. Dr. Ir. Veljkovic, M. (Milan)	Delft University of Technology
	Dr. Ir. Steenbergen, M.J.M.M. (Michaël)	Delft University of Technology
	Ir. Dorgelo, G. (Gerjan)	Antea Group

Preface

Dear reader,

This report has been written to obtain a masters degree in Civil Engineering at Delft University of Technology. It is related to the location of the first fatigue crack of a specific fatigue detail in an orthotropic steel bridge deck. It explores an uncommon approach to find the first fatigue crack. In this exploration the two parts which made me love civil engineering were combined. It uses a lot of structural mechanics to (try to) accurately determine stresses in an object. But above all, it does so in a bridge. An object one comes across often in their life.

I would never have been able to perform this research without the help of Antea Group. They provided me with the necessary environment, hardware, software, knowledge, experts, etcetera. It was always possible to ask anyone to help me. And even if they could not help me themselves, they would help me to find someone who could. Even though my thesis occupied me full time they made me part of their team. Inviting me for all social team building events. It should be clear, I am very grateful for the help that Antea Group provided me. In this regard ir. Gerjan Dorgelo deserves some extra attention. He went the extra mile. Traveling for hours, just to make sure that I could combine a meeting with him with an ice speed skating marathon in the afternoon. Reading a hundred-page report for the tenth time, just because I wanted feedback for the tenth time. And teaching me the mysteries of the bullpen. Gerjan, thanks.

This report would never have been finished without the help of my graduation committee. Therefore, I would like to show my gratitude to dr. ir. Alice Cicirello, prof. dr. ir. Veljkovic and dr. ir. Steenbergen. Without their feedback my master thesis would still have been in its infancy.

Lastly, I would like to express my gratitude to my friends and family. Those who gave me a moment to unwind while ice speed skating. Or offered to make dinner when studying made me tired. The few who have been my classmates, the fun we had together might be the reason I needed some extra time as a student. To my brothers, who were brave enough to criticize me when I needed it. And my parents, who have been supporting me unconditionally since before I was born. Friends, family, I would not have been able to achieve this without you.

Enjoy your readings,

Coen Stellinga

Delft, April 2023

Abstract

To reduce the environmental impact or cost of a civil engineering structure their designs are optimized. A promising method to optimize are iterative optimization algorithms. If both the design calculations and the iterative optimization algorithm are automated, an optimized design solution can be found within a feasible timeframe. To be able to automate the design calculations they need to be fully parameterizable. In this context it becomes interesting to research whether yet unparameterizable calculation processes can be made parameterizable. One of these processes is the determination of the locations in which the fatigue resistance has to be determined in a steel orthotropic bridge deck. This location is the location where the first fatigue crack is expected. Therefore, Antea Group requested if a study could be performed with the objective to answer the following research question:

How can the determination of the location of the first fatigue crack in the deck, at a stiffener to deck plate weld toe, be parameterized?

To answer the research question, the (in the Netherlands active) regulations are studied. Based on the regulations the process of determining fatigue damage of a point in the bridge can be understood. As well as the reason why, this process is too computational demanding and complex to be able to be applied to all points in all welds.

In response to this an alternative method is proposed. This method reduces the complexity and the computational budget that is needed, by using 1D elements instead of the currently prescribed 2D elements. To determine if this method can be used it was decided to apply it on a case study. The bridge which served as the case study was the Goereese bridge. The alternative method was applied to determine the expected distribution of fatigue damages in all welds in the case study. Based on this obtained distribution a limited number of interesting locations in the deck could be identified. At these points to regulatory required method was used to obtain results which can be compared with the alternative method.

It is concluded that the predicted location of the first fatigue crack of both methods is directly next to each other. However, the distribution of the remaining points suggest by the alternative method does not agree with the obtained results of the regulatory method. Remarkable enough, both these methods predict a location which is counter intuitive to the structural engineers participating in the research.

Therefore, the following general recommendations are given:

- Research if the regulatory method, to determine the location of the first fatigue crack, can be simplified.
- Research the cause(s) of the differences between the regulatory method and the alternative method.
- Increase the awareness of structural engineers regarding their intuition on the location of the first fatigue crack.

Table of contents Page

List of Figures

List of Tables

1 Introduction

Background:
Due to the rise of computers design calculations can be executed quicker and with less effort. This makes it possible to iteratively optimize designs. Recent experiences of Antea Group have shown that this can result in design solutions in which less materials are used, the costs are reduced and/or the environmental impact is lowered [1, 2]. Due to these successes Antea Group researches if the same method can be applied on more design calculations. An optimization algorithm can be applied if the design stage meets the following conditions:

- The calculation related to each design solution takes a lot of time. Therefore, automating the calculation is likely to be worth the time and effort.
- The (lawfully required) design calculations leave no room for interpretations of the structural engineer[1]. Therefore, they can be fully automated.
- It is expected that the (lawfully required) design calculations will have no significant changes in the near future. Therefore, the automation and optimization algorithm are expected to be useful for a longer period. Thus, worth the time and effort to be implemented.
- It is expected that current designs can be significantly improved. Therefore, the benefits of optimizing them are significant.

Recently the department of waterways of the Netherlands (Rijkswaterstaat) updated the lawfully required design calculations on the determination of the fatigue resistance of steel orthotropic bridge decks [3]. Thereby significantly reducing the freedom of the structural engineering in the determination of the fatigue resistance of a bridge deck. As well as (assumably) setting a precedent of the required design calculations for the upcoming years. This means that all requirements are met for this design calculation. Thus, Antea Group would like to research if the design solution of a steel orthotropic bridge deck regarding the fatigue resistance can be optimized.

This master thesis started with the goal to optimize the design of a steel orthotropic bridge deck regarding the fatigue resistance. However, during the research it was realized that the required design calculations are not yet defined strict enough to be able to be fully automized. To be able to optimize a design using an iterative optimization algorithm this will be necessary. Therefore, the goal changed to research the possibility to parametrize the design calculations regarding the fatigue resistance of steel orthotropic bridge decks.

Problem:
According to the Dutch regulations [3] the resistance of all points in all welds of a bridge has to be sufficient. Therefore, the stresses in all points in all welds due to all possible load combinations have to be determined. This takes a lot of computational power and will not be possible to do within a feasible time. As a result of this, only one point is usually analysed for each of the potential fatigue cracks (fatigue details [3]). For each of the fatigue details, the point chosen is the point where the highest fatigue damage is expected. In choosing this point a problem occurs. Since there is no parametrizable method to determine this point without doing a computational expensive calculation on all the points in all the welds. To be able to optimize a design with an iterative optimization algorithm this will be necessary. To remain within the scope of a master thesis this problem is researched for only one fatigue detail. This resulted in the following research question:

How can the determination of the location of the first fatigue crack in the deck, at a stiffener to deck plate weld toe, be parameterized?

---

[1] This is freedom in the design calculations. Structural engineers, designers and architects do have freedom in the design itself. But, not on the calculations resulting from the design.

Scope

To be able to perform the research some boundaries to the scope are necessary. For this research the Goereese bridge (51°49'27.5''N 4°02'18.4''E) acted as a case-study. A description of a model of the Goereese bridge is given in Chapter 3.

The problem being researched in this report relates to the application of Dutch regulations. The scope of this research will be limited to the application of these regulations, it will not extend to potential changes in the regulations themselves. Therefore, all proposed methods in this research should be permissible according to the regulations.

In the research question it is stated that the fatigue crack in the deck at a stiffener to deck plate weld toe is being researched. To determine if a bridge has enough fatigue resistance several other potential fatigue cracks need to be analysed [3]. These fatigue cracks all defined by their own fatigue detail. Since the Goereese bridge has continuous troughs a total of 16 fatigue details can be identified. There are several reasons to consider the fatigue detail researched in this report:

- In this report a method is proposed which uses 1D elements (Chapter 4). The applied Timoshenko beam elements assume no internal deformation [4, 5, 6]. Therefore, the stresses occurring perpendicular on the cross section are most reliable. As a result of this it is decided not to research any fatigue cracks occurring in a direction which is not perpendicular to the cross section of the element in which the fatigue crack occurs. This leaves 7 potential fatigue details to be researched.
- Since it is unknown where in the Goereese bridge the deck plate splice joints and the stiffener splice joints are, these cannot be used to apply the proposed method on. This leaves 4 potential fatigue details to be researched.
- The proposed 1D elements method uses cross beams with constant cross section properties. In doing so it removes the cope holes from the cross beams, there by changing the troughs from being continuous to discontinuous. It is assumed that this could have an influence on the stresses found close to the troughs. But that this effect will be negligible for fatigue details not related to the cross beams. This leaves 2 potential fatigue details to be researched.
- It is expected that any results of this research will have to be verified by experiments. To be able to do so the start of the first fatigue crack will have to be researched. Since fatigue cracks starting at the inside of a trough can only be located after they propagated through the entire element these fatigue cracks will be omitted. This leaves only one fatigue detail. The fatigue crack through the deck plate at a stiffener-to-deck plate weld toe (Figure 2).

According to the Eurocode there is a double logarithmic relation between the value of a stress interval and the fatigue damage due to a stress interval (Figure 12). As a result of this it is assumed that the first fatigue crack will occur at the location of the highest expected stress interval. A discussion on this assumption is held in Chapter 9.1.

Studies have shown that the highest stress values in the deck plate, at trough web-to-deck plate welds occur very close to the applied loads [7, 8]. The area significantly affected by a local wheel is about two to three trough webs. In the longitudinal direction the significant effects only occur at the loading area. Therefore, the influences of an axle positioned away from the considered location are neglected. As a results of this only the influences of individual axles are analysed. A discussion on this assumption can be found in Chapter 9.1.

If the location, in which the fatigue resistance has to be determined, is known, the process of determining the fatigue damage can start. In this process it is often the case that different influence lines are made of the stresses in the found location due to the different applied axles. Previously performed research shows that the compressive stresses found in the considered detail are up to 8.75 times higher than the found tensile stresses [9]. According to the Eurocode [10] the fatigue damage due to a compressive stress is 60% of the fatigue damage due to a tensile stress of the same magnitude. To account for this, the compressive stresses are reduced by 40%. This would still result in the corrected compressive stress being up to 5.25 times higher than the maximum tensile stress. The results from this report were obtained via numerical experiments preformed on a sub-model of an orthotopic steel bridge deck. More recent studies determined the stresses of this detail on a full-sized model which was in service during the determination of the stresses [11]. The results obtained with the full-scale model suggest that the maximum obtained compressive stress is approximately an order 4 times bigger than the maximum obtained tensile stress. Therefore, it is assumed that the considered fatigue detail will fail due to stress intervals mainly consisting out of compressive stresses.

Reading guide

Chapter 2 is a literature study in which the research problem is explored. Some assumptions are made based on the literature study resulting in a demarcation of the research. Chapter 3 looks at the problems occurring when a 3D model consisting out of 2D plate elements (without weld details) is used. After which Chapter 4 proposes and explains a 3D model with 1D beam elements to determine the point with the highest stress interval. Chapter 5 explains how 1D beam elements, can be solved analytically thereby having no mesh dependency. As a result of this the 3D model with 1D elements can be solved without mesh dependency. Chapter 6 makes use of the 3D model with 1D elements without mesh dependency to determine the point most likely to propagate the first fatigue crack. As well noting some remarkable results of this model. After which Chapter 7 will focus on the calculation of the highest stress interval (using the computational expensive method enforced by the regulations [3]) in the points considered most interesting according to current experts and the results obtained in chapter 6. These results can be compared with the results of the 3D model with 1D elements without mesh dependency to give information of the useability of the latter model. In the last two chapters some conclusions are drawn, some recommendations are given, and the research is discussed.

2 Literature review

To be able to put this report in context it is necessary to have an overview of the research done in related topics. Therefore, this chapter presents an overview of the resources used in the research. It starts by explaining the concept of fatigue and how the resistance against fatigue of steel orthotropic bridges is determined. This is followed by an overview in the methods applied to determine the stresses in a structure.

2.1 Fatigue

To be able to research the location of the first fatigue crack the concept of fatigue should be understood. As well as the method used to determine the fatigue resistance of an orthotropic steel bridge deck. This paragraph explains both.

2.1.1 Fatigue cracks

Fatigue is the weaking of a material due to cyclic loading [12]. If a material has underwent more fatigue damage than it can resist fatigue cracks will occur. The development of a fatigue crack is divided in two stages. The crack initiation phase, in which the phenomenon works on a microscopic scale and is not visible with the naked eye. And the crack growth phase, in which the fatigue crack reached a macroscopic scale and is visible to the naked eye. When the crack growth phase is reached only a small percentage of the total life remains [13].

Crack initiation
The fatigue cracks usually start at the surface of the material. This is because those grains have less constraints regarding slip. At this location plastic deformations can start occurring at low stress levels. This can result in a slip step (Figure 1).

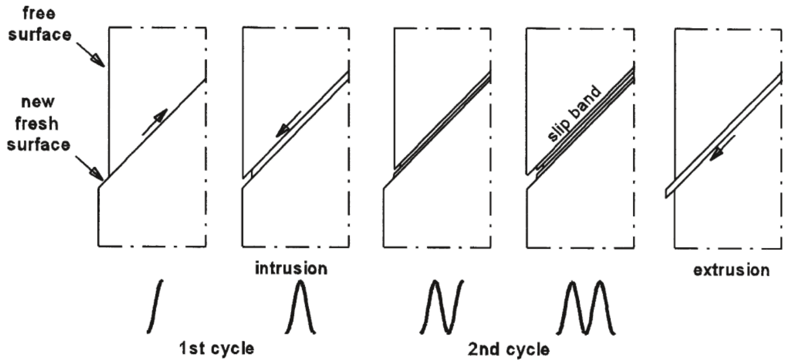

Figure 1:Development of slip band [13]

This slip step immediately results in a local reduction of the strength of the material. Each new loading cycle will cause crack extension. The chaces of a fatigue crack increase at an inhomogeneous stress distribution (for example at a weld). Since at such a location a peak stress occurs. Another factor increasing the chances of a fatigue crack is the surface roughness.

Crack growth
Slowly the fatigue cracks will grow. After a while the crack direction will not following the direction of the initial slip band anymore. Instead, it will tend to grow in a direction perpendicular to the main principal stress [13]. At this stage the resistance against the fatigue cracks is no longer depending on the surface properties. Instead, it depends on the material properties as a bulk [13].

Every increase of the crack size results in a reduction of the surface contributing to the resistance against the occurring stresses. If this surface becomes too small (thus the fatigue crack becomes too big), it will not be able to withstand to occurring stresses anymore. As a result of this (local) failure of the structure will occur [13].

2.1.2 Determine fatigue resistance

Fatigue detail

The regulations [3] divides all commonly occurring fatigue cracks in an orthotropic steel deck into 27 different fatigue details. In this report detail 1a is considered (Figure 2).

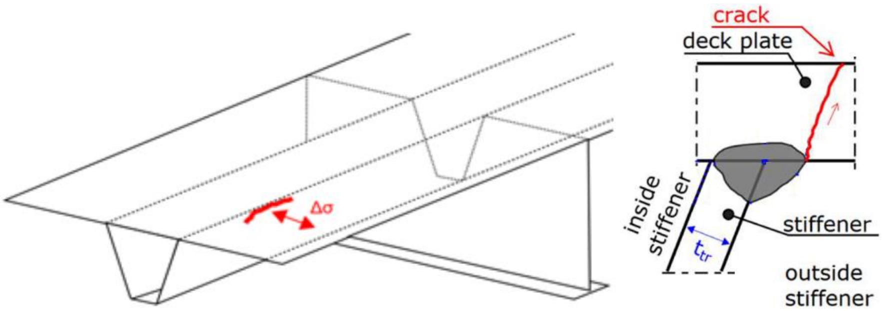

Figure 2: Stiffener-to-deck plate weld, weld toe crack in deck plate [3]

Based on the fatigue details requirements are given for the geometry of the weld and the method in which the stresses should be analysed. The fatigue detail considered in this report regards the stiffener-to-deck plate weld with a crack in the deck plate starting from the weld toe.

Weld modelling

There has been a lot of research into three different ways in which welds can be modelled [14, 15]. This resulted in the modelling method as provided in the regulations [3] (Figure 3).

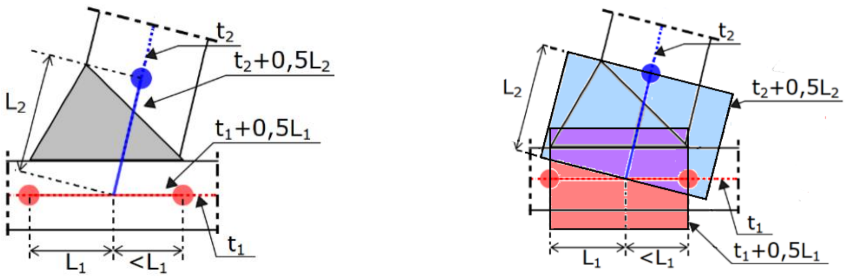

Figure 3: Weld modelling method [3], L_i is the length of the locally applied increase in thickness and t_i is the thickness of element i

This method states to locally increase the thickness of the plate elements at the locations of welds. A summary of this method is given in Chapter 7.3.2 a detailed description of the application of this method on to the considered case study is given in Appendix VII Elaboration calculating maximum stress interval 2D FE model.

Fatigue load model

The load cases which should be considered are given by a fatigue load model. In the case of steel orthotropic bridge, fatigue load model 4a should be used [3]. This model is given in the Dutch annex of Eurocode 1 part 2 [16]. The load model is shown in Figure 4.

Type voertuig		Verkeerstype				
Afbeelding van de vrachtwagen	Afstand tussen de assen m	Gelijkwaardige aslast kN	Lange afstand %	Middellange afstand %	Lokaal verkeer %	Wiel-type
	4,5	70 130	20,0	50,0	80,0	A B
	4,20 1,30	70 120 120	5,0	5,0	5,0	A B B
	3,20 5,20 1,30 1,30	70 150 90 90 90	40,0	20,0	5,0	A B C C C
	3,40 6,00 1,80	70 140 90 90	25,0	15,0	5,0	A B C C
	4,80 3,60 4,40 1,30	70 130 90 80 80	10,0	10,0	5,0	A B C C C

Figure 4: Fatigue load model 4a [16]

This model states which trucks should be accounted for. The loads of the different axles of the trucks. The distribution of the total amount of trucks in the 5 different separate trucks. And which axles make up a single truck. In this report it is assumed that the location of the maximum fatigue damage can be determined via applying single axles. Since the stresses are determined via a geometric and linear finite element analyses the maximum stress will always occur due to the maximum applied load. Therefore, for each of the three types of axles the maximum load is considered. This leaves the load cases given in Figure 5.

aslast kN	Wiel-type
70	A
150	B
90	C

Figure 5: Relevant axles and loads, assuming that the location of the maximum fatigue damage can be determined by analysing individual axles

Types of axles

To be able to place these axles on the bridge the configuration of an axle needs to be known. According to the ROK [3] the configuration stated in NEN 8701 [17] should be used in which the length of the wheels should be changed to 220mm. This results in the configuration in Figure 6.

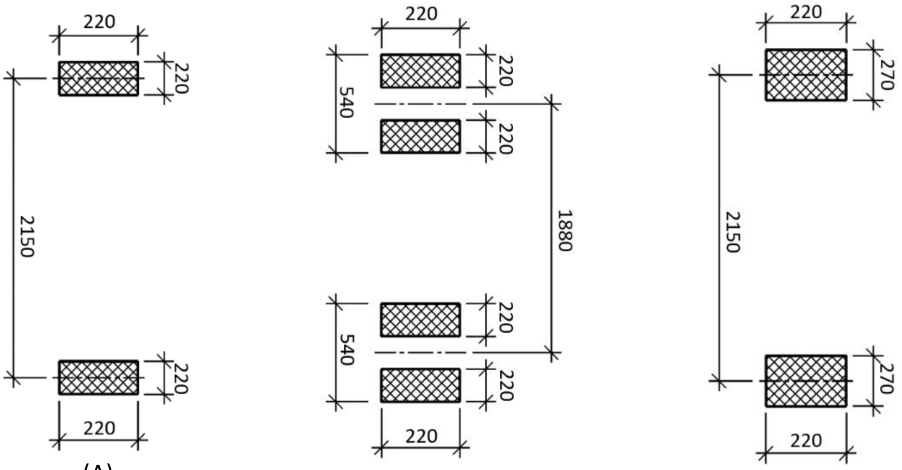

Figure 6: Axle dimensions of axle (A), (B) and (C) [17]

Wheel track location and spreading

The loads are all defined however, the position where to put the load still needs to be determined. Therefore, a location of a wheel track is determined. Depending on the location where the fatigue resistance needs to be determined there are three positions of the wheel track that needs to be determined [3]. Which are shown in Figure 7.

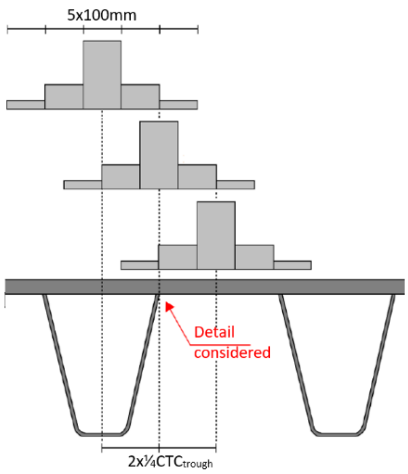

Figure 7: Locations of the wheel tracks [3]

These are locations of wheel tracks. As a result of this the other wheel of an axle can be on either side the considered wheel track. If the considered location is close to the edge of the bridge only the theoretical possible configuration has to be considered. If both configurations are possible both these configurations need to be considered.

Number of trucks

Because fatigue is a result of cyclic loading not only the loading is needed but also the number of cycles. In this case that means the number of trucks that pass the bridge during the considered lifespan. The Eurocode divides bridges in 4 different types, depending on the type of road that uses the bridge a different number of trucks pass the bridge. However, the Dutch ROK [3] states that all steel orthotropic bridge decks should be designed to withstand the highest number of trucks given by the Eurocode. This gives the results presented in Figure 8.

	Verkeerscategorie	$N_{obs,a,sl}$ **per jaar en per rijstrook voor zwaar verkeer**
1	Autosnelwegen (A-wegen) en wegen met twee of meer rijstroken per rijrichting en met intensief vrachtverkeer	$2{,}0 \times 10^6$

Nob

Figure 8: Number of trucks passing the bridge per year [16]

Extrapolation

The stresses at a weld cannot be determined by reading the results of a FE model directly at the weld. The ROK [3] gives methods to determine the stresses at fatigue details depending on the fatigue category. In the case of the considered fatigue detail the stresses have to be determined using the hot-spot method (Figure 9).

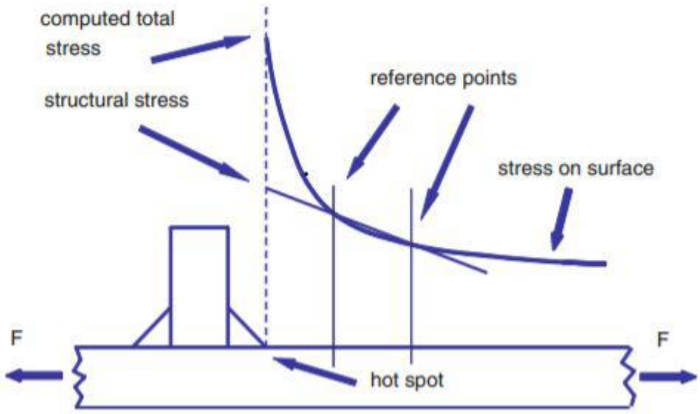

Figure 9: Sketch of hot-spot method [18]

This method states that the stresses should be determined at two reference points. After which linear extrapolation can be used to determine the stresses at the weld toe. The location of the reference points differs per considered fatigue detail. A summary of this method is explained in Chapter 7.3.2 and an elaboration on the application to the considered case study can be found in Appendix VII Elaboration calculating maximum stress interval 2D FE model.

Influence line / stress history

If all load cases are known, the hot-spot method can be used to determine the stresses from all the load cases. Thus, an influence line of all trucks can be made. Since the number of each type of truck passing the bridge can be determined using the fatigue load model, an influence line over the entire lifespan of the bridge can be made. In the case of fatigue this influence line considers the stresses at the weld detail. An example of such a line is given in the Eurocode [10] (Figure 10).

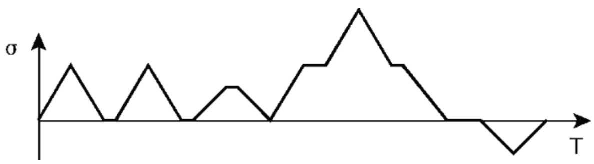

Figure 10: Example of influence line of stresses in a fatigue detail [10]

Dynamic amplification factor
When a truck passes an expansion joint it causes some dynamic effects. To account for this, within a static model, a dynamic amplification factor has to be applied. According to the ROK [3], an amplification factor of 1.15 has to be applied on all stresses of fatigue details within 6m from an expansion joint. In the considered case study, an expansion joint is situated at both ends of the bridge. Every point in this bridge is within 6m of one of these expansion joints. As a result of this all stresses (thus the entire influence line) have to be multiplied with a factor 1.15.

Reduced stress in compression
Since the compressive stresses have a lower contribution to fatigue damage then tensile stresses, the Eurocode [10] states that the compressive stresses should be reduced with 40%. As a result of this all compressive stresses in the found influence line of the considered fatigue detail are reduced with 40%.

Stress interval spectrum
The influence line of the fatigue details is currently determined. The next step is to determine the stress interval spectrum. This is a spectrum containing the values of the stress intervals of the influence line and the number of times they are expected occur during the life span of the bridge. To determine the stress interval spectrum an iterative procedure has to be used. An example of the development of the stress interval spectrum (and the influence line) throughout the different iterations is presented in Figure 11

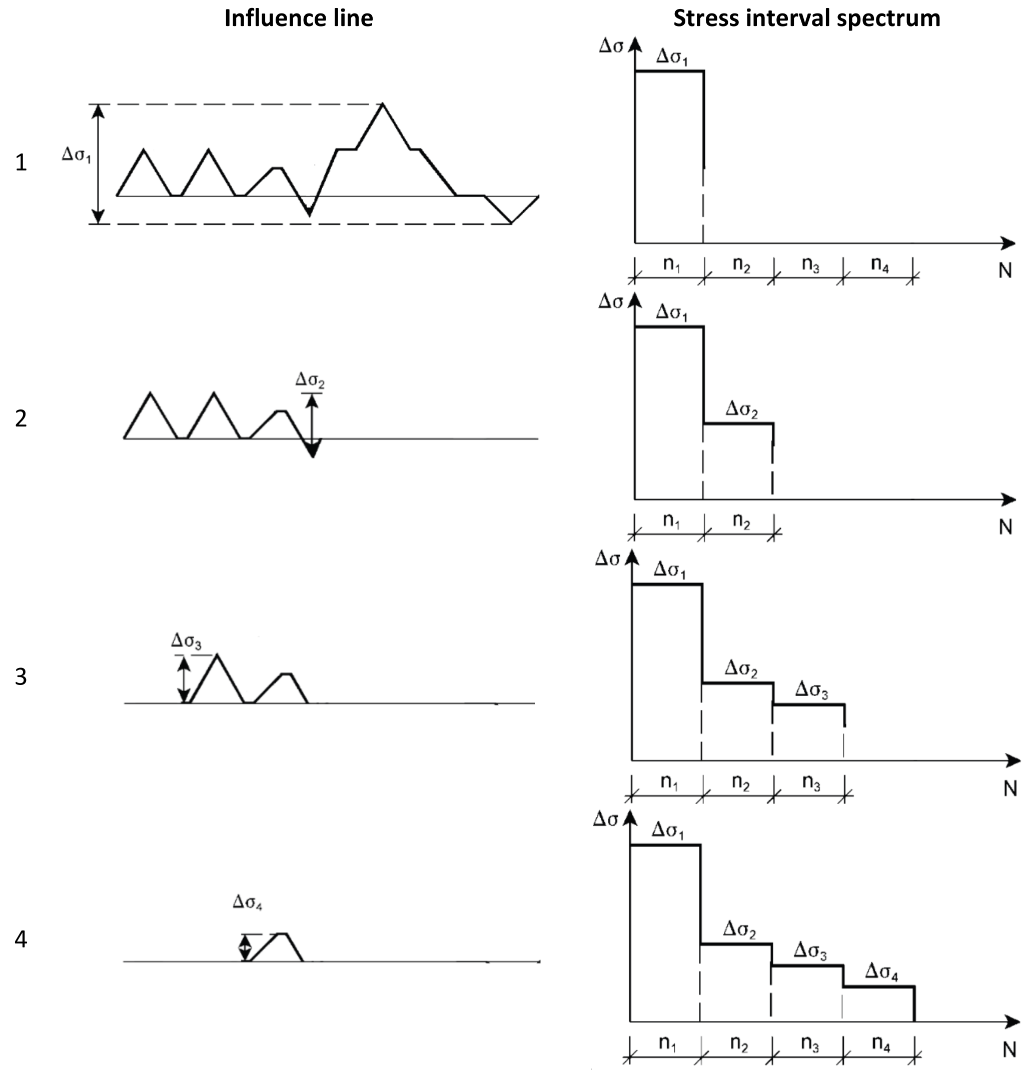

Figure 11: Overview of determination of stress interval spectrum [10]

For each of these iterations the following steps have to be completed:

1) The maximum compressive and tensile stress are determined. The summation of the two (excluding sign differences) is the considered stress interval (Δσ).
2) The number of times the compressive part and the tensile part, of the considered stress interval, occurs is determined. The lowest of the two numbers is the number of times the stress interval occurs (n).
3) The stress interval (Δσ) and the corresponding number of times (n) it occurs are added to the stress interval spectrum
4) The found compressive part and tensile part of the stress interval are removed n times from the influence line.
5) The process repeats until the obtained stress interval has a value smaller than the cut-off limit. Or the obtained fatigue damage of the considered stress interval spectrum results in a fatigue damage value greater than 1.

Cycles to failure

Research [9] has been performed to find a relation between a stress interval and the resulting fatigue damage. This resulted in a relation between the value of the stress interval (Δσ) and the number of times it can occur until a weld is considered to have failed due to fatigue (N). These relations differ for each of the fatigue details and the design of the bridge [3]. For the considered fatigue detail in this report and the considered case study the following relation is given in the Eurocode [10].

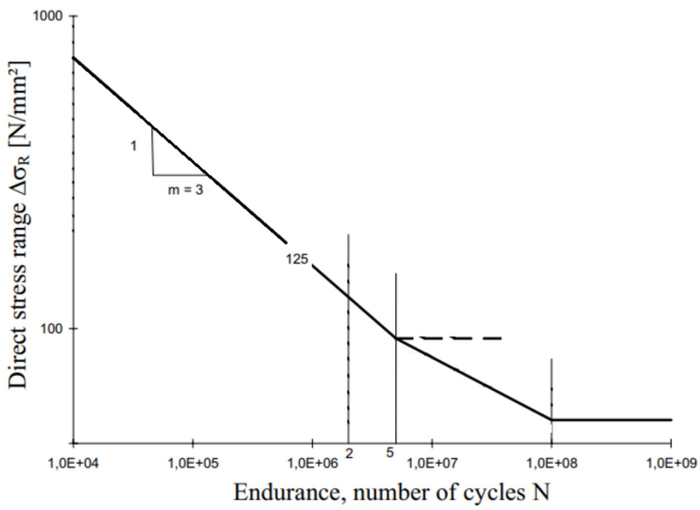

Figure 12: Relation between stress interval (Δσ) and the number of times it can maximally occur (N) [10]

This relationship can be used to determine the maximum allowable number of times of each of the stress intervals in the stress interval spectrum can occur. It can be observed that there is a double logarithmic relation between the value of the stress interval and the number of times it can maximally occur. Therefore, it is assumed that the location of the value of the maximum stress interval is the same as the location of the maximum fatigue damage.

Fatigue damage

In the case of the weld in an orthotropic steel bridge deck the stress intervals contributing to the fatigue damage have different values. Therefore, the damage due to the different stress intervals has to be combined. This can be done using the rule of Palmgren-Miner [10]:

$$\sum \frac{n_i}{N_i} \leq D_L$$

In which i is the number of stress intervals in the stress interval spectrum. n_i is the number of times stress interval i occurs. And N_i is the number of times that stress interval i is maximally allowed to occur should occur. The total damage should be smaller than the fatigue accumulation (D_L) which is usually set as 1.

2.2 Stress determination

In Chapter 2.1.2 it is explained how the fatigue damage should be determined using a FE model. During the research problems occurred relating to the mesh dependency of the FE model. To be able to understand the proposed alternative methods some knowledge about the determination of stresses in structures is needed. An overview of the methods to determine the stresses in structures is explained in this chapter.

This chapter is divided in 3 parts. The first part discusses the different 1D beam theories. The second paragraph extends the 1D beams theories into 2D theories. The third part discusses the commonly used FE method to numerically solve the equations describing the physics of the structure according to the applied 1D beam or 2D theory.

2.2.1 1D beam theories

There are several beam theories which can be used to determine displacements, strains and stresses in 1D beam elements. A clear overview of the most used ones is given by Simone [4]. Which explains 4 different elements. In this chapter 3 of those beam theories will be summarised.

Truss elements (normal deformation only)
Truss elements are elements which only account for normal deformations. A sketch of these elements is given in Figure 13.

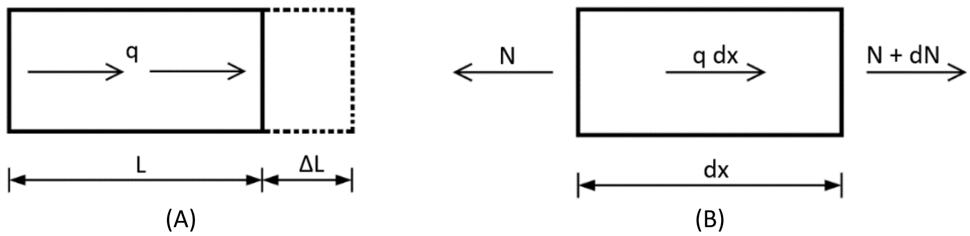

Figure 13: Illustration of truss element: (A) deformations; (B) forces on small segment [4]

In Figure 13 several symbols are used, for the applied load (q), the length of the element (L), the increase in the length of the element (ΔL), the size of a subsegment (dx), the normal force (N) and the increase in the normal forces (dN). It can be observed that such an element assumes that the cross-section area remains constant. The forces on a small segment can be used to determine the differential equation describing the physics of the element in a similar way as for a 1D Timoshenko beam element in a 3D space (Appendix I Derivation system of differential equations of a Timoshenko beam element). An application of this can be found in existing literature [4, 19]. The obtained differential equation is:

$$-EA\frac{d^2u}{dx^2} = q$$

In which the elasticity modulus (E), the cross-section area (A) and the displacement (u) are used. This differential equation can be solved analytically. The obtained solution is:

$$u(x) = -\frac{q}{2EA}x^2 + C_1x + C_2$$

In which C_i is an integration constant. The integration constants can be determined by substitution of the boundary conditions and/or interface conditions of the considered structure.

Euler-Bernoulli elements (includes bending deformations)

This theory includes the bending deformations of an element. It is only valid under small deformations. The most important assumption of this theory is the Bernoulli-Navier hypothesis. It states that the cross section remains planar and normal to the axis of the beam under bending.

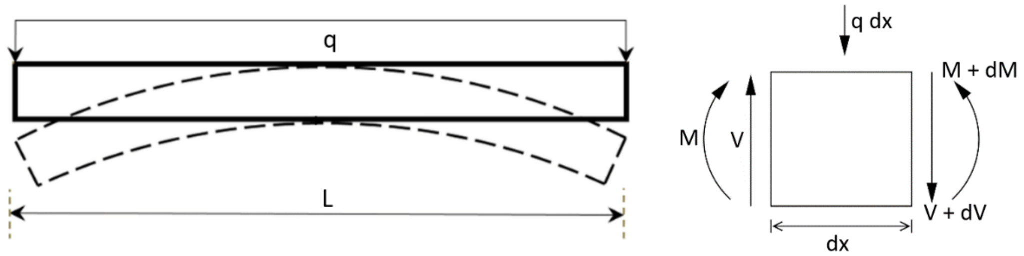

(A) (B)

Figure 14: Illustration of Euler-Bernoulli element: (A) deformations [20]; (B) forces on small segment [4]

Figure 14 introduces some extra quantities: the internal moment (M), the increase of the internal moment(dM), the internal shear force (V) and the increase in internal shear force (dV). The forces on a small segment can be used to determine the differential equation describing the physics of the element in a similar way as for a 1D Timoshenko beam element in a 3D space (Appendix I Derivation system of differential equations of a Timoshenko beam element). The relation between the moments on a segment and the displacements is explained in pre-existing literature [4, 21, 22]. An application of this can be found in the lecture notes written by Simone [4]. If this is combined with the truss element the following system of differential equations is obtained:

$$-EA\frac{d^2u}{dx^2} = q_x \; ; \; EI\frac{d^4v}{dx^4} = q_y$$

In which q_i is an external force applied in the direction of i, I is the second moment of area of the cross section and v is the vertical displacement. This system of differential equations can be solved analytically. The obtained solutions are:

$$u(x) = -\frac{q_x}{2EA}x^2 + C_1x + C_2 \; ; \; v(x) = \frac{q_y}{24EI}x^4 + C_3x^3 + C_4x^2 + C_5x + C_6$$

The integration constants can be determined by substitution of the boundary conditions and/or interface conditions of the considered structure.

Timoshenko elements (includes shear deformations)

The Timoshenko beam element does not only describe bending deformations, but it also includes shear deformations. Shear deformations of a 1D beam element are sketched in Figure 15.

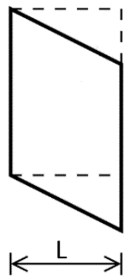

Figure 15: Sketch of shear deformation in 1D beam element [4]

An elaborate explanation of this type of element is given in Appendix I Derivation system of differential equations of a Timoshenko beam element. The methods add an extra degree of freedom (additional rotation of the bending slope), which results in the cross section being able to rotate relative to the neutral axis of the beam. Due to this degree of freedom shear strains are generated. In a 2D plane, if normal deformations are included, the following system of differential equations can be obtained:

$$-EA\frac{d^2u}{dx^2} = q_x\ ;\ EI\frac{d^2\varphi}{dx^2} + GA_s\left(\frac{dv}{dx} - \varphi\right) = 0\ ;\ GA_s\left(\frac{d^2v}{dx^2} - \frac{d\varphi}{dx}\right) = -q_y$$

This equation introduces: φ which is the rotation of the cross section, G which is the shear modulus and A_s which is the cross section shear area. This system of differential equations can be solved analytically. The obtained solutions are:

$$u(x) = -\frac{q_x}{2EA}x^2 + C_1x + C_2$$
$$v(x) = \frac{q_y}{24EI}x^4 + \frac{C_3}{6}x^3 + \frac{C_4}{2}x^2 + C_5x + C_6$$
$$\varphi(x) = \frac{q_y}{6EI}x^3 + \frac{C_3}{2}x^2 + \left(\frac{q_y}{GA_s} + C_4\right)x + \frac{EIC_1}{GA_s} + C_5$$

The integration constants can be determined by substitution of the boundary conditions and/or interface conditions of the considered structure.

Elements including warping deformations

The two most applied theories accounting for warping deformations are the De Saint Venant theory and the Vlasov theory [23, 24]. Most FE software uses De Saint Venant theory. As a results of this the effects of restraint warping are being ignored. Resulting in computed deformations being larger than the real deformations. As a result of this it can be argued that the De Saint Venant theory is safe to be applied.

In Chapter 4 it is argued that warping deformations are not relevant to determine the stresses in the proposed 1D method. Therefore, no literature review will be given on the addition of warping deformations to the 1D beam theories.

2.2.2 2D theories

There are several theories regarding 2D elements. In this chapter, 3 theories, related to this research, are discussed. All these theories are elaborated on in the notes given by Blaauwendraad [25].

Plates loaded in plane

The theory related to a 1D truss element (Chapter 2.2.1) can be extended to a 2D plane. A presentation on this was given by Hendriks based on the notes by Blaauwendraad [26, 25]. It derives the following system of differential equations:

$$-\frac{Et}{1-\nu^2}\left(\frac{\partial^2 u_x}{\partial x^2}+\frac{1-\nu}{2}*\frac{\partial^2 u_x}{\partial y^2}+\frac{1+\nu}{2}*\frac{\partial^2 u_y}{\partial x\partial y}\right)=p_x$$
$$-\frac{Et}{1-\nu^2}\left(\frac{\partial^2 u_y}{\partial y^2}+\frac{1-\nu}{2}*\frac{\partial^2 u_y}{\partial x^2}+\frac{1+\nu}{2}*\frac{\partial^2 u_x}{\partial x\partial y}\right)=p_y$$

The system uses t as the thickness of the plate, v as the Poisson ratio, u_i as the in-plane deformation in direction i, v as the out of plane deformation, p_i as the external applied in plane force in direction i. This system is not generally solvable.

Kirchhoff-Love (includes bending deformations)

The theory related to a 1D Euler-Bernoulli element (Chapter 2.2.1) can be extended to a 2D plane. A presentation on this was given by Hoogendoorn based on the notes by Blaauwendraad [27, 25]. It derives the following differential equation:

$$D\left(\frac{\partial^4}{\partial x^4}+2\frac{\partial^4}{\partial x^2\partial y^2}+\frac{\partial^4}{\partial y^4}\right)w=p_z$$

In this equation D is the plate stiffness and w refers to the out of plane deformation. This differential equation is not generally solvable.

Mindlin-Reissner (includes shear deformations)

The theory related to a 1D Timoshenko element (Chapter 2.2.1) can be extended to a 2D plane. A presentation on this was given by Hendriks based on the notes by Blaauwendraad [28, 25]. It derives the following system of differential equations:

$$-D_\gamma\left(\left(\frac{\partial^2}{\partial x^2}+\frac{\partial^2}{\partial y^2}\right)w+\frac{\partial}{\partial x}\varphi_x+\frac{\partial}{\partial y}\varphi_y\right)=p_z$$
$$D_\gamma\frac{\partial}{\partial x}w+\left(D_\gamma-D\frac{\partial^2}{\partial x^2}-\frac{(1-\nu)D}{2}*\frac{\partial^2}{\partial y^2}\right)\varphi_x-\frac{(1+\nu)D}{2}*\frac{\partial^2}{\partial x\partial y}*\varphi_y=p_x$$
$$D_\gamma\frac{\partial}{\partial y}w-\frac{(1+\nu)D}{2}*\frac{\partial^2}{\partial x\partial y}*\varphi_x+\left(D_\gamma-\frac{(1-\nu)D}{2}*\frac{\partial^2}{\partial x^2}-D\frac{\partial^2}{\partial y^2}\right)\varphi_y=p_y$$

In which D_γ is a measurement for the shear stiffness of the plate and φ_i is the rotation around axis i. This differential equation is not generally solvable.

2.2.3 Numerical solution method (FEM)

There are several methods to solve partial differential equations numerically. In the case of the system of differential equations belonging to complex geometries the FEM is usually chosen to numerically solve the system [29]. An extensive explanation can be found in the notes by Wells [29].

The FEM is a numerical method which has the following general approach:

- The domain is split in several sub-domains (meshing)
- The solution is assumed to be continuous, and linear on each sub-domain
- The system of differential equations is replaced by a system of linear equations
- The system of linear equations is solved numerically

If the domain is split in a higher number of sub-domains a higher level of accuracy of the numerical solution is obtained. However, with the increase in sub-domains the system of linear equations that needs to be solved increases as well. As a result of this computation time to determine a solution with a higher level of accuracy can be unpractically large.

3 Traditionally used 2D plate model

Since the stresses occurring in a weld have to be determined with a plate model containing locally detailed welds [3]. It seems logical to use a similar model to find the location where additional detailing is needed. To do so this chapter describes the traditionally used 2D plate model [30]. Starting with an overview and several paragraphs about the different plate elements. After which, in the last paragraph, the useability of this model is analysed.

3.1 General properties

The model itself does not contain any detailed welds, since the location of the (point in) the weld which needs to be used for the design calculation still has to be determined. The bridge is entirely made of steel quality S355 thus the elasticity modulus, Poisson ratio and a shear modulus are constant throughout the entire model (Table 1).

Table 1: Material properties of Goereese bridge

Description	Symbol	Value
Elasticity modulus	E	210,000 N/mm²
Shear modulus	G	80,769 N/mm²
Poisson ratio	v	0.3

The model takes normal, bending, shearing, and warping deformations in account. The model is fully consists of 2D plate elements and is divided in several sub parts: the main girders, the crossbeams, the stiffeners and the deck plate (Figure 16).

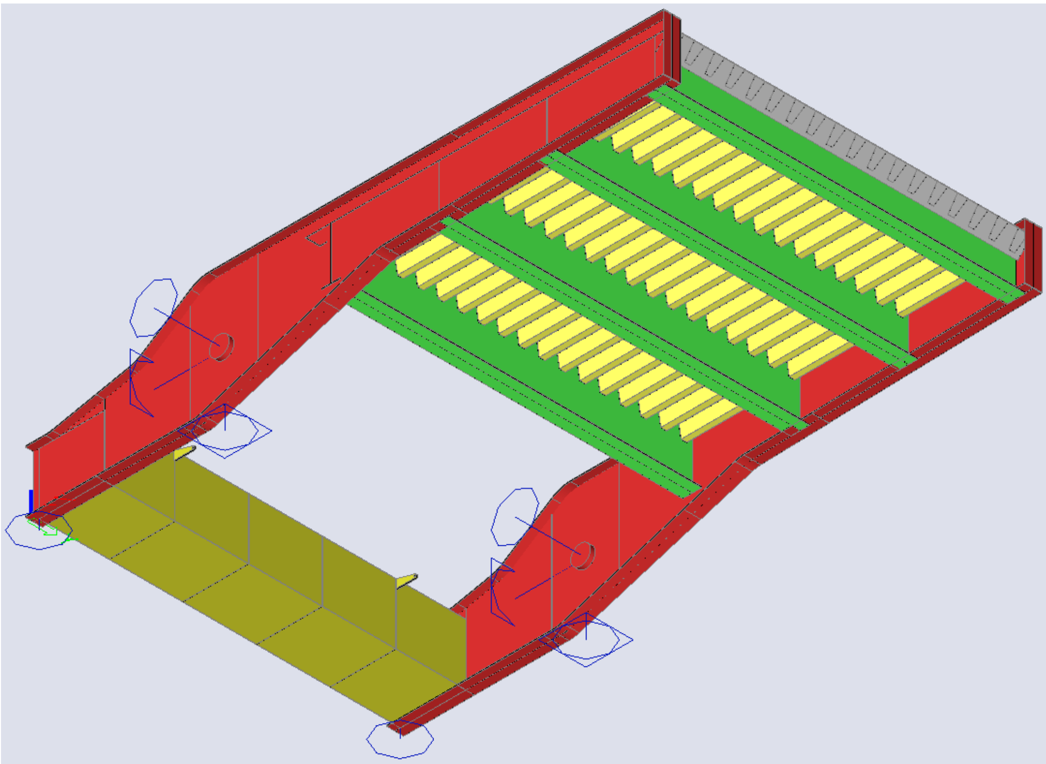

Figure 16: Goereese bridge with red main girders, green crossbeams, yellow stiffeners, and grey deck plate

The bridge is only supported at one side. At the end of the main girders, where the ballast box is situated, the displacement in down- and upward direction is fixed. In between the ballast box and the start of the deck plate a hinge is situated which fixes all displacement and rotations except of the rotation around the axes perpendicular to the main girders. Together the supports make sure that the model cannot have any star deformations. A full description of the FE model can be found in the data repository [30].

3.2 Main girders

The main girders connect the orthotropic bridge deck to the ballast box. The crossbeams and the side of the deck plate are welded to the web of the main girders. The main girders have variable cross section properties. At the end, at which the ballast box is situated, the main girders have a support constraining the displacement in up- and downward direction. In between the ballast box and the start of the deck plate a hinge support is situated. The entire orthotropic bridge deck is an overhang of the main girders. The two main girders are situated parallel from each other with a centre-to-centre distance of 10,700 mm. The main girders are shown in Figure 17.

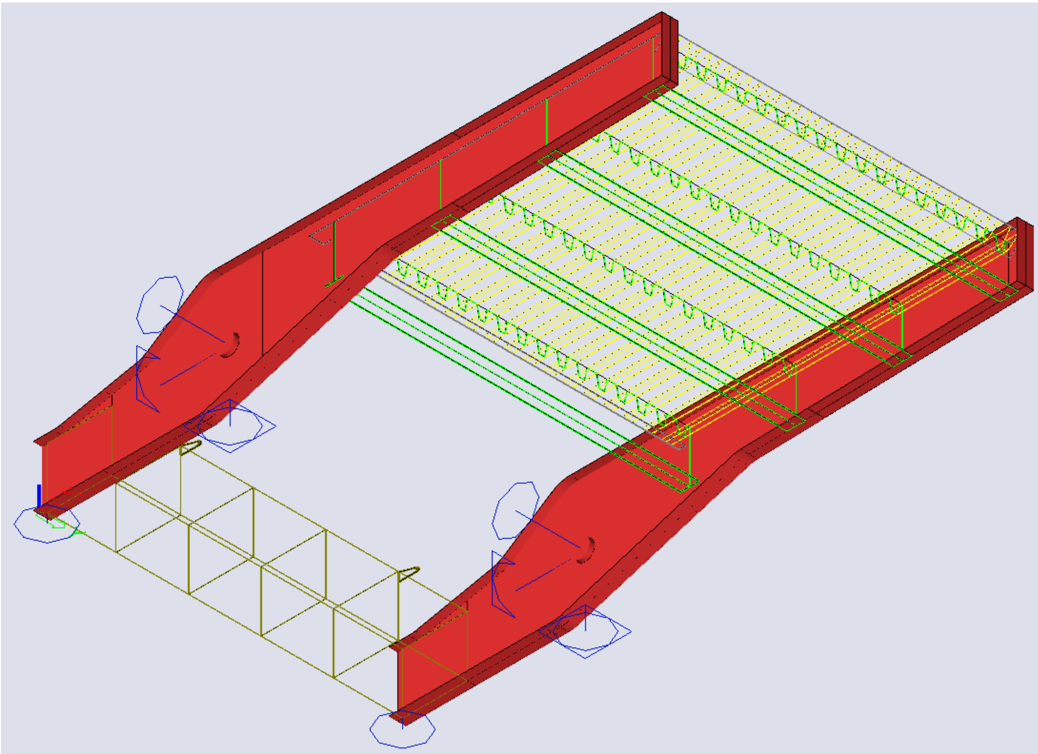

Figure 17: Visualisation of main girders (red) in relation to the Goereese bridge

The geometrical properties of the main girders can be found in Appendix III FE analysis main girder with variable cross section.

3.3 Crossbeams

The crossbeams are in between the two main girders and welded to the web of the main girders, the stiffeners, and the deck plate. In the traditionally used 2D plate model the stiffeners are continuous resulting in a cope hole in the crossbeams at the location of every stiffener. The crossbeams differ in height (Figure 19) and have a length of 10,700 mm. The crossbeams are shown in Figure 18.

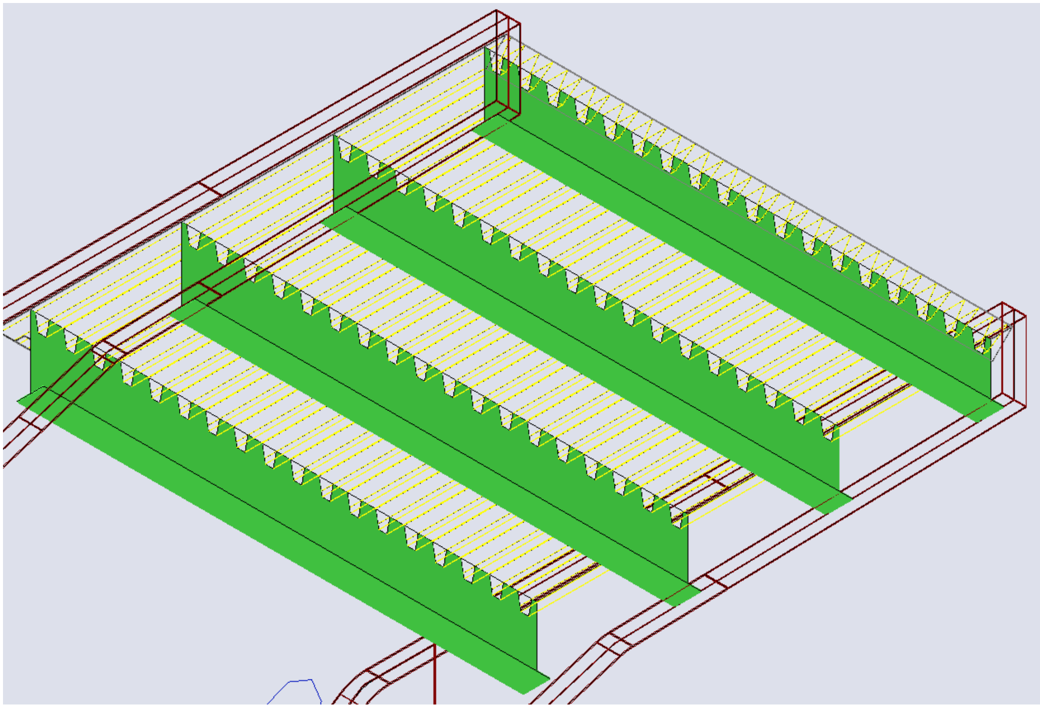

Figure 18: Visualisation of crossbeams (green) in relation to the Goereese bridge

The cross-section geometries of the different cross beams is given in Figure 19.

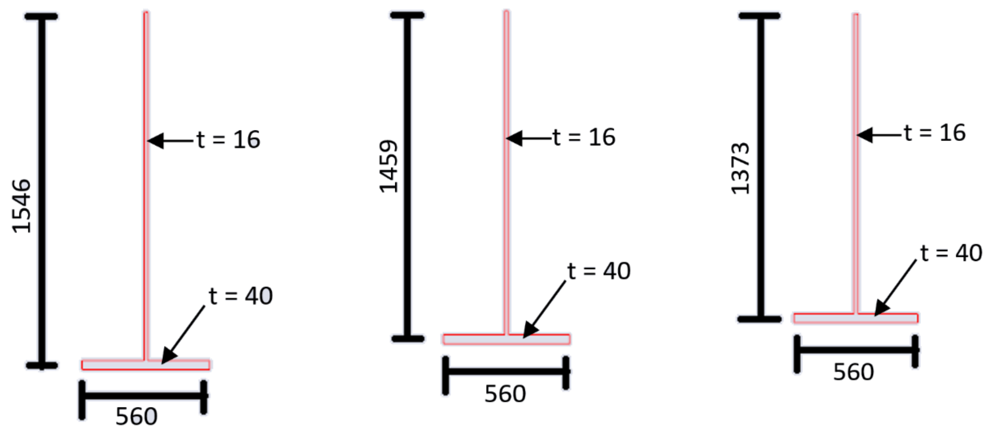

(A) (B) (C)

Figure 19: Cross section geometries of (A) cross beam 1 and 2, (B) cross beam 3 and (C) cross beam 4; all in mm with t being the thickness of the element

3.4 Stiffeners

In the Goereese bridge the stiffeners are so called troughs. This means they have the shape of a trapezium. The stiffeners are continuous and all identical. They are welded to the crossbeams and the deck plate. The stiffeners cover the entire length of the bridge deck of 10,810 mm. There are a total of 18 stiffeners which are equally spaced with a centre-to-centre distance of 300 mm. This means that the first and last stiffener have 250 mm between the stiffener centre and the web of the nearest main girder. The stiffeners are shown in Figure 20.

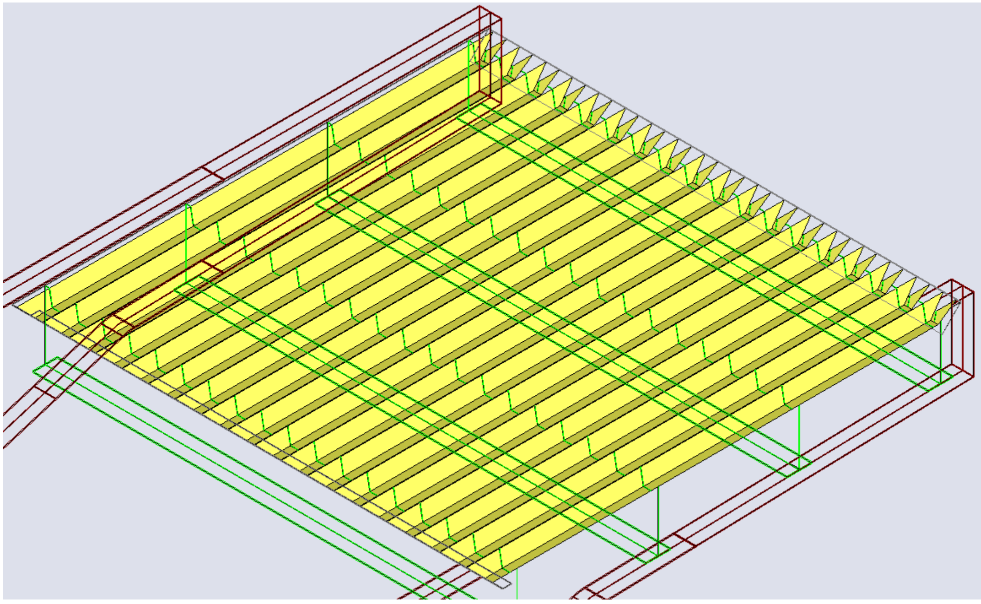

Figure 20: Visualisation of the stiffeners (yellow) in relation to the Goereese bridge

The cross-section geometry of the stiffeners is given in Figure 21.

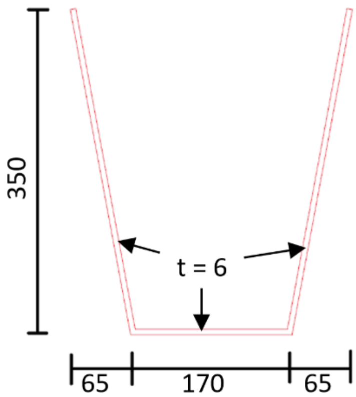

Figure 21: Cross-section geometry of stiffeners; all in mm, t is the thickness

3.5 Deck plate

The deck plate sits on top of the stiffeners and crossbeams and in between the two main girders. It is welded to the stiffeners, crossbeams, and the web of the main girders. It has a continuous thickness of 20 mm, a width of 10,700 mm and a length of 10,810 mm. In the traditionally used 2D plate model it is modelled as one continuous element. The deck plate is shown in Figure 22.

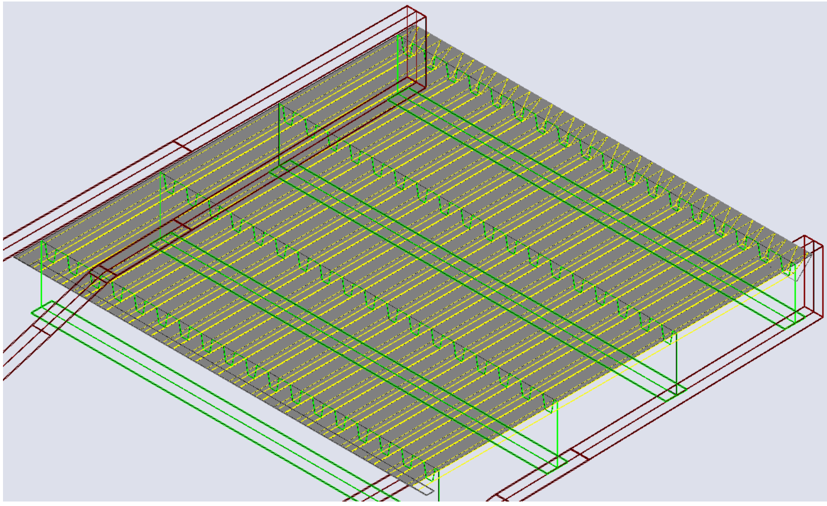

Figure 22: Visualisation of the deck plate (grey) in relation to the Goereese bridge

3.6 Useability

Since the weld details are not included in this model the stresses found at the locations of the welds cannot be used to calculate the required resistance of the bridge. However, it might be possible to use these stresses to find the weld with the highest stresses interval. To check whether this is the case several analyses have been done. These analyses use a limited amount of load cases to reduce the computation time. The FE models can be found in the data repository [30]. The relevant results are presented in Table 2.

Table 2: Point expected to have the highest maximum stress interval after use of traditionally used 2D plate model with different mesh sizes

Mesh size [m]	X coordinate [m]	Y coordinate [m]	Contributing loads
0.4	4.800	3.2	BG56 + BG265
0.2	4.703	3.5	BG196 + BG242
0.1	4.850	1.7	BG12 + BG311
0.05	4.850	3.2	BG35 + BG288

These analyses show that a different point will have the maximum stress interval, caused by a different load combination when a finer mesh is applied. This suggest that a still finer mesh is needed to determine the point with the highest stress interval. The model with the finest mesh (0.05 m) takes approximately 5 hours to run. This model had a limited amount of load cases applied. For a full analysis all potential load locations should be considered, resulting in more than 100 times the amount of load cases currently considered. Therefore, this model is considered unsuitable to determine the location of the point where the highest stress interval is expected[2]. It can be concluded that the x-coordinate of the point with the highest stress interval is close to 4.8 m in the applied analysis. This is also the x-coordinate of all the applied loads. Therefore, it is assumed that the maximum stress interval in a point is the result of loads applied with the same x coordinate as the considered point.

[2] Some of the models found a point with a maximum stress interval which, in more refined models had a maximum stress interval 20% lower than the maximum stress interval in that refined model.

4 Analytically solvable 1D elements model

Since the traditionally used 2D plate model is too mesh dependent it could not be used to determine the point most likely to propagate the first fatigue crack within a reasonable computation time. Because 1D elements usually need less computation time, it might be interesting to use those in an alternative model. Besides, often a system of differential equations belonging to a 1D element can be solved analytically (see Chapter 5) therefore, there is no mesh dependency. Even if a 1D element has no (useful) analytically solution they can be replaced with a set of boundary conditions (see Chapter 5.5), therefore, there is no need to discretize these elements. This means that it is be possible to make a model, constructed out of 1D elements, having no mesh dependency. However, it is not known if a model constructed out of 1D elements has the highest maximum stress interval at the same location as a model constructed out of 2D plate elements. A preliminary investigation is presented in this chapter. The chapter presents the different elements in the analytically solvable 1D elements model.

4.1 General properties

The model itself does not contain any detailed welds, since the location of (the point in) the weld which need to be used for the design calculation still has to be determined. The bridge is entirely made of steel quality S355 thus the elasticity modulus, Poisson ratio, and shear modulus are constant throughout the entire model (Table 1). The model takes bending, shearing, and warping in account. The model is constructed out of 1D beam elements and divided in several sub parts: the main girders, the crossbeams, the stiffeners and the deck plate strip (Figure 23).

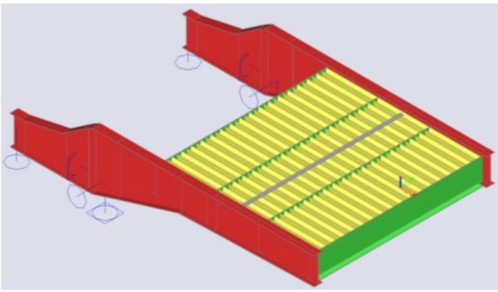

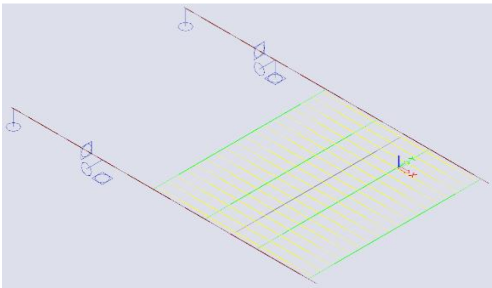

Figure 23: FE model of Goereese bridge out of 1D elements with element surfaces (left) and without element surfaces (right)

The 1D model does not contain the ballast box since it is not expected to influence the stresses in the deck plate. Details of the individual elements can be found in the remaining paragraphs of this chapter. The full 1D FE model can be found in the data repository [30].

4.2 Main girders presented as 1D elements

Due to limitations of the FE software used the main girders are supported at the height of the neutral axis at location of the ballast box. The main girders are the only elements with a changing cross section. Therefore, it is split in several regions as can been seen in Figure 24.

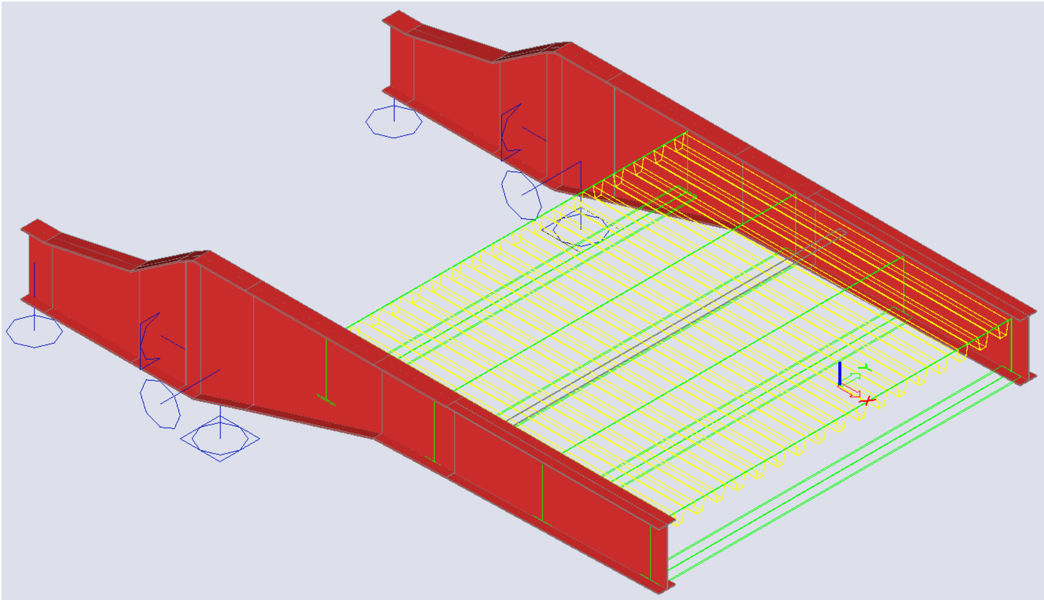

Figure 24: Visualisation of main girders (red) as 1D elements

The traditionally used 2D plate model makes use of plates with curved edges. The used software (SCIA) does not allow 1D elements to have curved edges thus all changes in the cross section are either stepwise or linear. In the calculations, done by the FE software, these are further simplified by further splitting the sub regions in part with constants cross section properties [31]. As a results of this the main girders need a very fine mesh to accurately determine the internal forces. The geometrical properties of the main girders can be found in Appendix III FE analysis main girder with variable cross section.

4.3 Crossbeams presented as 1D elements

In the traditionally used 2D plate model the stiffeners are continuous, and the crossbeams have cope holes where the stiffeners intersect with the crossbeams. Since the considered weld detail (Figure 2) only has to be accounted for at a distance of more than 150mm from the crossbeams [3] it could be the case that modelling the crossbeams with or without a constant cross section (see Figure 25) will not influence the location of the maximum stress interval.

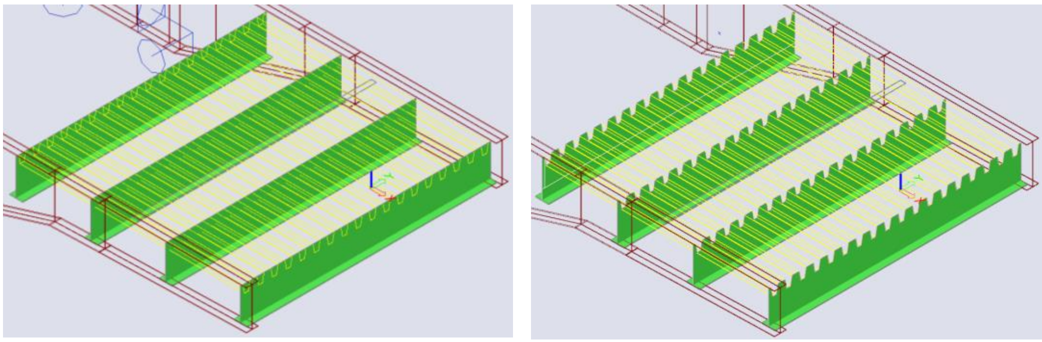

(A) (B)

Figure 25: Visualisation of crossbeams (green) as 1D elements with (A) or without (B) cope holes

The influence of the presence of a cope hole on the location of the maximum stress interval is investigated in Chapter 4.6. All the crossbeams have the same length and shape however the height of the crossbeams differ (Figure 19). From the cross-section geometry, the following cross section properties can be derived (Table 3):

Table 3: Cross section properties of 1D cross beams

Description	Symbol	Value
Cross section area of cross beam 1 & 2	A_{DD1} ; A_{DD2}	47,136 mm²
Shear area in horizontal direction of cross beam 1 & 2	$A_{sy;DD1}$; $A_{sy;DD2}$	20,533 mm²
Shear area in vertical direction of cross beam 1 & 2	$A_{sz;DD1}$; $A_{sz;DD2}$	22,563 mm²
Second moment of area around the y axis of cross beam 1 & 2	$I_{y;DD1}$; $I_{y;DD2}$	11,953,800,324 mm⁴
Second moment of area around the z axis of cross beam 1 & 2	$I_{z;DD1}$; $I_{z;DD2}$	585,914,368 mm⁴
Second polar moment of area of cross beam 1 & 2	$I_{t;DD1}$; $I_{t;DD2}$	14,057,472 mm⁴
Warping constant of cross beam 1 & 2	$I_{w;DD1}$; $I_{w;DD2}$	$1 * 10^{-17}$ mm⁶
Cross section area of cross beam 3	A_{DD3}	45,744 mm²
Shear area in horizontal direction of cross beam 3	$A_{sy;DD3}$	20,525 mm²
Shear area in vertical direction of cross beam 3	$A_{sz;DD3}$	21,608 mm²
Second moment of area around the y axis of cross beam 3	$I_{y;DD3}$	10,227,287,957 mm⁴
Second moment of area around the z axis of cross beam 3	$I_{z;DD3}$	585,884,672 mm⁴
Second polar moment of area of cross beam 3	$I_{t;DD3}$	13,938,688 mm⁴
Warping constant of cross beam 1 & 2	$I_{w;DD3}$	$1 * 10^{-16}$ mm⁶
Cross section area of cross beam 4	A_{DD4}	44,368 mm²
Shear area in horizontal direction of cross beam 4	$A_{sy;DD4}$	20,518 mm²
Shear area in vertical direction of cross beam 4	$A_{sz;DD4}$	20,476 mm²
Second moment of area around the y axis of cross beam 4	$I_{y;DD4}$	8,680,996,621 mm⁴
Second moment of area around the z axis of cross beam 4	$I_{z;DD4}$	585,855,317 mm⁴
Second polar moment of area of cross beam 4	$I_{t;DD4}$	13,821,269 mm⁴
Warping constant of cross beam 1 & 2	$I_{w;DD4}$	$3 * 10^{-17}$ mm⁶

4.4 Stiffeners presented as 1D elements

In the traditionally used 2D plate model the stiffeners consisted of 3 plate elements. In the 1D model the stiffeners are all modelled as a 1D beam element (Figure 26).

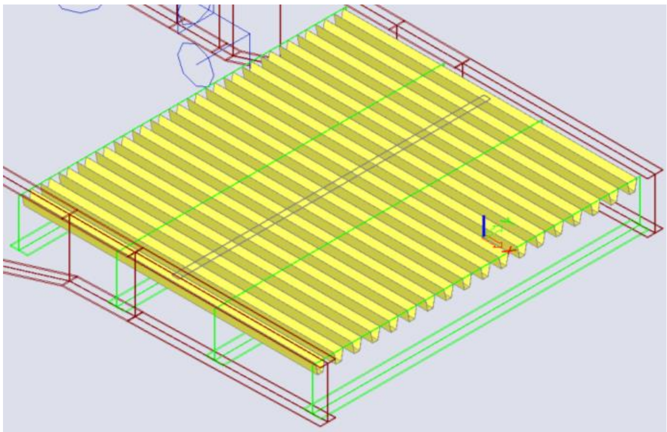

Figure 26: Visualisation of stiffeners (yellow) as 1D elements

The stiffeners are troughs (or u-ribs) of which the webs are welded to the deck plate, thereby making a closed cross section. This results in two possible options for the cross section of the 1D stiffeners: an open cross section or a closed cross section (Figure 27).

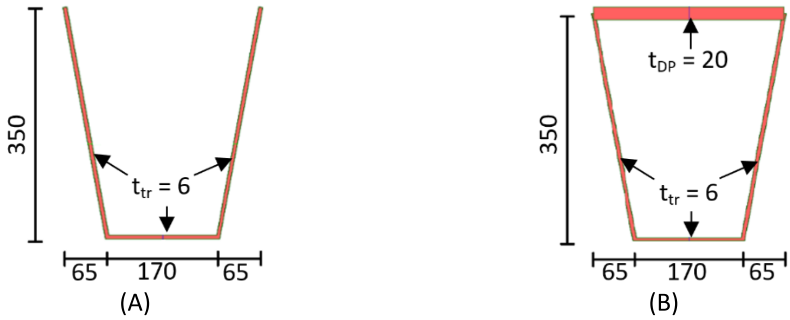

Figure 27: Options for 1D stiffener cross section (A) an open stiffener; (B) a closed stiffener. All dimensions are in mm. t_{tr} is the thickness of the trough and t_{DP} is the thickness of the deck plate

Using the cross-section geometries, the cross-section properties can be determined.

Table 4: Cross-section properties of 1D stiffener elements

Description	Symbol	Value Open	Value Closed
Cross section area	A_{tr}	5,292 mm^2	11,292 mm^2
Shear area in horizontal direction	$A_{sy;tr}$	1,924 mm^2	7,394 mm^2
Shear area in vertical direction	$A_{sz;tr}$	3,902 mm^2	4,323 mm^2
Second moment of area around the y axis	$I_{y;tr}$	68,841,506 mm^4	191,560,919 mm^4
Second moment of area around the z axis	$I_{z;tr}$	62,957,395 mm^4	107,957,395 mm^4
Second polar moment of area	$I_{t;tr}$	63,502 mm^4	167,907,392 mm^4
Warping constant	$I_{w;tr}$	203,693,164,282 mm^6	140,784,373,310 mm^6

The open cross section does not represent any of the deck plate, thus outside of the deck plate strip there will be no deck plate at all. Leading to an underrepresentation of the stiffness. The closed cross section does locally represent the deck plate. There by having a stiffness closer to the 2D model than the open cross section counterpart. However, a closed cross section has a deck plate part where it crosses the deck plate strip. This means that at all the stiffener with deck plate strip crossings the deck plate will be represented twice. Leading to locally overrepresentation of the stiffness. The influence of the choice of the cross section on the location of the point with the highest maximum stress interval is discussed in Chapter 7.2.

4.5 Deck plate presented as 1D Deck plate strip

The deck plate is represented by a 1D strip in the direction of the width of the bridge. This direction is the direction of stresses which needs to be accounted for (Chapter 2.1.2). The width of the strip is equal to the length of a single wheel (Figure 28).

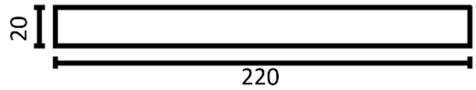

Figure 28: Cross section geometry of 1D deck plate strip

Using the geometry defined in Figure 28 the cross-section properties of the deck plate strip can be determined (Table 5).

Table 5: Cross-section properties of deck plate strip

Description	Symbol	Value
Cross section area	A_{DP}	4,400 mm²
Shear area in horizontal direction	$A_{sy;DP}$	3,667 mm²
Shear area in vertical direction	$A_{sz;DP}$	3,667 mm²
Second moment of area around the y axis	$I_{y;DP}$	146,667 mm⁴
Second moment of area around the z axis	$I_{z;DP}$	17,746,667 mm⁴
Second polar moment of area	$I_{t;DP}$	553,067 mm⁴
Warping constant	$I_{w;DP}$	0 mm⁶

The ends of the deck plate strip are connected to the first and last stiffener (Figure 29).

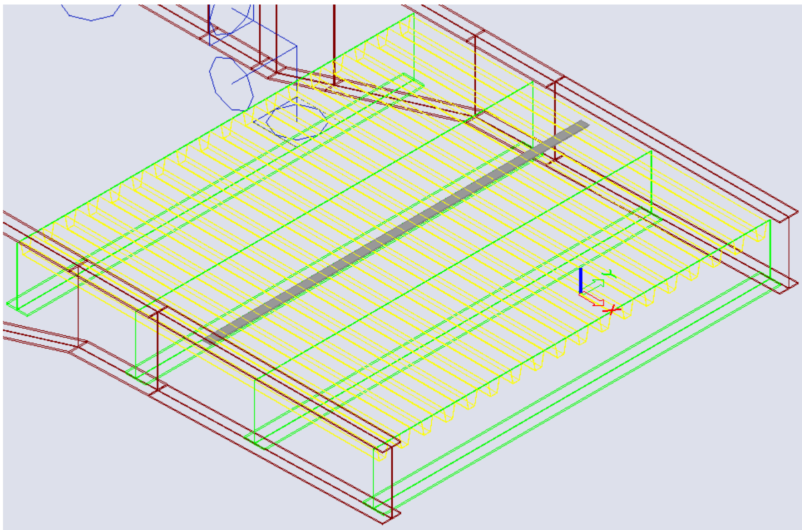

Figure 29: Visualisation of deck plate strip (grey) as 1D element

Since the point with the highest stress interval is expected to be situated directly next to the applied load (Chapter 3.6) the point with the highest stress interval due to a load applied at the deck plate strip is expected to be within the deck plate strip. To account for all potential load locations on the deck plate the loads have to be iteratively moved over the width of the bridge. Therefore, the deck plate strip has to be iteratively moved over the length of the bridge as well. Since the deck plate strip is iteratively moved over the length of the bridge the location of the connection between the main girder and the deck plate strip is changing throughout the iterations. Because the main girder is replaced by a set of boundary conditions (Chapter 5.5) a new set of boundary conditions needs to be determined for each iteration. This would lead to a computational expensive analysis of the main girder for all potential locations of the deck plate strip.

Since it is expected that the connection between the deck plate and the main girder has no effect on the location of the point with the highest maximum stress interval, the deck plate strip will not be connected to the main girders but to the outer first stiffeners.

4.6 Influence of cope holes and stiffener cross section

To investigate if the influence of cope holes and the cross section of the stiffener, on the location of the point with the highest maximum stress interval four models are compared. These models consisted of 1D elements with or without the presents of cope holes in the crossbeams. For this test all models used the same load combinations (the same as applied to determine the results from Table 2). The results can be found in Figure 30 and Table 6.

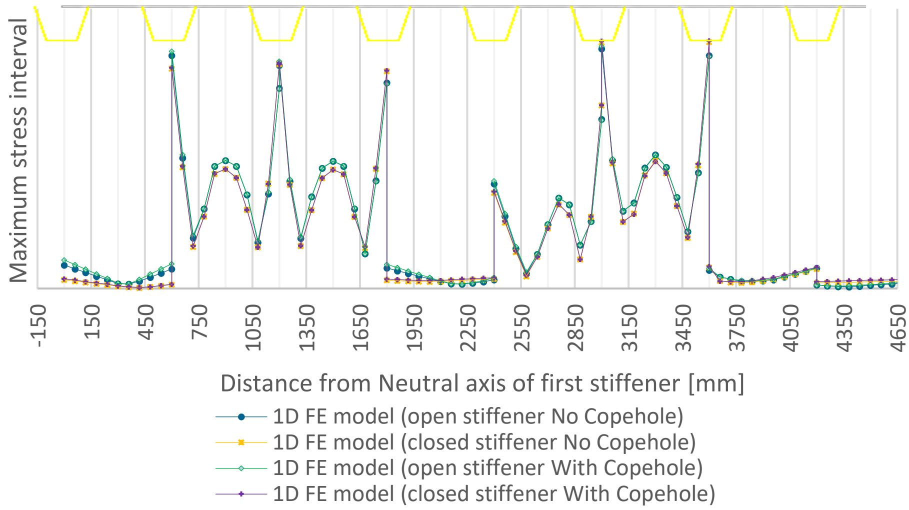

Figure 30: Maximum stress interval at bottom of deck plate at the same cross section in 1D and 2D FE model

Table 6: Comparison of locations of maximum stress intervals in different 1D FE models

	Open cross section No cope hole		Closed cross section No cope hole	
	Distance from first stiffener [mm]	Difference with maximum stress interval	Distance from first stiffener [mm]	Difference with maximum stress interval
Maximum stress interval	3150	-	3450	-
	750	2.68%	3150	0.11%
	3450	2.87%	1350	8.55%
Lower stress intervals	1350	6.95%	1050	8.97%

	Open cross section With cope hole		Closed cross section With cope hole	
	Distance from first stiffener [mm]	Difference with maximum stress interval	Distance from first stiffener [mm]	Difference with maximum stress interval
Maximum stress interval	3150	-	3450	-
	750	2.05%	3150	0.09%
	3450	4.29%	1350	8.95%
Lower stress intervals	1350	6.20%	1050	9.43%

The inclusion of a cope hole and choice of stiffener cross section can influence the location of the point with the maximum stress interval. The difference between the results of the different 1D FE models is small. However, the differences in the maximum stress intervals occurring in different points is also small. Therefore, the choice in different stiffener cross sections can lead to a different point having the highest maximum stress interval. Based on the results, obtained by applying a traffic lane at the theorized position[3], it can be concluded that if one of the models is used, and all points within 5% of the found maximum are considered the maximum of all models is likely to be within in the remaining points (see Table 6). Therefore, any of the 1D models could be used. In this report the model without cope holes and an open stiffener cross section is researched.

Currently the 1D FE models are made in FE software. This software does not use the exact solutions of the 1D elements but meshes the elements in smaller subparts. As a result, there still is mesh dependency and an increase in computation time. To determine the location of the point with the highest stress interval the loads and deck plate strip will have to be moved iteratively. Resulting in new FE models being made for each iteration. By writing code using the exact solutions of 1D elements both these disadvantages can be reduced.

[3] The current regulations do not allow to base the load cases on the theoretical traffic lane position. Elaboration on this can be found in the discussion (Chapter 9.1).

5 Mesh independent solutions of 1D elements

To get rid of the mesh dependency of the 1D model the analytical solutions of the 1D elements need to be used. To do so a system of differential equations describing the behaviour of the 1D elements has to be derived. After which this system can be solved. The obtained solutions still has unknown integration constants which can be determined after formulating the boundary and interface conditions between all elements. After which all displacements (and by extension the stresses) of the 1D model are known without any mesh dependency.

5.1 System of differential equations

The 1D elements used are Timoshenko beam elements. These elements account for shear deformations [4, 5, 6] as is required by the ROK [3]. To simplify the calculations warping deformations are ignored, it is assumed that these deformations are negligible. In the considered case study, all elements perceive a constraint regarding torsional deformations due to their connection with the deck plate. Since the warping deformations are linked to the torsional deformations it is assumed that these can be neglected [32]. In the derivations of the system of differential equations normal deformations are accounted for. Since all elements have constant material properties the system of differential equation can be simplified. It is not assumed that all elements have constant geometrical properties since the main girders have variable cross section properties. To be able to understand the system of differential equations a coordinate system needs to be agreed upon. The used coordinate system is presented in Figure 31. The positive direction of the applied forces is the same as the positive direction of the axis.

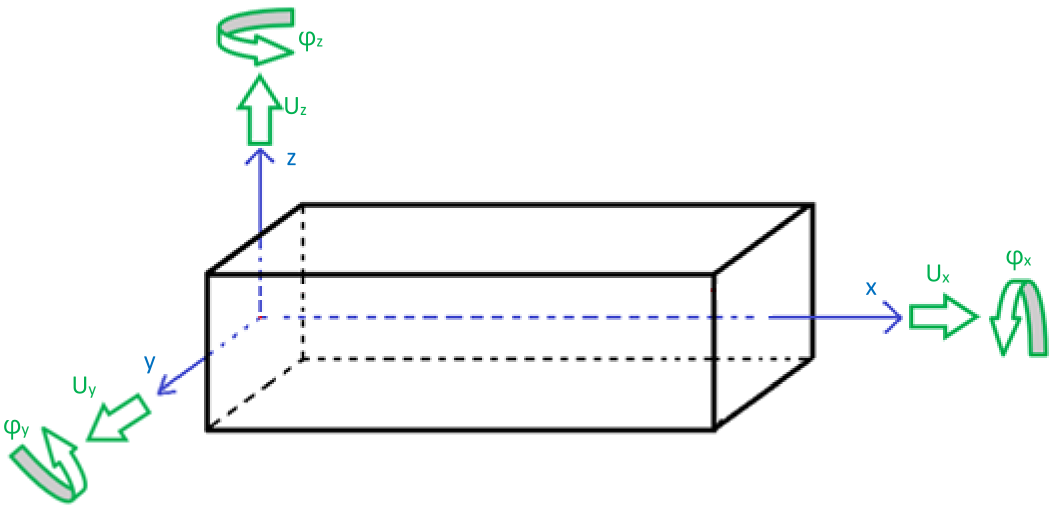

Figure 31: Sign conventions

A lot of derivations of Timoshenko beam elements in a 2D space can found in existing literature [4, 5, 6], however an extension of this in a 3D space is scarce. Therefore, the derivations of a Timoshenko beam element (including normal deformations) can be found in Appendix I Derivation system of differential equations of a Timoshenko beam element. By carefully collecting the material and cross section properties in three matrices ($\boldsymbol{K}_{(1)}\,;\boldsymbol{K}_{(2)}\,;\boldsymbol{K}_{(3)}$). And constructing a vector containing all the displacement ($\boldsymbol{u}$) as well as a vector containing all applied forces ($\boldsymbol{q}$). The system of differential equation describing the physics of a 1D Timoshenko beam element can be written as:

$$\boldsymbol{K}_{(1)}\frac{d^2}{dx^2}\boldsymbol{u} + \boldsymbol{K}_{(2)}\frac{d}{dx}\boldsymbol{u} + \boldsymbol{K}_{(3)}\boldsymbol{u} = \boldsymbol{q} \tag{1}$$

5.2 General solutions of 1D Timoshenko beam elements

The system of a 1D Timoshenko beam element including normal deformations has a solution. To be able to understand the solutions several terms need to be introduced (Table 7).

Table 7: Terms used in solutions Timoshenko beam element

Symbol	Description	Symbol	Description
$\boldsymbol{U_i}$	Displacement in direction of i	E	Elasticity modulus
$\boldsymbol{A}$	Cross section area	q_i	Distributed load applied in direction of i
$\boldsymbol{C_i}$	Integration constant number i	$I_y\,;I_z$	Second moment of area around axis y or z
$\boldsymbol{G}$	Shear modulus	A_{si}	Shear area in direction i
$\boldsymbol{t_i}$	Distributed moment applied around axis i	φ_i	Rotation around axis i
$\boldsymbol{I_t}$	Second polar moment of area		

Now the solution can be written as:

$$U_x(x) = -\frac{1}{E}\int \frac{x}{A(x)}dx * q_x + \int \frac{1}{A(x)}dx * C_1 + C_2 \tag{2A}$$

$$\begin{aligned} U_y(x) = {} & \left(\frac{1}{E}\iint \frac{x}{I_z(x)}dxdx - \frac{1}{G}\int \frac{x}{A_{sy}(x)}dx\right) * q_y + \frac{1}{E}\iint \frac{x}{I_z(x)}dxdx * t_z \\ & - \iint \frac{1}{I_z(x)}dxdx * C_3 + \int \frac{1}{A_{sy}(x)}dx * C_4 - C_5 x + C_6 \end{aligned} \tag{2B}$$

$$\begin{aligned} U_z(x) = {} & \left(\frac{1}{E}\iint \frac{x}{I_y(x)}dxdx - \frac{1}{G}\int \frac{x}{A_{sz}(x)}dx\right) * q_z - \frac{1}{E}\iint \frac{x}{I_y(x)}dxdx * t_y \\ & + \iint \frac{1}{I_y(x)}dxdx * C_7 + \int \frac{1}{A_{sz}(x)}dx * C_8 + C_9 x + C_{10} \end{aligned} \tag{2C}$$

$$\varphi_x(x) = -\frac{1}{G}\int \frac{x}{I_t(x)}dx * t_x + \int \frac{1}{I_t(x)}dx * C_{11} + C_{12} \tag{2D}$$

$$\varphi_y(x) = \frac{1}{E}\int \frac{x}{I_y(x)}dx * q_z - \frac{1}{E}\int \frac{x}{I_y(x)}dx * t_y + \int \frac{1}{I_y(x)}dx * C_7 + C_9 \tag{2E}$$

$$\varphi_z(x) = -\frac{1}{E}\int \frac{x}{I_z(x)}dx * q_y - \frac{1}{E}\int \frac{x}{I_z(x)}dx * t_z + \int \frac{1}{I_z(x)}dx * C_3 + C_5 \tag{2F}$$

This solution contains several integrals which are hard to evaluate. The considered bridge mostly has elements with constant cross section properties. The next paragraph simplifies the solution for the case with constant cross section properties.

5.3 Solution 1D Timoshenko beam element with constant cross section properties

When a 1D Timoshenko beam element has constant cross section properties both the system of differential equations (1) as well as the solutions of the system (2) can be simplified. An even further simplification can be found when only a load in the direction of the z axis has to be accounted for. In the case of the considered bridge both these statements are true for the crossbeams, the stiffeners and the deck plate strip. The solution is:

$$\begin{bmatrix} U_x \\ U_y \\ U_z \\ \varphi_x \\ \varphi_y \\ \varphi_z \end{bmatrix} = \begin{bmatrix} 0 & 0 & 0 & C_1 & C_2 \\ 0 & -\frac{1}{6}C_3 & -\frac{1}{2}C_4 & \frac{EI_z}{GA_{sy}}C_3 - C_5 & C_6 \\ \frac{q_z}{24EI_y} & \frac{1}{6}C_7 & -\frac{q_z}{2GA_{sz}} + \frac{1}{2}C_8 & -\frac{EI_y}{GA_{sz}}C_7 + C_9 & C_{10} \\ 0 & 0 & 0 & C_{11} & C_{12} \\ 0 & \frac{q_z}{6EI_y} & \frac{1}{2}C_7 & C_8 & C_9 \\ 0 & 0 & \frac{1}{2}C_3 & C_4 & C_5 \end{bmatrix} \begin{bmatrix} x^4 \\ x^3 \\ x^2 \\ x \\ 1 \end{bmatrix} \tag{3}$$

This solution does not contain any integrals anymore. Before this solution can be used the integration constants need to be determined.

5.4 Solving integration constants

The solution of the system with constant cross section properties (3) contains twelve unknown integration constants. These constants can be determined if twelve conditions are known. The elements with constant cross section properties (crossbeams, stiffeners, and deck plate strip) are mainly connected with interface conditions to each other. Only the ends of the crossbeams are connected to the main girder for which interface conditions are hard to formulate. In the other cases a connection of i number of elements is made. As shown in Figure 32.

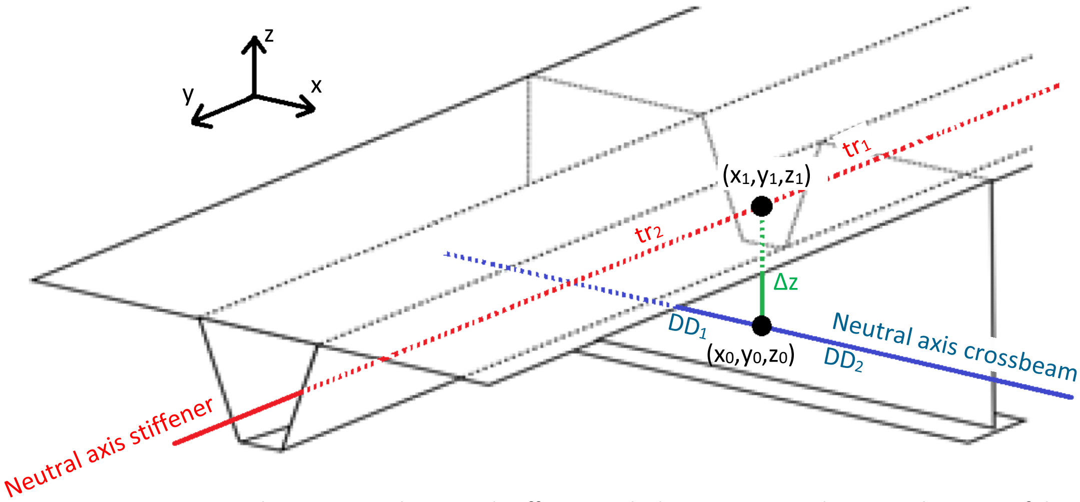

Figure 32: Connection between crossbeam and stiffener in which tr_1, tr_2, DD_1 and DD_2 are the name of the names of the elements. (x_i, y_i, z_i) are the coordinates of a point and Δz is the distance between the neutral axis of the stiffener and the cross beam [3]

The following interface conditions can be formulated based on the requirement of the elements to be connected and in equilibrium:

$$\begin{aligned} u_x^{DD_1}(x_0,y_0,z_0) &= u_x^{DD_2}(x_0,y_0,z_0) = u_x^{tr_1}(x_1,y_1,z_1) + \Delta z\varphi_y^{tr_1}(x_1,y_1,z_1) \\ &= u_x^{tr_2}(x_1,y_1,z_1) + \Delta z\varphi_y^{tr_2}(x_1,y_1,z_1) \end{aligned} \tag{4A}$$

$$\begin{aligned} u_y^{DD_1}(x_0,y_0,z_0) &= u_y^{DD_2}(x_0,y_0,z_0) = u_y^{tr_1}(x_1,y_1,z_1) - \Delta z\varphi_x^{tr_1}(x_1,y_1,z_1) \\ &= u_x^{tr_2}(x_1,y_1,z_1) - \Delta z\varphi_x^{tr_2}(x_1,y_1,z_1) \end{aligned} \tag{4B}$$

$$u_z^{DD_1}(x_0,y_0,z_0) = u_z^{DD_2}(x_0,y_0,z_0) = u_z^{tr_1}(x_1,y_1,z_1) = u_z^{tr_2}(x_1,y_1,z_1) \tag{4C}$$

$$\varphi_x^{DD_1}(x_0,y_0,z_0) = \varphi_x^{DD_2}(x_0,y_0,z_0) = \varphi_x^{tr_1}(x_1,y_1,z_1) = \varphi_x^{tr_2}(x_1,y_1,z_1) \tag{4D}$$

$$\varphi_y^{DD_1}(x_0,y_0,z_0) = \varphi_y^{DD_2}(x_0,y_0,z_0) = \varphi_y^{tr_1}(x_1,y_1,z_1) = \varphi_y^{tr_2}(x_1,y_1,z_1) \tag{4E}$$

$$\varphi_z^{DD_1}(x_0,y_0,z_0) = \varphi_z^{DD_2}(x_0,y_0,z_0) = \varphi_z^{tr_1}(x_1,y_1,z_1) = \varphi_z^{tr_2}(x_1,y_1,z_1) \tag{4F}$$

$$N_x^{DD_1}(x_0,y_0,z_0) + N_x^{DD_2}(x_0,y_0,z_0) + N_x^{tr_1}(x_1,y_1,z_1) + N_x^{tr_2}(x_1,y_1,z_1) = 0 \tag{4G}$$

$$V_y^{DD_1}(x_0,y_0,z_0) + V_y^{DD_2}(x_0,y_0,z_0) + V_y^{tr_1}(x_1,y_1,z_1) + V_y^{tr_2}(x_1,y_1,z_1) = 0 \tag{4H}$$

$$V_z^{DD_1}(x_0,y_0,z_0) + V_z^{DD_2}(x_0,y_0,z_0) + V_z^{tr_1}(x_1,y_1,z_1) + V_z^{tr_2}(x_1,y_1,z_1) = 0 \tag{4I}$$

$$\begin{aligned} M_x^{DD_1}(x_0,y_0,z_0) &+ M_x^{DD_2}(x_0,y_0,z_0) + M_x^{tr_1}(x_1,y_1,z_1) + \Delta z V_y^{tr_1}(x_1,y_1,z_1) \\ &+ M_x^{tr_2}(x_1,y_1,z_1) + \Delta z V_y^{tr_2}(x_1,y_1,z_1) = 0 \end{aligned} \tag{4J}$$

$$\begin{aligned} M_y^{DD_1}(x_0,y_0,z_0) &+ M_y^{DD_2}(x_0,y_0,z_0) + M_y^{tr_1}(x_1,y_1,z_1) - \Delta z V_x^{tr_1}(x_1,y_1,z_1) \\ &+ M_y^{tr_2}(x_1,y_1,z_1) - \Delta z V_x^{tr_2}(x_1,y_1,z_1) = 0 \end{aligned} \tag{4K}$$

$$M_z^{DD_1}(x_0,y_0,z_0) + M_z^{DD_2}(x_0,y_0,z_0) + M_z^{tr_1}(x_1,y_1,z_1) + M_z^{tr_2}(x_1,y_1,z_1) = 0 \tag{4L}$$

In equation (4) the following terms are used:

Table 8: Terms used in equation (4)

Symbol	Description
$u_i^j(a,b,c)$	Displacement in the direction of i of element j at point (a, b, c)
Δz	Distance between the neutral axis of the stiffener and the cross beam
$\varphi_i^j(a,b,c)$	Rotation in around axis i of element j at point (a, b, c)
$N_x^j(a,b,c)$	Normal force of element j at point (a, b, c)
$V_i^j(a,b,c)$	Shear force in the direction of i of element j at point (a, b, c)
$M_i^j(a,b,c)$	Internal moment around axis i of element j at point (a, b, c)

These interface conditions are formulated in terms of a global coordinate system. Since the displacement field (3) and internal forces (11) are determined in terms of a local coordinate system they should be rewritten to the global coordinate before they can be substituted in the given interface conditions. At the ends of the stiffeners there is no crossing of two crossbeams and two stiffeners but a crossing of two cross beams with only one stiffener. In these cases, the interface conditions presented here are still valid. However, the terms related to the non-existent stiffener have to be neglected. As a result of this there are less interface conditions, this is no problem since one less stiffener means that there are less integration constants which will have to be solved.

To be able to determine the total displacement field of the bridge all integration constants need to be solved. This cannot be done by only using the interface conditions shown here (4) since this does not give enough equations to solve all integration constant. The remaining equations have to do with the connections of the cross beams with the main girders. These cannot be determined in the way that is presented here since the main girders have a variable cross-section. Substitution of the displacement field of the main girder (2) in the interface equations does not lead to solvable equations. An alternative method is presented in the next paragraph.

5.5 Boundary conditions modelling behaviour of main girders

The solutions of a beam with variable cross section properties (2) have potentially hard to solve integrals and are therefore not useful. As a result of this the interface equations (4) cannot be used and some integration constants remain unsolved. However, if the proper displacements of the main girders can be determined without using the analytical solution these can be used as boundary conditions. To see if this is possible the properties of the solution of an element with constant cross section properties is being analysed. After which a property of the solution of an element with constant cross section properties is assumed. Which will be combined with a numerical analysis of the main girder to formulate the needed boundary conditions.

5.5.1 Properties of solution of simplified, constant cross section, main girder

If a main girder with constant cross section properties is assumed. The solution can be determined using the standard solution (3) in combination with the general interface conditions (4). On the main girders there is no distributed load present. However, all the cross beams transfer their internal forces to the main girders, leading to point forces at the locations where the cross beams and the main girder are connected. The simplified, constant cross section, main girder is visualized in Figure 33.

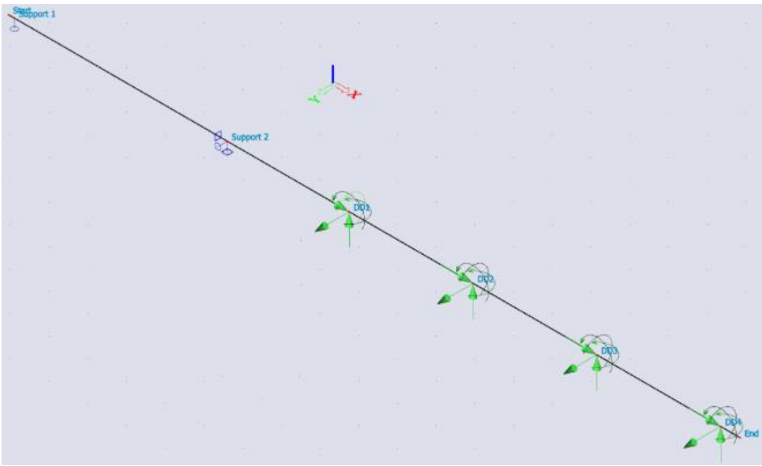

Figure 33: Visualisation of 1D main girder with crossbeams modelled as point loads[4]

This simplified main girder consists of 7 elements with a constant cross section having the solutions discussed in Chapter 5.3 and presented in formula (3). The solution still contains unknown integration constants. All integration constants can be solved using the interface conditions presented in (4)[5]. In combination with the equations following from the physical constraints and the necessity from an equilibrium at the supports and the end of the beam. An elaboration of this calculation can be found in Appendix II Solution main beam with constant cross section properties. The displacements at the location ($x_{(i)}$) of the different cross beams are:

$$\boldsymbol{u}^{(i)} = \boldsymbol{K}^{(i)}(A_{tot}, E, G, I_t, I_y, I_z, x_{Support1}, x_{Support2}, x_{DD1}, x_{DD2}, x_{DD3}, x_{DD4}, x_{(i)})\boldsymbol{p} \qquad (5)$$

In equation (5) $\mathbf{u}^{(i)}$ is a vector containing the displacements at cross beam number (i). $\mathbf{K}^{(i)}$ is a matrix depending on the material and geometry properties, and the location of cross beam i ($x_{(i)}$). Vector $\mathbf{p}$ contains the forces that the cross beams apply to the main girder. Since the responses can be expressed as a matrix (independent of the force vector) multiplied with the force vector the response is linearly related to the force vector. This means that the response of a combination of loads is the summation of the responses of the individual loads in that combination.

---

[4] The cross beams are not connected to the main girders at the height of the neutral axis of the main girders. Thus, the internal normal and shear forces of the crossbeams result in an additional moment in the case that the main girders are modelled as shown in Figure 33.

[5] If a force is applied at a point this should be included in the force equilibrium

5.5.2 Hypothesized form of replacement boundary condition

In the previous paragraph it was determined that, in the case of geometrically constant main girder, the displacements at the locations of the connection between the cross beams and the main girder are linearly related to the internal forces of the cross beams (5). This formula can be rewritten as:

$$\boldsymbol{u}^{(i)} = \sum_{j=1}^{24} \boldsymbol{K}_{*,j}^{(i)} \boldsymbol{p}_j \tag{6}$$

In the case of constant geometrical properties, the components of $\boldsymbol{K}_{*,j}$ could be analytically determined and are depended on material and geometrical properties of the main girder (Appendix II Solution main beam with constant cross section properties). In the case of a geometrically variable main girder the component of $\boldsymbol{K}_{*,j}$ can not be determined analytically. However, if it is assumed that the displacements of the cross beams will remain linearly related to the internal forces in the crossbeams, equation (6) is still valid. In that case a single component of $\boldsymbol{K}_{*,j}$ can be determined by obtaining the displacements for a load case in which only a single component of the load vector is unequal to zero. This can be easily shown by stating that for j=l all $\boldsymbol{p}_j$ are equal to zero except $\boldsymbol{p}_l$. In that case (6) can be rewritten to:

$$\boldsymbol{K}_{*,l}^{(i)} = \frac{1}{\boldsymbol{p}_l} \boldsymbol{u}^{(i)}$$

By preforming 24 numerical analyses of the main girder. In which a single internal force of a cross beam was applied as a unit load, and the displacements of the main girder at the location of the connection with the crossbeams are determined. All values of $\boldsymbol{K}$ can be determined. For a description of the numerical analysis and the results see Appendix III FE analysis main girder with variable cross section.

Since all components in $\boldsymbol{K}_{*,l}^{(i)}$ are now known the displacements of the main girder, at the point they intersect with the cross beams, can now be determined by substituting these values in (6).

In the model with 1D elements described in Chapter 4 the only loads applied on the 1D model are the internal forces of the cross beams. This means that the displacements of the main girders at the location of the cross beams can be expressed in terms of the internal forces of the cross beams. The found expression is:

$$\boldsymbol{u}^{(i)}(x_0) = \boldsymbol{K}^{(i)} \begin{bmatrix} \boldsymbol{f}_{int_1}^{(DD1)}(x_0) \\ \boldsymbol{f}_{int_1}^{(DD2)}(x_0) \\ \vdots \\ \boldsymbol{f}_{int_6}^{(DD4)}(x_0) \end{bmatrix} \tag{7}$$

In which $\boldsymbol{f}_{int_i}^{(j)}$ is the i^{th} component of the internal force vector of cross beam j as defined in Appendix I Derivation system of differential equations of a Timoshenko beam element. Adding these boundary conditions (7) to those established to the set determined in the previous chapter (4) makes it possible to solve the model of 1D element as described in Chapter 4 without discretising in space. Therefore, the solution obtained in this manner will have no mesh dependency.

6 Results of mesh independent 1D elements model

In the previous chapters the theory and idea behind the use of a mesh independent model existing out of 1D elements was discussed. After applying the theory results can be obtained. In this chapter different options on the interpretation of these results are discussed. As well as the conclusions that can be drawn from these results.

6.1 Use of mesh independent 1D model

The proposed 1D elements model has to be used in an iterative manner (Chapter 4.5). For this research several iterations were performed. The locations at which the maximum stress intervals were determined are shown in Figure 34.

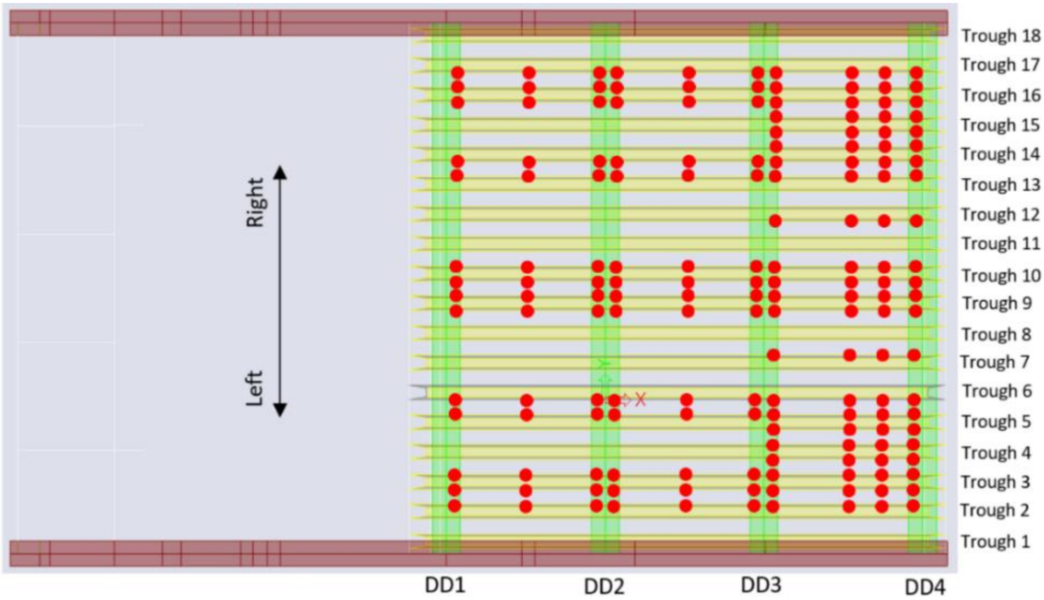

Figure 34: Iteration locations

Since the considered bridge has an axis of symmetry only half of the iteration locations have to be used. According to the Dutch regulations [3] at each of these locations 3 possible central points of the spread of a wheel of a truck have to be considered to determine the fatigue damage (Figure 7). These being on top of the centre of the considered trough, on top of the considered web of a trough and in between the two troughs next to the considered trough web. However, in the proposed 1D elements model the troughs are connected to the deck plate at the neutral axis of the trough (not at the webs of the trough). Therefore, only two locations are considered for the central point of the spread of a wheel of a truck. These being on top of the neutral axis of the considered trough and in between the troughs next to the considered trough web. In some cases, the position of the spread of the wheel of the trucks was such that the other wheel of the truck had a set location (since setting it at the opposite side of the given location meant that it would be placed outside of the bridge). In the other cases both the placement of the left and right wheel at the given spread locations had to be considered. Note that left and right refer to a local definition which is shown in Figure 34.

The very first iterations were chosen evenly distributed over the entire bridge. Extra iterations were added close the maximum of the previous iterations. As a result of this a global maximum might have been missed. An improvement in both the change of missing the global maximum as well as the number of iterations needed to find it can be reached by applying optimization algorithm [33, 12].

For every load case (between 30 and 60) in every considered trough web a linear system of equations has to be solved[6]. This system will have slightly different sizes but always exceeds 2025 equations. Due to the size of these system and a limit in computation time this system is solved numerically.

6.2 Interpretation of results of mesh independent 1D model

In the proposed mesh independent 1D model the troughs are not connected to the deck plate at their webs but directly above the neutral axis of the trough. Therefore, the points with the maximum stress interval are not located at the trough webs but at the neutral axis of the trough (Figure 41). As a result of this, and some numerical interpolation issues (Appendix IV Uninterpreted results mesh independent 1D elements model) a different way of interpretating the results is necessary. In this research two interpretation methods are used and compared.

In this paragraph all results of the mesh independent 1D model are presented in dimensionless units (percentages). This is because the results cannot be used to determine stress values accurately and presenting stress values might suggest that the model can be used to determine those values. However, the model might still be able to determine the location where the maximum stress interval can be found. All results in Paragraph 6.2.1 are in relation to the same maximum thus these figures can be compared with each other. The results of Paragraph 6.2.2 are in relation to a different maximum.

[6] Another reduction of less than 20% can be reached by noting that some load cases can be used to analyse two different trough webs. Therefore, in these cases, the system of equations has to be solved only once to get the stresses in two trough webs.

6.2.1 Interpretation method 1: Stress in trough web assumed to be stress at corresponding side of neutral axis, only right sided trough webs

The first interpretation method which will be discussed is only taking the right web of all troughs in account. Since the bridge is symmetric the value of a left web of a trough is equal to right web of the trough at the other side of the symmetry axis (e.g. the maximum stress interval in the left web of trough 3 is the same as in the right web of trough 15). This leads to the following results (Figure 35):

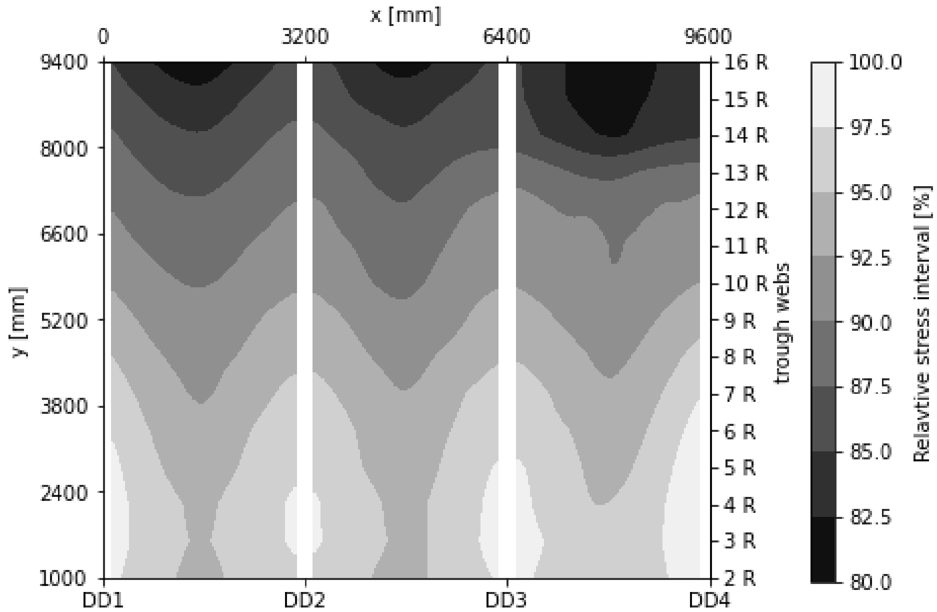

Figure 35: Contour plot of max stress interval obtained with method 1

This contour plot has some notable properties:

- All fields between the cross beams have a similar shape
- The maxima are found close to the crossbeams while the minima are found in between the crossbeams
- The maximum of the plot does not exceed 100%
- The maxima look to be close to one main girder while the minima look to be close to the opposite main girder

That the fields between the crossbeams have a similar shape but do not have identical values is expected. It is expected that the local design of the bridge has the most influence on the local stresses. Since the design is locally identical the stress values are expected to be similar. However, the global design will still have a small influence. And since the full design is not fully symmetric (the support conditions, main girders and cross beams are not symmetric in all axes, see Chapter 3) some small difference between the stresses are expected.

Having the highest and lowest value of the stress intervals either in the middle or at the ends of the fields in between the crossbeams is expected. This is due to high stiffness expected close to the cross beams and low stiffness expected the be in the middle between two cross beams. often the maximum and minimum stresses can be found close to the location of the maximum and minimum stiffness (Appendix V Shortlist of potential critical points).

That no value in the contour plot exceeds 100% means that the point with the highest expected maximum stress interval is already within the points which have been analysed in the previous iterations. Therefore, it is assumed that further iterations are not likely to suggest that a different point will have a higher expected maximum stress interval. Thus, it is decided that the iterative process has been repeated enough times.

The results suggest that the highest maximum stress interval is at an outer side of the bridge while the lowest is at the opposite side of the bridge. To better examine this the maximum stress interval is graphed in several cross sections (Figure 36).

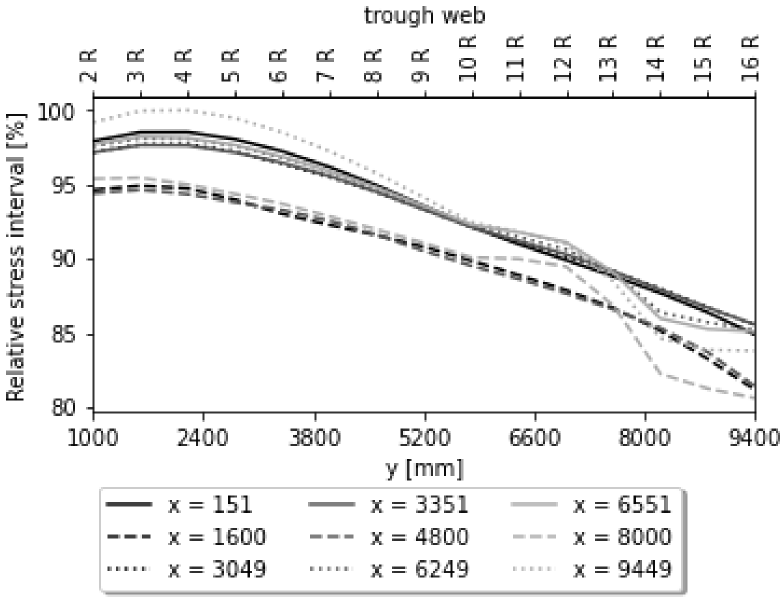

Figure 36: Maximum stress interval in cross sections, obtained with interpretation method 1

This graph has some notable properties:

- The highest expected maximum stress interval is found at the end of the bridge (x = 9449) in the right web of trough 4 (y = 2200)
- The lowest expected maximum stress interval is found in the centre of the field between crossbeam 3 and crossbeam 4 (x = 8000) in the right web of trough 16 (y = 9400)
- In some cross sections there is a kink at trough 14
- The cross sections in the middle of two cross beams (x = 1600, x = 4800 and x = 8000) contain maximum stress intervals which have a lower value than the cross sections which are close to the cross beams

The highest value of the maximum stress interval is at the end of the bridge (x = 9449). This is one of the locations identified as likely to have the highest maximum stress interval (Appendix V Shortlist of potential critical points). However, it is found in the fourth trough, this is not a trough which is considered to be likely to have the highest maximum stress interval. Since the bridge is symmetric there is another point expected to have the same maximum stress interval. That point is also at the end of the bridge (x = 9449) but in the left web of trough fifteen.

The lowest expected maximum stress interval is found in the left web of trough 16 for all analysed cross sections. This is remarkable since this means that both the lowest and highest maximum stress interval is found to be close to the main girders and close to each other.

In Figure 36 some cross sections show a kink at the location of the right web of trough 14 while other cross sections do not. It is noted that the cross sections with a kink are located at x is 6249, 6551, 8000, 8750 and 9449. These cross sections are all close (or at) an analysed point in the right web of trough 14. While the remaining cross sections are further away from a preformed iteration on the right web of trough 14. Therefore, the remaining cross sections will have a smooth curve at this location (Since a cubic surface is used to interpolate between iteration points the curve has to be smooth between these points [34]). The cross sections with a kink have those because troughs 14, 15 and 16 have fewer load cases which can be applied (the trucks have to be positioned in such a manner that both wheels fit on the bridge). In the next trough these extra load cases can be added. This results in a sudden increase in the expected maximum stress interval.

It can be observed cross sections which are situated in between the cross beams have lower maximum stress interval values than the cross sections close to the cross beams. To research this behaviour the maximum stress intervals in the length of troughs are graphed (Figure 37).

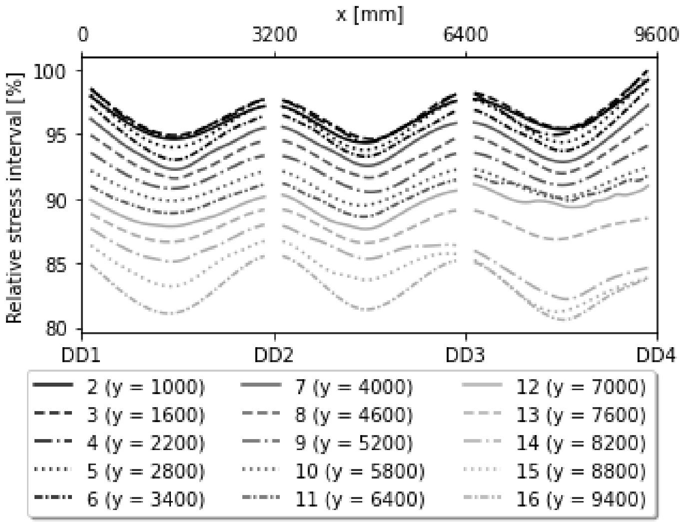

Figure 37: Maximum stress interval in right sided trough webs, obtained with interpretation method 1

This graph has some notable properties:

- All troughs have a maximum stress interval at the points close to the cross beams and a minimum in the middle between two cross beams
- Troughs at the right side of the considered bridge (troughs with a low number) have higher expected stress interval values than the troughs at the left side of the considered bridge
- Between the third and the fourth cross beam the differences between the maximum stress intervals in the different troughs is bigger than in between the other cross beams

Each trough shows a similar behaviour of the maximum stress interval. All troughs have local maximum stress intervals at the cross beams and local minimum stress intervals in between two cross beams. This agrees with the cross sections in between two cross beams having lower stress interval values than the cross sections close to the cross beams as presented in Figure 36.

It can be observed that the right sided trough webs at the right side of the bridge have higher expected maximum stress intervals than the right sided trough webs at the left side of the bridge. This agrees with the cross sections in between two cross beams having lower stress interval values than the cross sections close to the cross beams as presented in Figure 36.

It is noted that the differences between the maximum stress values is bigger between the troughs at the left side of the bridge between cross beam 3 and 4 than at the other locations of the bridge. This agrees with the kink in the graph of Figure 36. The reason for this behaviour is explained in the paragraphs concerning Figure 36.

The proposed mesh independent 1D model does not account for the connection between the trough webs and the deck plate. This might be the reason for the remarkable difference occurring between left and right webs of troughs (Appendix IV Uninterpreted results mesh independent 1D elements model). Therefore, an alternative interpretation for the results will be examined.

6.2.2 Interpretation method 2: Averaging trough webs, difference in trough webs determined using nearest trough

By applying interpretation method 1 it was found that one web (right) of a trough has a remarkably higher expected maximum stress interval than the other web (left) of the trough. This might be due to the simplifications applied in the connection between the troughs and the deck plate strip. To account for this it can be argued to average the found values at either side of the neutral axis of the trough and use those for both webs of a trough. This would give a sense of the maximum stress interval of each trough. The difference between the webs in a trough could be determined by looking at the adjacent troughs at either side of the considered web. The trough with a higher expected stress interval could be argued to be on the side in which the trough web is expected to have a higher maximum stress interval as well. Applying this method, the following result can be obtained (Appendix VI Results mesh independent 1D element model interpretated via method 2, Figure 38):

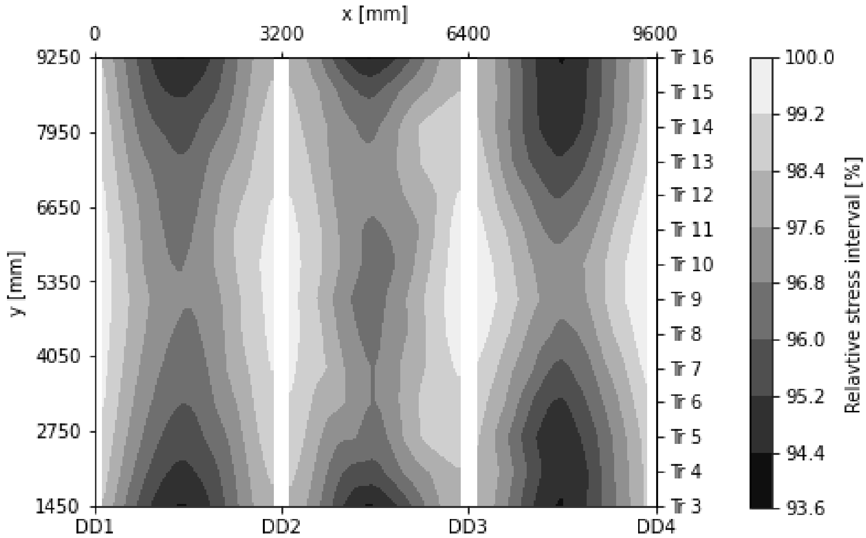

Figure 38: Contour plot when averaging between trough webs

This contour plot (Figure 38) has some notable properties:

- The highest maximum stress interval is found in the middle of the bridge (y = 5050 and 5650) and at the last cross beam (x = 9449). It is expected to be in the trough web closest to the middle of the bridge.
- The lowest maximum stress interval is found in the middle of the field between crossbeam 3 and 4 (x = 8000) and close to the main girders (y = 1450 and 9250).
- It is close the perfectly symmetric.
- The maximum of the plot does not exceed 100%
- In the fields between cross beam 1,2 and 2,3 a saddle point is situated in the middle. While in the field between cross beam 2 and 3 a local minimum is found in the middle. This minimum sits between two saddle points.

The highest maximum stress interval is found at one of the locations where it would have been expected in advance (Appendix V Shortlist of potential critical points).

The lowest maximum stress interval is found at one of the locations where it would have been expected in advance (Appendix V Shortlist of potential critical points).

The contour plot is almost symmetric. The bridge is entirely symmetric thus the contour plot is expected to be so too. The small deviation from symmetry is due to the accuracy of the applied interpolation method.

The fact that no value in the contour plot exceeds 100% means that the point with the highest expected maximum stress interval is already within the points which have been analysed in the previous iterations. Therefore, it is assumed that further iterations are unlikely to suggest that a different point will have a higher expected maximum. Thus, it is decided that the iterative process has been repeated a sufficient number of times.

In the fields between crossbeam 1, 2 and 3, 4 a saddle point can be found in the middle. While the field between crossbeam 2 and 3 has a local minimum at this point. In this research the focus is on the highest maximum stress interval thus no extra attention will be given to this remarkable property.

6.3 Differences in results of interpolation methods

Both the methods discussed in this chapter have wildly different results (Figure 35 and Figure 38). The points with the highest maximum stress interval found by applying the two interpolation methods are given in Table 9.

Table 9: Results of 1D elements model using interpretation method 1 and method 2

	Method 1			Method 2		
	x [mm]	y [mm]	Through web	x [mm]	y [mm]	Through web
Maximum stress interval	9449	2200	4R	9449	5200	9R
	9449	1600	3R	9449	4900	9L
	9449	2800	5R	9449	4600	8R
Lower stress intervals	9449	1000	2R	9449	4300	8L

Both interpretation methods result in an expected point with the highest expected stress interval at the end of the bridge next to the last cross beam (x = 9449). However, both interpretation methods result in a different trough having the expected highest maximum stress interval. Method 1 suggest that there is a significant difference in the maximum stress interval between the two webs of a trough while method 2 states that the stress interval in different webs of a trough are similar.

7 Verification

In the previous chapters several simplifications on the traditionally used 2D plate model have been preformed of which the influence, on the location of the highest maximum stress interval, have to be studied. The following simplifications will be studied in reversed order:

- Change from traditionally used 2D plate FE model to 1D elements FE model
- Change from 1D elements FE model to mesh independent 1D model

To see whether these simplifications have influences on the location with the highest maximum stress interval several case studies will be performed. The choice for these cases (choice in the points analysed). Is based on the results in the previous chapter (Paragraph 6.3) and the judgement of two structural engineers.

The verification will be done by comparing the results of the proposed mesh independent 1D model with the 1D elements FE model. Comparing the results of a 1D FE model with the results of a 2D elements FE model with weld details (as required with the regulations [3]). And by comparing the results of the proposed mesh independent 1D model with the 2D elements FE model (with weld details).

7.1 Proposed mesh independent 1D model vs. 1D elements FE model

In the previous chapter it was shown that the maximum stress interval is expected in right web of trough 4 or the right web of trough 9. In this comparison the right web of trough 4 is considered. Since all load cases, which have to be considered in this point, create a compressive stress (Appendix IV Uninterpreted results mesh independent 1D elements model) only 1 load case will be needed to determine the maximum stress interval of the two models. The load case used for the comparison is one of the load cases which has to be used for the determination of the maximum stress interval in both the right web of trough 4 and the left web of trough 5. This load case is related to a truck with axis type B (Figure 6) on the field at the right side (Figure 40) of the considered trough web. The resulting stresses found in the bottom of the deck plate strip are shown in Figure 39 and Figure 40. These figures show the stresses found in both models. However, these values are not representative for the stress occurring in a 2D element model nor a full 3D model. **<u>These stresses cannot be used to determine fatigue damages</u>**.

Figure 39: Stress in bottom of deck plate strip using proposed mesh independent 1D model

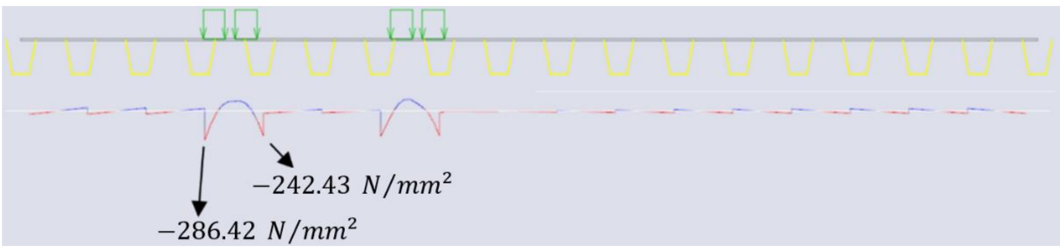

Figure 40: Stress in bottom of deck plate strip using 1D elements FE model (without cope hole)

It can be noted that the stress interval found at the considered web is (to at least two digits after the comma) identical in both 1D models. Therefore, it can be concluded that replacement of the main girders by alternative boundary conditions as presented in Chapter 5.5 is done properly.

7.2 1D elements FE model vs. traditionally used 2D plate model

To compare the 1D FE model with the traditionally used 2D plate several FE analyses are compared. For these analyses both models used the same load combinations (the same as applied to determine the results from Table 2). Since it is likely that point with the highest stress interval is directly next to the applied loads (Chapter 3.6) only the points in line with the loads are considered. The results can be found in Figure 41.

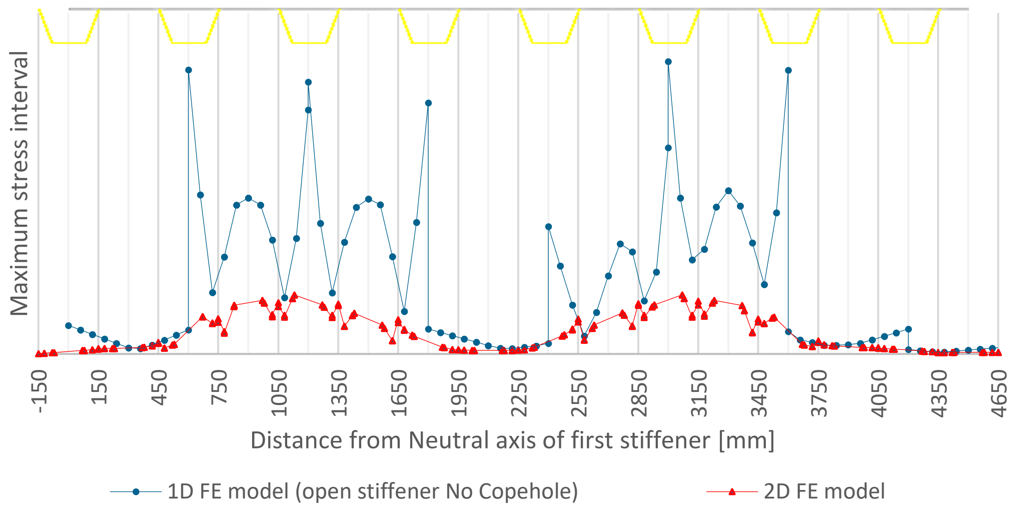

Figure 41: Maximum stress interval at bottom of deck plate at the 1D and 2D FE model

The traditionally used 2D plate model used to make this graph has a mesh of 0.4m with local refinements around the welds of 0.05m. For a thorough description see the FE model in the database [30]. Some observation can be made based on Figure 41:

- The values of stresses in the 1D FE models differ from the traditionally used 2D plate model. This is expected since the 1D FE model only a small deck plate strip is modelled (Chapter 4.5).
- The traditionally used 2D plate model and 1D FE model have their maximum stress intervals in the same region. As a result of this the highest stress intervals could be at the same locations. The traditionally used 2D plate model (without weld details) is not able to determine the exact point the maximum stress interval is likely to occur (Chapter 3.6).

7.3 Proposed mesh independent 1D model vs. 2D FE model

The traditionally used 2D plate model cannot be used to determine the location of the maximum stress interval (Chapter 3.6). However, now that some points potentially having the maximum stress interval are determined (Chapter 6.3) the traditionally used 2D plate model can be updated. At the relevant locations the required [3] weld details and mesh refinement can be added. And the total amount of load cases considered can be reduced. After which this updated 2D FE model can be used to determine the value of the maximum stress interval at the relevant locations. These maximum stress intervals can be compared with the results of the proposed mesh independent 1D model.

An overview on how to update the traditionally used 2D plate model is given in the Chapter 2.1.2. In this chapter only a short summary is given of this method. The calculation as applied on the considered case study (of the Goereese bridge) can be found in the appendix (Appendix VII Elaboration calculating maximum stress interval 2D FE model).

7.3.1 Comparison points

Since the results required by the proposed mesh independent 1D model interpretated via method 1 suggest significant difference between the maximum stress values at different webs of a trough (Chapter 6.2.1), for every point in a trough (if possible[7]) both webs will be considered. A total of four points will be considered. 2 of these points (1 and 2) are at the maxima found by the two different interpolation methods applied on the results of the 1D elements model (Figure 35 and Figure 38). The last two points are determined by asking experts on their opinion. One of these points (A) was given by structural engineer "A" who was not informed of the results of the proposed 1D elements model. The second point (B) was given by structural engineer "B" who was aware of the results and details of the proposed 1D elements model. Both structural engineers were familiar with the design of the bridge. In Figure 42 the points are shown.

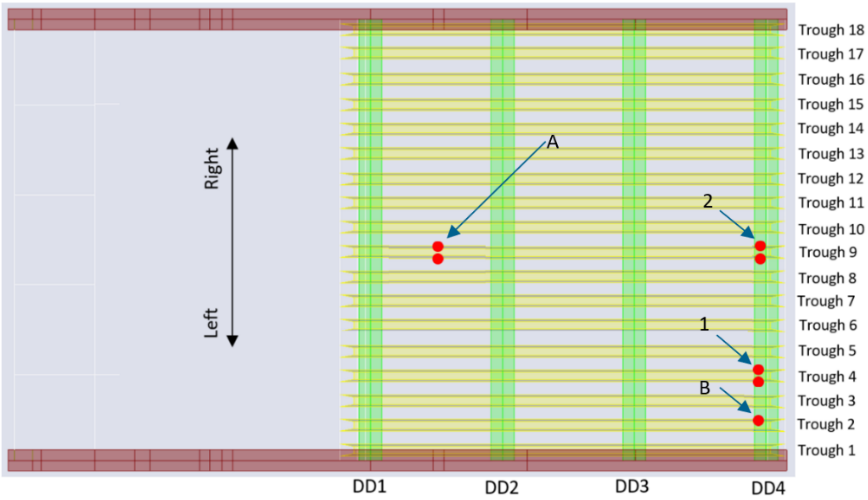

Figure 42: The four points analysed with a 2D elements SCIA model.

Both structural engineer "A" and "B" explained their choice for their expected point A and B.

Point A

As stated before, this point was chosen without the results obtained by the proposed mesh independent 1D model. The short list obtained by this structural engineer was the same as explained in Appendix V Shortlist of potential critical points. Next, the structural engineer mentioned that the fields at the ends are expected to have a higher maximum stress interval since a dynamic amplification factor has to be applied. When this argument surfaced the structural engineer was told that the new regulations (ROK [3] article 00910) state that over a distance of 6m from any expansion joint a constant dynamic amplification factor of 1.15 has to be applied. Since there is an expansion joint at both ends of the bridge and the bridge is less than 12 meter long all points have the same constant dynamic amplification that has to be applied. Thus, this factor will not have an influence[8]. However, this did not change the chosen point since the structural engineer argued that the asymmetry in support conditions might still lead to point A having the highest maximum stress interval. The structural engineer stated that the difference between the trough webs is expected to be extremely small (therefore, the difference might not be measurable). However, if a difference can be found the structural engineer expect the trough web at right side (Figure 42) to have the highest maximum stress interval.

[7] For point "B" only the right trough web could be considered since the left trough web is too close to the main girder. Resulting in not all load cases, which have to be considered according to the regulations [3], fitting on the designed bridge. In this analysis the left trough web was omitted. In real live applications this point would either be analysed using the remaining possible load combinations or be omitted due to extra applied vehicle retaining barriers (see Chapter 9.1).

[8] In the previous version of the ROK [31] was published a linear decreasing dynamic amplification factor had to be applied which would have had an influence.

B

This point was chosen by a structural engineer who was informed on the results of the proposed mesh independent 1D model. Again, the same short list of points was obtained (Appendix V Shortlist of potential critical points). After examining the results, the first thing the structural engineer started to do was trying to argue why the first interpretation method of the 1D elements model suggest a highest maximum stress interval at a point which is not on the short list. After looking at Figure 36 the structural engineer concluded that they simplification of the deck plate not being connected to the main girder but to the nearest trough (Chapter 4.5) might lead to inaccurate maximum stress intervals in the most outer 3 troughs. Therefore, the structural engineer expect that a more accurate estimation would be a further increase in the maximum stress interval when reaching the outer sides (Figure 43). Therefore, the prediction of this structural engineer was a point at the end of the bridge at the right trough web of the trough closest to the main girder (Figure 42).

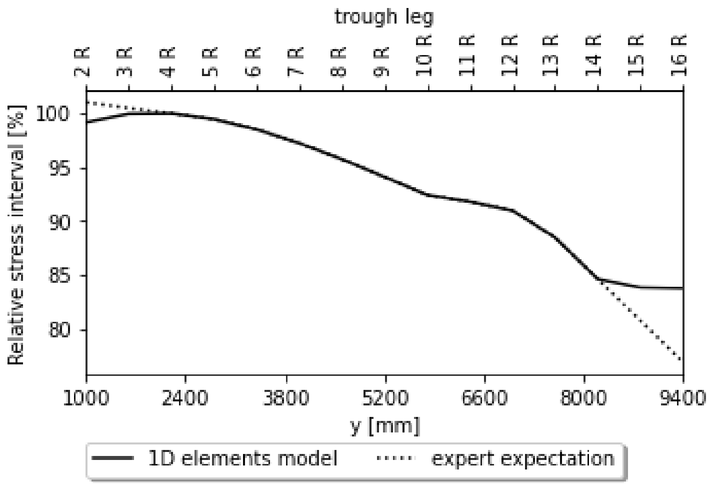

Figure 43: Results 1D elements model plus expected reality by expert at the end of the deck plate (x=9449)

7.3.2 Update 2D elements model (element thickness and mesh sizes)

The regulations [3] provide a method to model the welds and determine the stresses occurring in the welds. For the considered weld detail (Figure 2) the most relevant articles are number 00912 and 00915. Together these articles, in combination with the design of the bridge, make it possible to determine all necessary information to model the welds. As well as determine the stresses which would have to be used to determine the fatigue damage. The calculation is provided in Appendix VII Elaboration calculating maximum stress interval 2D FE model. The obtained weld model is shown in Figure 44.

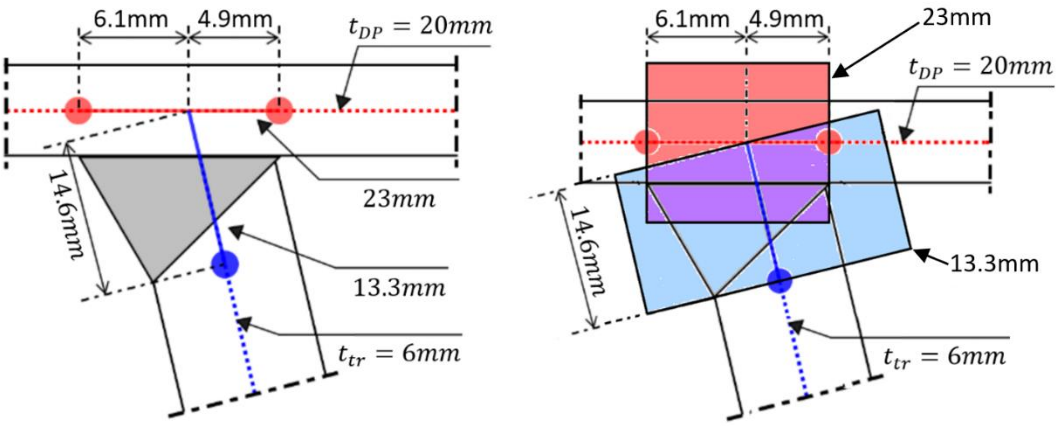

Figure 44: Detailed weld (drawing not to scale) [3]

In Figure 44 the prescribed method on how to model the weld is shown. In this the red area is the local increase in element thickness (from 20 to 23mm) in the deck plate. In blue a local increase in the element thickness (from 6 to 13.3mm) in the trough is shown.

To determine the stresses in the considered detail (Figure 2) it is not allowed to use the stresses reported by the FE model at the weld toe. Instead, the stresses have to be determined at two points (A and B) at a certain distance from the weld toe. After which the stresses at the weld toe can be determined via the application of linear interpolation (from A and B to C). To determine the location of points used for the interpolation article 00915 of the ROK [3] can be used. The obtained points are sketched in Figure 45.

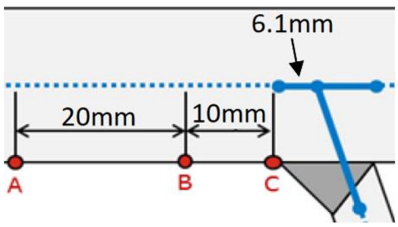

Figure 45: Interpolation points for stress determination [3]

The regulations [3] also provides the maximum allowed mesh size. This size should be smaller or equal to half the deck plate thickness. For the considered case study that results in a local mesh size of 10mm.

7.3.3 Results 2D elements SCIA model

After applying the calculation method as provided in the ROK [3], in combination with the results obtained from a FE analysis (see the database [30]) the results in Table 10 are obtained.

Table 10: Results of 2D elements SCIA model

Point			Load case	Maximum Stress interval
Name	Trough	Web	(see Figure 46)	[N/mm²][9]
A	9	Left	7 (A)	55.47
A	9	Right	13 (D)	56.00
B	2	Right	13 (D)	53.90
1	4	Left	7 (C)	63.28
1	4	Right	13 (D)	63.24
2	9	Left	7 (C)	61.76
2	9	Right	13 (B)	61.99

From the results in Table 10 some observations can be made:
- The stresses in the different webs of a trough are comparable
- Every analysed point has a maximum stress interval due to a spread location which result in only compressive stresses happening in at the analysed point. As a result of this the maximum stress interval is the result of only one truck.[10]
- The load case resulting in the maximum stress interval is always due to a truck with an axle type B having a wheel directly positioned on top of the considered trough web (Figure 46).
- Of all the considered points (Figure 42) the left side of point 1 has the highest maximum stress interval. This point is not within the points expected to contain the maximum stress interval (Appendix V Shortlist of potential critical points)

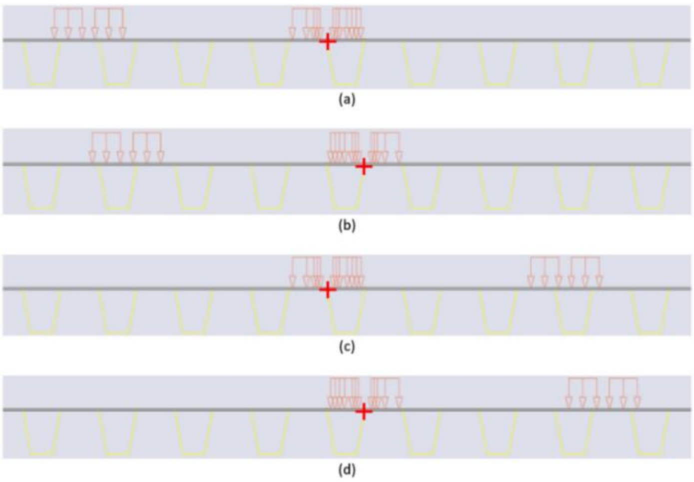

Figure 46: Different load cases. (a) the right wheel of a truck with axle type B positioned on track 7. (b) the right wheel of a truck with axle type B positioned on track 13. (c) the left wheel of a truck with axle type B positioned on track 7. (d) the left wheel of a truck with axle type B positioned on track 13. The red plus is positioned at the location which has the maximum stress during the shown load case.

[9] These result follow from the FE analysis after the dynamic amplification factor (1.15) is applied. The reduction for compressive stresses of 60% was not applied. This would not change the location of the maximum stress interval since all stresses are compressive.

[10] It can be noted that other analysed spread location sometimes had a maximum stress interval due to a combination of two different tucks. However, these are lower than the maximum stress interval of another spread location. This is unlikely to be the case for other detail categories. The ROK [3] specifically mentions detail 2a and 2b being prone the stresses in both compression and tension (article 00909).

7.4 Comparison

The 2D FE model including weld details was used to determine the maximum stress interval in a limit set of points (Figure 42). The results of the 2D FE model with weld details (Table 10) for these points can be compared with the results of the different interpretations of the 1D analytical solutions model (Figure 35 and Figure 38). In Table 11 the points for which both models have results are ordered in order from highest maximum stress interval to lower maximum stress intervals.

Table 11: Comparison of results of 2D FE model with weld details and proposed mesh independent 1D model

	2D FE model with weld details			*Proposed mesh independent 1D model*					
				Interpretation method 1			**Interpretation method 2**[11]		
	Trough	**web**	**x[mm]**	**Trough**	**web**	**x[mm]**	**Trough**	**web**	**x[mm]**
Max.	4	Left	9449	4	Right	9449	9	Right	9449
stress	4	Right	9449	2	Right	9449	9	Left	9449
interval	9	Right	9449	9	Right	9449	4	Right	9449
	9	Left	9449	9	Left	9449	4	Left	9449
Lower	9	Right	1600	9	Right	1600	2	Right	9449
stress	9	Left	1600	9	Left	1600	9	Right	1600
interval	2	Right	9449	4	Left	9449	9	Left	1600

This comparison leads to some observations.

- The proposed mesh independent 1D model predicts a highest maximum at the end of the bridge (x = 9449) which agrees with the 2D FE model with weld details.
- All models have a different point in width direction of the bridge containing the maximum stress interval
- The 2D FE model with weld details and the proposed mesh independent 1D model interpreted via method 1 have the same trough with the maximum stress interval but in a different web
- The 2D FE model with weld details and the proposed mesh independent 1D model interpreted via method 2 suggest that the difference of maximum stress interval between two trough webs is small

Since all compared models have several points in the same cross section (x=9449) a graph containing these results can be made (Figure 47).

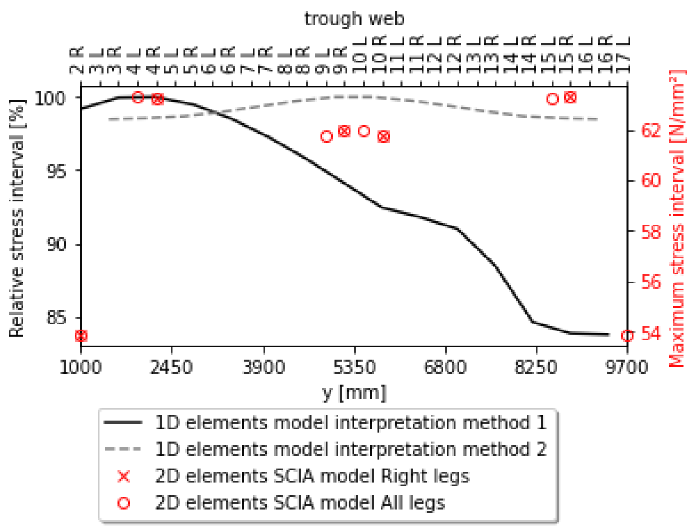

Figure 47: Maximum stress interval at x = 9449 resulting from the different models

It can be observed that all models predict a different distribution of the maximum stress intervals over this cross-section.

[11] This interpretation method (Chapter 6.2.2) cannot be applied on through 2. Thus, the result of trough 2 was obtained via extrapolation.

8 Conclusion and recommendations

In the previous chapters results are shown regarding:

- The useability of a 2D model without containing weld details (Chapter 3.6). Where the problems regarding mesh dependency of this model is shown.
- The distribution of the maximum stress interval of the 1D model interpreted in 2 different ways (Figure 35 and Figure 38). Including a comparison of these distributions with the 2D model containing weld details at the end of the bridge (Figure 47). It is observed that the distributions are dissimilar.
- The obtained location of the maximum stress interval of the 1D model interpreted in two different ways and the 2D model containing weld details (Table 11). It is observed that all three points are found in the same cross section. However, they are located at different trough webs. Two of the three points are at different legs of the same trough while the third point is several troughs away.
- The load cases resulting in the maximum stress interval at a considered point in the 2D model containing weld details (Figure 46). It is observed that the load cases (resulting in the maximum stress interval) are similar.

From these results conclusions can be drawn, and recommendations can be given. This will be done in this chapter. A discussion on these conclusions and recommendations is given in Chapter 9.

8.1 Conclusions

In this report an investigation is presented of the answer the following research question:

How can the determination of the location of the first fatigue crack in the deck, at a stiffener to deck plate weld toe, be parameterized?

From this investigation six conclusions can be drawn:

- It can be concluded that a model made from mesh independent 1D elements is unlikely to determine the location of the expected first fatigue crack in agreement with the prediction of a detailed 2D FE model.

- A traditionally used, 2D FE model not containing any weld details cannot be used. Since the found location for the first fatigue crack is highly mesh depended. As a result of this a very small mesh size is needed resulting in unpractically large computation times (with the currently available computation power).

- The results from 1D model as presented in the report predicts differences between the maximum stress intervals at the two webs of the same trough of a higher magnitude then the 2D detailed FE model.

- All models in this report predict a location of the first fatigue crack. All these predictions stated that the crack will occur in a cross section at the end of the bridge (x = 9449).

- The predictions of all models in this report suggest a point counterintuitive to the structural engineers participating in this research. Therefore, the intuition of structural engineers regarding the location of the first fatigue crack might sometimes be incorrect.

- The number of load cases considered in the 2D FE model including weld details can be reduced.

  Since this conclusion is based on a limited number of considered locations and for a single case study this conclusion has a limited degree of certainty. The higher the number of concluded irrelevant load cases the higher the degree of uncertainty. In order of increasing uncertainty, it can be concluded that:

  - In a 2D FE model containing weld details (of the case study), the maximum stress interval at a trough web-to-deck plate weld toe occurs when the spread location of a wheel of a truck is applied directly on top of the considered trough web.

  - In a 2D FE model containing weld details (of the case study). If the spread location of a wheel of truck is directly above the considered trough web, all load cases result in a compressive stress in the considered trough web-to-deck plate weld toe. Therefore, only the influence of individual truck axles has to be accounted for in the determination of the location of the maximum stress interval at a trough web-to-deck plate weld toe.

  - In a 2D FE model containing weld details (of the case study), the maximum stress in a point at a trough web-to-deck plate weld toe occurs when an axle type B (Figure 66) is placed directly on top of the considered point.

8.2 Recommendations

Based on the obtained results and related conclusion recommendations can be given. In this chapter these recommendations are split in three parts. First, recommendations are given on research into potential improvements of a 2D FE model. Secondly, recommendations are given on gaining knowledge to help explaining the differences in the results of the proposed 1D method and the 2D FE model containing weld details. Lastly, recommendations are given on the immediate use of the obtained knowledge.

8.2.1 Possible simplifications of a 2D FE model for the determination of the location of the highest maximum stress interval

To potentially reduce the computational time needed to solve the 2D FE models the following actions are recommended:

- Investigate if the number of load cases necessary to determine the maximum stress interval in a point can be reduced. This can be done by researching the following questions and their general applicability:
    - Is the maximum stress interval in every trough web always caused by a load combination occurring when the spread of a truck wheel is applied directly on top of a trough web?
    - Do all load cases, in the spread location resulting in the maximum stress interval in a trough web, cause compressive stresses?
    - Is the maximum stress always occurring if an axle type B is directly on top of the considered trough web?
    - Does the presence of a second axle (away from the analysed point) of a truck influence the location of the highest maximum stress interval?
    - Does the presence of a second wheel of an axle influence the location of the highest maximum stress interval?

- Investigate if the modelling requirements (as required by the regulations [3]) can be simplified for the determination of the location of the maximum stress interval. This can be done by investigating the following questions and their general applicability:
    - Does the addition of weld details influence the location of the highest maximum stress interval?
    - Does the omittance of the extrapolation method influence the location of the highest maximum stress interval?

  To research the two questions stated above a FE model including all the suggested simplifications can be made. The results of this FE model can be compared with the results of a FE model without the proposed simplifications. If necessary, a next set of models could be made in which a single simplification is lifted to research the influence of this specific simplification.

Independent of the results presented in this report some general recommendations on the research in improving the computation time needed to solve the system of differential equation can be given (improving FE method, researching alternative methods, or improving computational power). However, in this report the recommendations will be limited to that what is discussed in the earlier chapters of the report.

8.2.2 Research difference between 1D method and 2D FE model

To be able to further explain the differences between the obtained results of the 1D method and 2D model several recommendations into further research are recommended.

- Research if the location where the highest maximum stress interval occurs is the location where the highest fatigue damage occurs. To do this not only the maximum stress interval should be determined with a the detailed 2D FE model and regulatory method in several points. But the entire fatigue damage should be determined (with the 2D FE model including weld details as required by the regulations) in (the same) several points.

- Research the influence of the difference between load cases considered in the 1D model and the 2D model containing weld details. This can be done by performing the analysis of the 2D model only considering the load cases which are accounted for in the 1D model.

- Research the influence of the extrapolation (hot-spot) method. This can be done by determining the results of the 2D model without the extrapolation method and compare those with the results obtained with the 1D model.

- Research the influence of the inclusion of the weld details. This can be done by determining the results of the 2D model without locally increased element thickness and compare those with the results obtained with the 1D model.

  Research the influence of the difference in the way the connection between the stiffeners and the deck plate are modelled. This can be done by analysing a bridge with stiffeners with only one connection point with the deck plate (e.g. bulb strips). And comparing the difference between the 2D and 1D model of these two bridges. It is recommended to start with a single load case.

- Research if the connection of the deck plate with the main girder has an influence on the location of the maximum stress interval. This can be by connecting the deck plate strip (in the 1D method) with the main girder and compare the result of that model with the results presented in this report.

8.2.3 Recommendation until knowledge, on the determination of the location with the highest expected fatigue damage, is acquired

To be able to correctly determine the location of the first expected fatigue crack more knowledge has to be acquired. Until then, some action can be advised.

- Inform current and future structural engineer on the unreliability of intuition with regards to the location of the first fatigue crack.

- Monitor and inspect bridges carefully. Especially the welds directly below a wheel track. Since fatigue crack usually are located below a wheel track [7].

- Design bridges in such a manner that fatigue cracks are easy to repair.

9 Discussion

Some remarks can be made related to the research presented in the report. In this chapter the assumptions and simplifications in the research are being discussed as well as the conclusions.

9.1 Discussion on the assumptions and simplifications

This paragraph mentions and discusses all assumptions and simplifications in this research. The order in which these are presented here is the same as the order in which they appear throughout the report.

- It is assumed that the highest stress interval will occur at the same location as the highest fatigue damage. This is based on the double logarithmic relation between a stress interval and the fatigue damage resulting from a stress interval [10].The relation between a single stress interval and allowable number cycles is given by Figure 48.

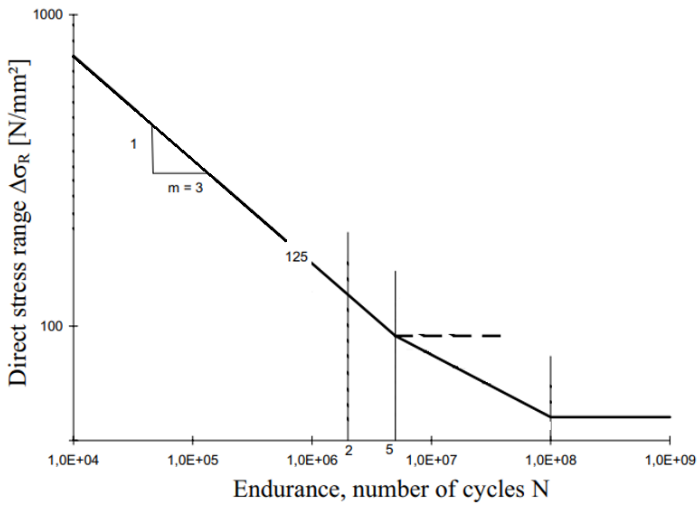

Figure 48: Relation between the size of a stress interval and the maximal allowable number of cycles [10]

It is assumed that the highest maximum stress interval would be in the part of the curve with the steepest (1/3) declination. From this part, the slope and a single point are given (Figure 48). This means that the analytical expression for this part of the curve can be determined. It can be written as a relation between the number of cycles (N) and the maximum allowable stress interval ($\Delta\sigma_R$):

$$N = \frac{2 * 10^{12}}{\Delta\sigma_R^3} \tag{10}$$

Suggesting that a small increase in the stress interval results in significant decrease in the maximal number of cycles (e.g., if the stress interval increases with 10% the maximum number of cycles decreases with 25%). However, for the determination of the fatigue damage not only the maximum stress interval has to be accounted. All the stress intervals higher than the cut-off limit need to be taken in account. As a result of this it is possible that the highest maximal stress interval occurs at a point in which the maximum fatigue damage is not found. Since the maximum observed stress interval (Table 10) is not withing the part of the curve with biggest decline, the chances this assumption being incorrect increases.

- In the determination of the useability of the traditionally used 2D plate model (Chapter 3.6) and in the investigation in the influence of cope holes and stiffener cross section (Chapter 4.6). Two discussable decisions are made:
    - The analyses were performed based on the choice of the central position of a traffic lane. While the current regulations [3] state that for each of the considered welds three positions of a wheel track should be considered. The benefit of the regulatory method is that only one point is analysed thus, mesh refinement has to be applied around only one point. The disadvantage is that more load cases need to be considered.
    - The load cases used are based on the axles of the trucks as defined by NEN 8701 [35] while Dutch regulations state that the axles presented in Figure 6 should be used.

  In this report it is assumed that these decisions have no influence on the drawn conclusions.

- Several discussable decisions are made in the design of the 1D model (Chapter 4).
    - It does not contain a ballast box. Since the ballast box is not directly connected to the bridge deck it is assumed that this choice has no influence on the location of the maximum stress interval.
    - The part of the bridge deck before the first and after the last cross beam is neglected. It is assumed that the point with the highest maximum stress interval will be found between the cross beams. And the presence of the bridge deck before the first and after the last cross beam will have no influence on the location of the highest maximum stress interval.
    - The deck plate is connected to most outer troughs instead of the main girder. Some discussion into the reason of this choice is presented in Chapter 4.5. And a recommendation on an investigation on the influence on this choice is given in Chapter 8.2.2. It is assumed that this choice has no influence on the location of the maximum stress interval. Especially since the considered case study has additional vehicle barriers (Figure 49) which were not included in this research. As a result of this the wheel track positions close to main girders can be omitted.

Figure 49: Outer vehicle retaining barriers on Goereese bridge [36]

- The 1D beam elements do not account for warping deformations. This might lead to differences between the 1D FE model and the 1D analytical solution. Which could potentially lead to change of the location of the highest maximum stress interval. However, it is assumed that the effect of warping deformations is negligible. The reasoning behind this assumption is given in Chapter 4. To check this assumption a comparison can be made of the 1D analytical method and the 1D FE model with a random load case (Figure 39 and Figure 40). It seems that the assumption was correct.

- The 1D method does not account for cope holes in the crossbeams. It was argued that this would not be a problem if all points within 5% of the found maximum would be used in the determination of the fatigue damage of the bridge (Chapter 4.6). From the results obtained of the 1D models (Figure 35 and Figure 38), the following remaining points can be obtained:

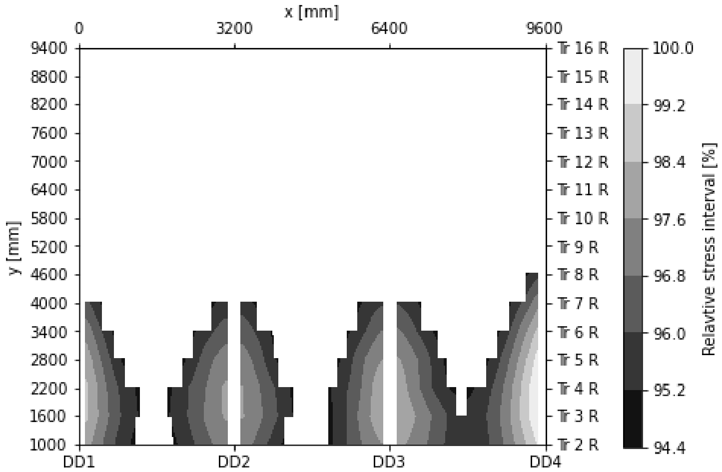

Figure 50: Results 1D model interpretation 1 for points >95%

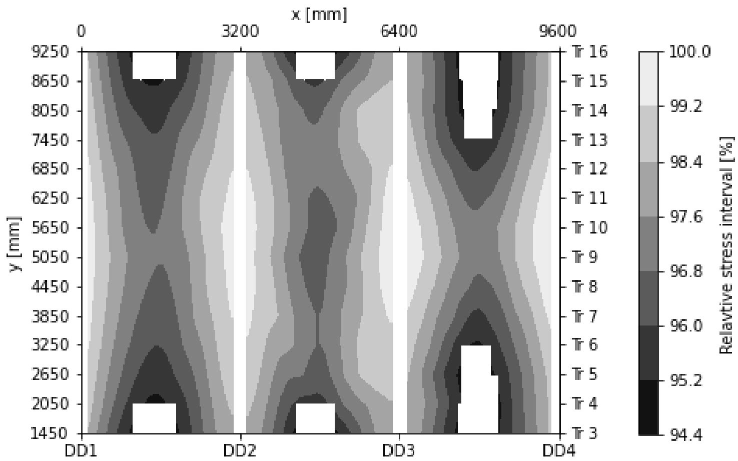

Figure 51: Results 1D model interpretation 2 >95%

From Figure 50 and Figure 51 it can be concluded that a lot of points are within 5% of the predicted maximum. Resulting in a significant amount of uncertainty regarding the point with the highest maximum stress interval.

- The 1D model is used in a limited number of points (Figure 34). The predicted maximum stress interval in the remaining points is determined via interpolation. At the interpolated points the obtained values have a degree of uncertainty. As a results of this the global highest maximum stress interval might be missed. Advanced algorithms to determine the next location for the next iteration can reduce the uncertainty [33].

- Only 4 points are used to compare with the 2D FE model (Figure 42). It can be argued that using more points leads to a better comparison.

9.2 Discussion on the conclusions

This paragraph discusses the conclusions which were made after the research was performed. It elaborates on how the conclusion can be drawn from the obtained results. It does not discuss the results themselves. Any discussion of the results can be found in Chapter 9.1. The conclusions are ordered in the way they are presented in Chapter 8.1.

- Even though the 1D model interpretated via method 1 predicts a point with the highest maximum stress interval close to the point found with the 2D model (Table 11). This similarity could be coincidental. This because Figure 47 shows that the 1D model predicts a distribution of the maximum stress intervals which is behaving unlike the results from the 2D model.

- From Table 2 it can be concluded that the 2D FE model without weld details needs a very fine mesh before the maximum stress interval can be determined without uncertainty.

- Looking at the results from the 1D model (Chapter 6.2.1) it can be concluded that a significant difference between the maximum stress interval is found between the different webs of a trough. However, in the detailed 2D FE model the results (Table 10), maximum stress intervals are shown which suggest that the maximum stress intervals between two trough webs are very similar.

- Based on the results in Table 11 it can be concluded that all models (1D with both interpretations and 2D detailed FE) suggest that the point with the highest maximum stress interval can be found at the end of the bridge (at x = 9449)

- Based on the results in Table 11 it can be concluded that all models (1D with both interpretations and 2D detailed FE) suggest that the point with the highest maximum stress interval can be found somewhere else than what is expected by structural engineers (Appendix V Shortlist of potential critical points). Therefore, it is concluded that the point with the highest maximum stress interval is counter intuitive to most structural engineers.

- In Figure 46, the load cases resulting in the maximum stress interval at the analysed points (Figure 42) are shown. This is a small number of the load cases which have to considered according to the regulations (Chapter 2.1.2). Therefore, it can be concluded that only a limited number of load cases has to be considered.

Bibliography

[1] Antea Group. B.V., „Hoe we dankzij nieuwe technologie de vervanginsopgave de baas blijven," *extraCT,* pp. 22-23, 1 April 2022.

[2] Antea Group B.V., „Hoe een kudde schapen de civiele wereld op zijn kop zet," *extraCT,* pp. 54-55, 1 April 2022.

[3] Rijkswaterstaat, „Richtlijnen Ontwerp Kunstwerken," Rijkswaterstaat, 2021.

[4] A. Simone, "Timoshenko beam theory," in *An Introduction to the Analysis of Slender Structures*, Draft ed., Delft, Zuid-Holland: Delft University of Technology, Faculty of Civil Engineering and Geosciences, Structural Mechanics Section, Computational Mechanics Group, 2011, pp. 25-27.

[5] S. P. Timoshenko, "On the correction for shear of the differential equation for transverse vibrations of prismatic bars," *Philosphical Magazine,* vol. 41, no. 245, pp. 744-746, 1921.

[6] S. P. Timoshenko, "On the transverse vibrations of bars of uniform cross-section," *Philosophical Magazine,* vol. 43, no. 253, pp. 124-131, 1922.

[7] L. Yunsheng, C. Chunlei, W. Yuanqing and P. Peng, "Stress Distribution of Orthotropic Steel Bridge Decks under Vehicle Wheel Loading," in *Nineteenth International Offshore and Polar Engineering Conference*, Osaka, 2009.

[8] X. Zhi-Gang, Y. Kentaro, Y. Samol and Z. Xiao-Ling, "Stress analyses and fatigue evaluation of rib-to deck joints in steel orthotropic decks," *International Journal of Fatigue,* vol. 30, no. 8, p. 11, 30 October 2007.

[9] M. H. Kolstein, "Fatigue Classification of Welded Joints in Orthotropic Steel Bridge Decks," M.H. Kolstein, Spijkenisse, 2007.

[10] Netherlands Standardization Institute, "Eurocode 3: Design of steel structures - Part 1-9: Fatigue," Netherlands Standardization Institute, 2012.

[11] Z. Zhiwen, Y. Tao, X. Ze, H. Yan, Y. Z. Edward and S. Xudong, "Behavior and Fatigue Performance of Details in an Orthotropic Steel Bridge with UHPC-Deck Plate Composite System under In-Service Traffic Flows," *Journal of Bridge Engineering,* vol. 23, no. 3, p. 21, 1 March 2018.

[12] H. W. Van der Laan, "Repository TU Delft," 9 July 2021. [Online]. Available: https://repository.tudelft.nl/islandora/object/uuid%3A29f4a730-500f-47e4-863b-a1765f1e9e02. [Accessed 22 Februari 2023].

[13] J. Schijve, Fatigue of Structures and Materials, Second Edition ed., Delft, Zuid-Holland: Springer, 2008, p. 627.

[14] D. J. van der Ende, "A state of art review on advanced modelling techniques for weld in structural steel," Delft University of Technology, Brielle, 2020.

[15] S. Pandit, "Finite element modelling of open longitudinal stiffener to crossbeam connection in OSD bridges for hot-spot stress determination," Delft University of Technology, Delft, 2020.

[16] Royal Netherlands Standardization Institute, "National Annex to NEN-EN 1991-2+C1: Eurocode 1: Actions on structures - Part2: Traffic loads on bridges," Royal Netherlands Standardization Institute, 2019.

[17] Stichting Koninklijk Nederlands Normalisatie Instituut, "Assessment of existing structures in case of reconstruction and disapproval - Actions," Stichting Koninklijk Nederlands Normalisatie Instituut, 2020.

[18] A. F. Hobbacher, Recommendations for Fatigue Design of Welded Joints and Components, 2 ed., C. Mayer, Ed., Wilhelmshaven: Springer, 2014, p. 19.

[19] J. F. Doyle, Static and Dynamic Analysis of Structures with An Emphasis on Mechanics and Computer Matrix Methods, West Lafayette: Springer, 1991.

[20] A. R. Hadjesfandiari, A. Hajesfandiari, H. Zhang and G. F. Dargush, “arxiv,” 20 December 2017. [Online]. Available: https://arxiv.org/abs/1712.08527. [Accessed 12 April 2023].

[21] J. P. Den Hartog, Strength of Material, New York: Dover Publications, 1968.

[22] E. P. Popov, Introduction to mechanics of solids, Berkeley: London: Macdonald & Co., 1968.

[23] P. C. J. Hoogenboom, “7 Vlasov torsion theory,” 2006.

[24] P. C. Hoogenboom and A. Borgart, “Method for including restrained warping in traditional frame analyses,” *HERON.,* vol. 50, no. 1, 2005.

[25] J. Blaauwendraad, Plate analysis, theory and application, vol. 1, 2006.

[26] M. A. N. Hendriks, *Plates loaded in their plane,* Delft, Zuid-Holland, 2017, p. 39.

[27] P. C. J. Hoogendoorn, *Thick slabs,* Delft, Zuid-Holland, 2017.

[28] P. C. J. Hoogendoorn, *Isotropic thick slabs,* Delft, Zuid-Holland, 2017, p. 39.

[29] G. N. Wells, “The Finite Element Method: An Introduction,” 2020, p. 125.

[30] C. Stellinga, “Database containing FE models,” 14 April 2023. [Online]. Available: https://doi.org/10.4121/eaa8ceb3-77cc-452b-b2f2-2796ba33e5ab.

[31] SCIA, “Analysis of a haunch versus mesh size,” SCIA, [Online]. Available: https://help.scia.net/22.0/en/analysis/calculation/analysis_of_a_haunch_versus_mesh_size.htm. [Accessed 16 March 2023].

[32] S. P. Timoshenko, “Theory of bending, torsion and buckling of thin-walled members of open cross section.,” *Journal of the Franklin Insitute,* vol. 239, no. 3, pp. 201-219, March 1945.

[33] A. Cicirello and F. Giunta, “arxiv,” 21 June 2021. [Online]. Available: https://arxiv.org/abs/2106.11215. [Accessed 22 Februari 2023].

[34] C. Vuik, F. J. Vermolen, M. B. Van Gijzen and M. J. Vuik, “Interplation,” in *Numerical Methods for Ordinary Differential Equations*, Delft, VSSD, 2015, p. 125.

[35] Netherlands Standardization Institute, “Eurocode 1: Actions on structures - Part 2: Traffic loads on bridges,” Netherlands Standardiztion Institute, 2015.

[36] Flakkee Nieuws, “Nieuwe brudgedelen voor Goereese brug,” FlakkeeNieuws, 30 October 2012. [Online]. Available: https://flakkeenieuws.nl/nieuws/nieuwe-brugdelen-voor-goereese-brug/5580. [Accessed 20 March 2023].

[37] C. Hartsuijker and J. W. Welleman, “Engineering Mechanics; Volume 2: Stresses, Strains, Displacements,” Springer, Delft, 2007.

[38] Rijkswaterstaat, “Richtlijnen Onterp Kunsterken ROK 1.4,” RWS GPO, 2017.

Appendix I Derivation system of differential equations of a Timoshenko beam element

In a 3D space including normal deformations

Appendix I Derivation system of differential equations of a Timoshenko beam element

A 1D Timoshenko beam element is a 1D shaped element in which it is assumed that the cross section remains plain. The cross section rotates and translates around the neutral axis of the beam. The sign conventions are shown in Figure 52. The external forces are considered positive if they are in the same direction as the axis.

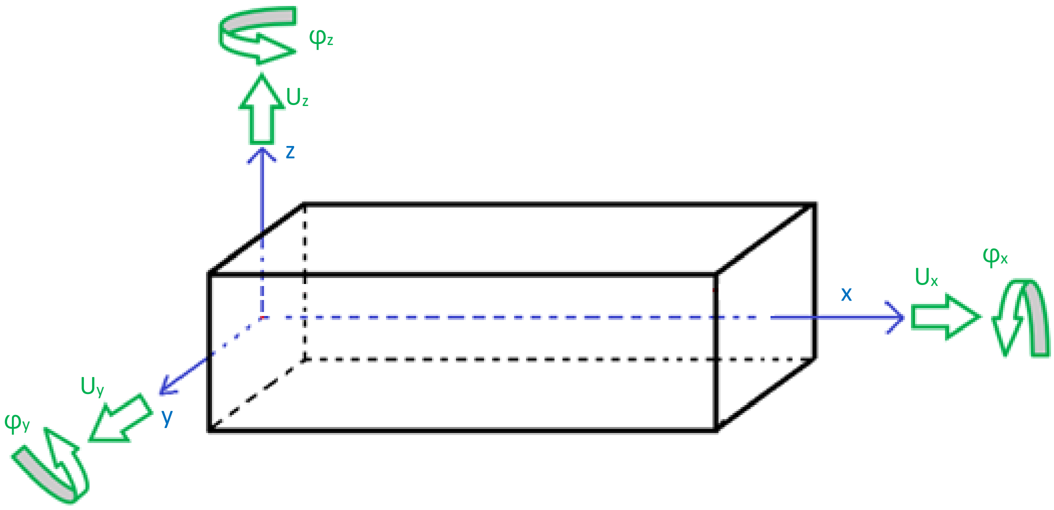

Figure 52: Sign conventions

The displacement of all points in the cross section can be expressed in the displacement of the neutral axis as:

$$S_x(x,y,z) = U_x(x) - z\varphi_y(x) + y\varphi_z(x)$$
$$S_y(x,z) = U_y(x) + z\varphi_x(x)$$
$$S_z(x,y) = U_z(x) - y\varphi_x(x)$$

The strains can be determined by taking the different derivatives in space.

$$\varepsilon_{xx}(x,y,z) = \frac{\partial S_x}{\partial x} \ ; \ \gamma_{xy}(x,z) = \frac{\partial S_x}{\partial y} + \frac{\partial S_y}{\partial x} \ ; \ \gamma_{xz}(x,y) = \frac{\partial S_x}{\partial z} + \frac{\partial S_z}{\partial x}$$

The stresses can be determined using Hooke's law.

$$\sigma_{xx}(x,y,z) = E\varepsilon_{xx} \ ; \ \tau_{xy}(x,z) = G\gamma_{xy} \ ; \ \tau_{xz}(x,y) = G\gamma_{xz} \tag{8}$$

The normal force in the cross section can be determined by taking the integral of the normal stress over the surface of the cross section. For the shear forces take the integral over the corresponding shear area. It is assumed that the material properties are constant in space. The internal moment can be determined by taking the integral over the surface of the equivalent stress multiplied with the corresponding arm.

$$N_x(x) = \oiint_{A(x)} \sigma_{xx} dA \ ; \ V_y(x) = \oiint_{A_{sy}(x)} \tau_{xy} dA \ ; \ V_z(x) = \oiint_{A_{sz}(x)} \tau_{xz} dA \tag{9}$$

$$M_x(x) = \oiint_{A_{sy}(x)\cap A_{sz}(x)} z\tau_{xy} - y\tau_{xz} dA \ ; \ M_y(x) = \oiint_{A(x)} -z\sigma_{xx} dA \ ; \ M_z(x) = \oiint_{A(x)} y\sigma_{xx} dA \tag{10}$$

By choosing the coordinate system in the neutral axis of the element and substituting (8) in (10) and (10) these expressions can be simplified to:

$$N_x(x) = EA(x)\frac{dU_x}{dx}\ ;\ V_y(x) = GA_{sy}(x)\left(\frac{dU_y}{dx} + \varphi_z(x)\right) \tag{11A}$$

$$V_z(x) = GA_{sz}(x)\left(\frac{dU_z}{dx} - \varphi_y(x)\right) \tag{11B}$$

$$M_x(x) = G\oiint_{A_{sy}(x)\cap A_{sz}(x)}(y^2 + z^2)dA\frac{d\varphi_x}{dx}\ ;\ M_y(x) = E\oiint_{A(x)}z^2dA\frac{d\varphi_y}{dx} \tag{12A}$$

$$M_z(x) = E\oiint_{A(x)}y^2dA\frac{d\varphi_z}{dx} \tag{12B}$$

The definitions of the moments of inertia (1313) can be substituted in these expressions (12). Leading to the following results.

$$I_y(x) = \oiint_{A(x)}z^2dA\ ; I_z(x) = \oiint_{A(x)}y^2dA\ ; I_t(x) = \oiint_{A_{sy}(x)\cap A_{sz}(x)}(y^2 + z^2)dA \tag{13}$$

$$M_x(x) = GI_t(x)\frac{d\varphi_x}{dx}\ ;\ M_y(x) = EI_y(x)\frac{d\varphi_y}{dx}\ ;\ M_z(x) = EI_z(x)\frac{d\varphi_z}{dx} \tag{14}$$

The next step is to determine the equilibrium equations. Here it is assumed that the applied load is constant over a distance dx and that second order terms can be neglected. To understand the equations describing the equilibrium equations sketches are added

Table 12: Equilibrium equations

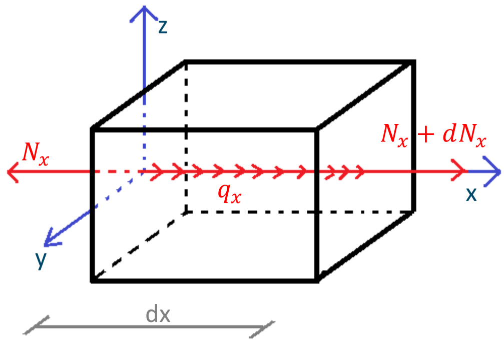

Translation equilibrium in x direction

$$\frac{dN_x}{dx} = -q_x$$

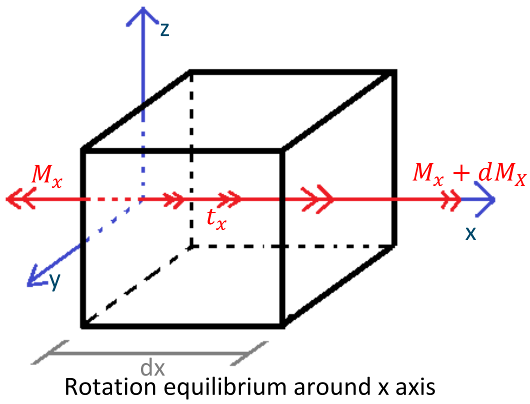

Rotation equilibrium around x axis

$$\frac{dM_x}{dx} = -t_x$$

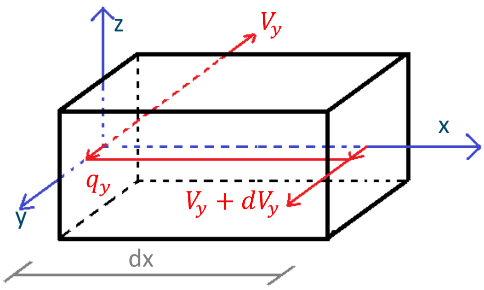

Translation equilibrium in y direction

$$\frac{dV_y}{dx} = -q_y$$

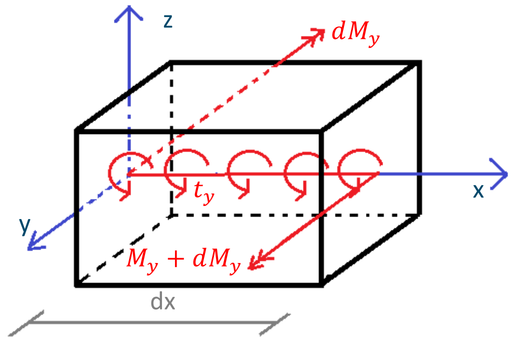

Rotation equilibrium around y axis

$$\frac{dM_y}{dx} + V_z = -t_y$$

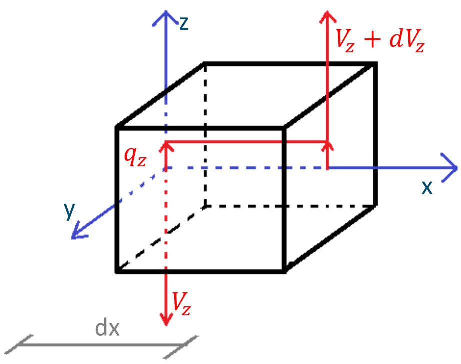

Translation equilibrium in y direction

$$\frac{dV_z}{dx} = -q_z$$

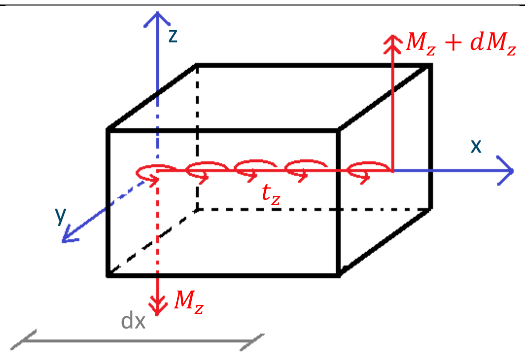

Rotation equilibrium around z axis

$$\frac{dM_z}{dx} - V_y = -t_z$$

The total set of equilibrium equations are:

$$\frac{dN_x}{dx} = -q_x \; ; \; \frac{dV_y}{dx} = -q_y \; ; \; \frac{dV_z}{dx} = -q_z \; ; \; \frac{dM_x}{dx} = -t_x \; ; \; \frac{dM_y}{dx} + V_z = -t_y \; \frac{dM_z}{dx} - V_y = -t_z \tag{15}$$

By substitution of (11) and (14) into (15) the following system of differential equations is obtained:

$$E\frac{d}{dx}\left(A(x)\frac{dU_x}{dx}\right) = -q_x$$

$$G\frac{d}{dx}\left(A_{sy}(x)\left(\frac{dU_y}{dx} + \varphi_z(x)\right)\right) = -q_y$$

$$G\frac{d}{dx}\left(A_{sz}(x)\left(\frac{dU_z}{dx} - \varphi_y(x)\right)\right) = -q_z$$

$$G\frac{d}{dx}\left(I_t(x)\frac{d\varphi_x}{dx}\right) = -t_x$$

$$GA_{sz}(x)\frac{dU_z}{dx} + E\frac{d}{dx}\left(I_y(x)\frac{d\varphi_y}{dx}\right) - GA_{sz}(x)\varphi_y(x) = -t_y$$

$$GA_{sy}(x)\frac{dU_y}{dx} - E\frac{d}{dx}\left(I_z(x)\frac{d\varphi_z}{dx}\right) + GA_{sy}(x)\varphi_z(x) = t_z$$

Or the following matrices and vector can be introduced:

$$\boldsymbol{K}_{shear}(x) = G\begin{bmatrix} A_{sy} & 0 \\ 0 & A_{sz} \end{bmatrix} ; \boldsymbol{K}_{bend}(x) = E\begin{bmatrix} I_y & 0 \\ 0 & -I_z \end{bmatrix} ; \boldsymbol{T}_{(1)} = \begin{bmatrix} 0 & 1 \\ -1 & 0 \end{bmatrix} ; \boldsymbol{T}_{(2)} = \begin{bmatrix} 0 & 1 \\ 1 & 0 \end{bmatrix}$$

$$\boldsymbol{K}_{(1)}(x) = \begin{bmatrix} EA & 0 \quad 0 & 0 & 0 \quad 0 \\ \begin{matrix} 0 \\ 0 \end{matrix} & \boldsymbol{K}_{shear} & \begin{matrix} 0 \\ 0 \end{matrix} & \begin{matrix} 0 \quad 0 \\ 0 \quad 0 \end{matrix} \\ 0 & 0 \quad 0 & GI_t & 0 \quad 0 \\ \begin{matrix} 0 \\ 0 \end{matrix} & \begin{matrix} 0 \quad 0 \\ 0 \quad 0 \end{matrix} & \begin{matrix} 0 \\ 0 \end{matrix} & \boldsymbol{K}_{bend} \end{bmatrix} ; \boldsymbol{K}_{(2)}(x) = \begin{bmatrix} E\frac{dA}{dx} & 0 \quad 0 & 0 & 0 \quad 0 \\ \begin{matrix} 0 \\ 0 \end{matrix} & \frac{d}{dx}\boldsymbol{K}_{shear} & \begin{matrix} 0 \\ 0 \end{matrix} & \boldsymbol{K}_{shear}\boldsymbol{T}_{(1)} \\ 0 & 0 \quad 0 & G\frac{dI_t}{dx} & 0 \quad 0 \\ \begin{matrix} 0 \\ 0 \end{matrix} & \boldsymbol{T}_{(2)}\boldsymbol{K}_{shear} & \begin{matrix} 0 \\ 0 \end{matrix} & \frac{d}{dx}\boldsymbol{K}_{bend} \end{bmatrix}$$

$$\boldsymbol{K}_{(3)}(x) = \begin{bmatrix} 0 & 0 & 0 & 0 & 0 \quad 0 \\ \begin{matrix} 0 \\ 0 \end{matrix} & \begin{matrix} 0 \\ 0 \end{matrix} & \begin{matrix} 0 \\ 0 \end{matrix} & \begin{matrix} 0 \\ 0 \end{matrix} & \frac{d}{dx}\boldsymbol{K}_{shear}\boldsymbol{T}_{(1)} \\ 0 & 0 & 0 & 0 & 0 \quad 0 \\ \begin{matrix} 0 \\ 0 \end{matrix} & \begin{matrix} 0 \\ 0 \end{matrix} & \begin{matrix} 0 \\ 0 \end{matrix} & \begin{matrix} 0 \\ 0 \end{matrix} & \boldsymbol{T}_{(2)}\boldsymbol{K}_{shear}\boldsymbol{T}_{(1)} \end{bmatrix} ; \; \boldsymbol{u}(x) = \begin{bmatrix} U_x \\ U_y \\ U_z \\ \varphi_x \\ \varphi_y \\ \varphi_z \end{bmatrix} ; \; \boldsymbol{q} = \begin{bmatrix} -q_x \\ -q_y \\ -q_z \\ -t_x \\ -t_y \\ t_z \end{bmatrix}$$

Such that the system of differential equation describing the physics of a 1D Timoshenko beam element can be written as:

$$\boldsymbol{K}_{(1)}\frac{d^2}{dx^2}\boldsymbol{u} + \boldsymbol{K}_{(2)}\frac{d}{dx}\boldsymbol{u} + \boldsymbol{K}_{(3)}\boldsymbol{u} = \boldsymbol{q}$$

Appendix II Solution main beam with constant cross section properties

Appendix II Solution main beam with constant cross section properties

The main girder as described in figure Figure 33 has seven elements all having six degrees of freedom. Each of these elements has the solution given as (3). This solution contains 12 unknown integration constants each. Leading to a total 84 unknowns which can be solved using 84 equations. At the six interfaces (at Support 1, Support 2, DD1, DD2, DD3 and DD4) we have 12 interface conditions as described in Chapter 5.4. At the start and the end of the beam we have another six boundary conditions leading to a total of 84 equations. To be able to formulate and understand the equations some conventions need to be established. The coordinate system (of all the elements) will be set at the start of the beam. In the subscript of the x coordinate the information of the location is contained. The superscript used refers to the element number, numbering starts with 1 from the start of the main girder. The following boundary conditions can be formulated[12]:

	Boundary conditions	Interface conditions		
	Neuman conditions	Dirichlet conditions		Neumann / Equilibrium conditions
Location	-	Continuity conditions	Support conditions	
x_{start}	$\boldsymbol{f}_{int}^{(1)} = \mathbf{0}$	-	-	
$x_{Support\ 1}$	-	$\boldsymbol{u}^{(1)} = \boldsymbol{u}^{(2)}$	$u_z^{(1)} = 0$	$\boldsymbol{f}_{int}^{(1)} - \boldsymbol{f}_{int}^{(2)} = \begin{bmatrix} 0 \\ 0 \\ V_z^{(1)} - V_z^{(2)} \\ 0 \\ 0 \\ 0 \end{bmatrix}$
$x_{Support\ 2}$	-	$\boldsymbol{u}^{(2)} = \boldsymbol{u}^{(3)}$	$\boldsymbol{u}^{(2)} = \begin{bmatrix} 0 \\ 0 \\ 0 \\ 0 \\ \varphi_y^{(2)} \\ 0 \end{bmatrix}$	$M_y^{(2)} - M_y^{(3)} = 0$
x_{DD1}	-	$\boldsymbol{u}^{(3)} = \boldsymbol{u}^{(4)}$	-	$\boldsymbol{f}_{int}^{(3)} - \boldsymbol{f}_{int}^{(4)} = \boldsymbol{p}_{(DD1)}$
x_{DD2}	-	$\boldsymbol{u}^{(4)} = \boldsymbol{u}^{(5)}$	-	$\boldsymbol{f}_{int}^{(4)} - \boldsymbol{f}_{int}^{(5)} = \boldsymbol{p}_{(DD2)}$
x_{DD3}	-	$\boldsymbol{u}^{(5)} = \boldsymbol{u}^{(6)}$	-	$\boldsymbol{f}_{int}^{(5)} - \boldsymbol{f}_{int}^{(6)} = \boldsymbol{p}_{(DD3)}$
x_{DD4}	-	$\boldsymbol{u}^{(6)} = \boldsymbol{u}^{(7)}$	-	$\boldsymbol{f}_{int}^{(6)} - \boldsymbol{f}_{int}^{(7)} = \boldsymbol{p}_{(DD4)}$
x_{End}	$\boldsymbol{f}_{int}^{(7)} = \mathbf{0}$	-	-	-

Substitution of (11), (14) and (3) in these conditions results in system of 84 equations with 84 unknowns. This system can be solved after which the integration constants can be substituted in the general solution (3). From this point on the superscript refers to the considered cross beam. The displacement at the cross beams are:

[12] Same variables and names are used as in earlier appendices. And a vector containing the applied forces p is introduced $\boldsymbol{p} = [P_x \quad P_y \quad P_z \quad T_x \quad T_y \quad T_z]^T$

Solution of cross beam at location i

We introduce the following vectors:

$$\boldsymbol{u}^{(i)} = \begin{bmatrix} u_x^{(i)} & u_y^{(i)} & u_z^{(i)} & \varphi_x^{(i)} & \varphi_y^{(i)} & \varphi_z^{(i)} \end{bmatrix}^T ; \boldsymbol{k}_{norm}^{(i)} = \frac{x_{(i)} - x_{Support2}}{EA} \begin{bmatrix} 1 \\ 1 \\ 1 \\ 1 \end{bmatrix}$$

$$\boldsymbol{k}_{2bend}^{(i)} = \frac{\left(x_{(i)} - x_{Support2}\right)^2}{6EI_z} \begin{bmatrix} 3x_{DD1} - x_{(i)} - 2x_{Support2} \\ 3x_{DD2} - x_{(i)} - 2x_{Support2} \\ 3x_{DD3} - x_{(i)} - 2x_{Support2} \\ 3x_{DD4} - x_{(i)} - 2x_{Support2} \end{bmatrix} ; \ \boldsymbol{k}_{2shear}^{(i)} = \frac{x_{(i)} - x_{Support2}}{GA_{sy}} \begin{bmatrix} 1 \\ 1 \\ 1 \\ 1 \end{bmatrix}$$

$$\boldsymbol{k}_{3bend}^{(i)} = -\frac{x_{(i)} - x_{Support2}}{2EI_z} \begin{bmatrix} 2x_{DD1} - x_{(i)} - x_{Support2} \\ 2x_{DD2} - x_{(i)} - x_{Support2} \\ 2x_{DD3} - x_{(i)} - x_{Support2} \\ 2x_{DD4} - x_{(i)} - x_{Support2} \end{bmatrix}$$

$$\boldsymbol{k}_{4bend}^{(i)} = \frac{x_{(i)} - x_{Support2}}{6EI_y} \begin{bmatrix} x_{(i)}\left(3x_{DD1} - x_{(i)}\right) - \left(x_{DD1} + x_{(i)} - 2x_{Support1}\right)x_{Support2} - 2x_{DD1}x_{Support1} \\ x_{(i)}\left(3x_{DD2} - x_{(i)}\right) - \left(x_{DD2} + x_{(i)} - 2x_{Support1}\right)x_{Support2} - 2x_{DD2}x_{Support1} \\ x_{(i)}\left(3x_{DD3} - x_{(i)}\right) - \left(x_{DD3} + x_{(i)} - 2x_{Support1}\right)x_{Support2} - 2x_{DD3}x_{Support1} \\ x_{(i)}\left(3x_{DD4} - x_{(i)}\right) - \left(x_{DD4} + x_{(i)} - 2x_{Support1}\right)x_{Support2} - 2x_{DD4}x_{Support1} \end{bmatrix}$$

$$\boldsymbol{k}_{4shear}^{(i)} = \frac{x_{(i)} - x_{Support2}}{GA_{sz}\left(x_{Support2} - x_{Support1}\right)} \begin{bmatrix} x_{DD1} - x_{Support2} \\ x_{DD2} - x_{Support2} \\ x_{DD3} - x_{Support2} \\ x_{DD4} - x_{Support2} \end{bmatrix}$$

$$\boldsymbol{k}_{5bend}^{(i)} = \frac{1}{6EI_y} \begin{bmatrix} 2x_{DD1}\left(3x_{(i)} - 2x_{Support2} - x_{Support1}\right) - 3x_{(i)}^2 + x_{Support2}^2 + 2x_{Support2}x_{Support1} \\ 2x_{DD2}\left(3x_{(i)} - 2x_{Support2} - x_{Support1}\right) - 3x_{(i)}^2 + x_{Support2}^2 + 2x_{Support2}x_{Support1} \\ 2x_{DD3}\left(3x_{(i)} - 2x_{Support2} - x_{Support1}\right) - 3x_{(i)}^2 + x_{Support2}^2 + 2x_{Support2}x_{Support1} \\ 2x_{DD4}\left(3x_{(i)} - 2x_{Support2} - x_{Support1}\right) - 3x_{(i)}^2 + x_{Support2}^2 + 2x_{Support2}x_{Support1} \end{bmatrix}$$

$$\boldsymbol{k}_{5shear} = \frac{1}{GA_{sz}\left(x_{Support2} - x_{Support1}\right)} \begin{bmatrix} x_{DD1} - x_{Support2} \\ x_{DD2} - x_{Support2} \\ x_{DD3} - x_{Support2} \\ x_{DD4} - x_{Support2} \end{bmatrix} ; \ \boldsymbol{k}_{tors}^{(i)} = \frac{x_{(i)} - x_{Support2}}{GI_t} \begin{bmatrix} 1 \\ 1 \\ 1 \\ 1 \end{bmatrix}$$

$$\boldsymbol{k}_{7bend}^{(i)} = \frac{\left(3x_{(i)} - x_{Support2} - 2x_{Support1}\right)\left(x_{(i)} - x_{Support2}\right)}{6EI_y} \begin{bmatrix} 1 \\ 1 \\ 1 \\ 1 \end{bmatrix}$$

$$\boldsymbol{k}_{7shear}^{(i)} = \frac{x_{(i)} - x_{Support2}}{GA_{sz}\left(x_{Support2} - x_{Support1}\right)} \begin{bmatrix} 1 \\ 1 \\ 1 \\ 1 \end{bmatrix} ; \ \boldsymbol{k}_{8bend}^{(i)} = \frac{3x_{(i)} - 2x_{Support2} - x_{Support1}}{3EI_y} \begin{bmatrix} 1 \\ 1 \\ 1 \\ 1 \end{bmatrix}$$

$$\boldsymbol{k}_{8shear} = \frac{1}{GA_{sz}\left(x_{Support2} - x_{Support1}\right)} \begin{bmatrix} 1 \\ 1 \\ 1 \\ 1 \end{bmatrix} ; \ \boldsymbol{k}_{9bend}^{(i)} = -\frac{\left(x_{(i)} - x_{Support2}\right)^2}{2EI_z} \begin{bmatrix} 1 \\ 1 \\ 1 \\ 1 \end{bmatrix}$$

$$\boldsymbol{k}_{10bend}^{(i)} = \frac{x_{(i)} - x_{Support2}}{EI_z} \begin{bmatrix} 1 \\ 1 \\ 1 \\ 1 \end{bmatrix}$$

$$\boldsymbol{p}_x = \begin{bmatrix} P_{xDD1} \\ P_{xDD2} \\ P_{xDD3} \\ P_{xDD4} \end{bmatrix} ; \boldsymbol{p}_y = \begin{bmatrix} P_{yDD1} \\ P_{yDD2} \\ P_{yDD3} \\ P_{yDD4} \end{bmatrix} ; \boldsymbol{p}_z = \begin{bmatrix} P_{zDD1} \\ P_{zDD2} \\ P_{zDD3} \\ P_{zDD4} \end{bmatrix} ; \boldsymbol{t}_x = \begin{bmatrix} T_{xDD1} \\ T_{xDD2} \\ T_{xDD3} \\ T_{xDD4} \end{bmatrix} ; \boldsymbol{t}_y = \begin{bmatrix} T_{yDD1} \\ T_{yDD2} \\ T_{yDD3} \\ T_{yDD4} \end{bmatrix} ; \boldsymbol{t}_z = \begin{bmatrix} T_{zDD1} \\ T_{zDD2} \\ T_{zDD3} \\ T_{zDD4} \end{bmatrix}$$

Now we can write the solutions as:

$$
\boldsymbol{u}^{(i)} = \begin{bmatrix}
\boldsymbol{k}_{norm}^{(i)} & \boldsymbol{0} & \boldsymbol{0} & \boldsymbol{0} & \boldsymbol{0} & \boldsymbol{0} \\
\boldsymbol{0} & \boldsymbol{k}_{2bend}^{(i)} + \boldsymbol{k}_{2shear}^{(i)} & \boldsymbol{0} & \boldsymbol{0} & \boldsymbol{0} & \boldsymbol{k}_{3bend}^{(i)} \\
\boldsymbol{0} & \boldsymbol{0} & \boldsymbol{k}_{4bend}^{(i)} + \boldsymbol{k}_{4shear}^{(i)} & \boldsymbol{0} & \boldsymbol{k}_{5bend}^{(i)} + \boldsymbol{k}_{5shear} & \boldsymbol{0} \\
\boldsymbol{0} & \boldsymbol{0} & \boldsymbol{0} & \boldsymbol{k}_{tors}^{(i)} & \boldsymbol{0} & \boldsymbol{0} \\
\boldsymbol{0} & \boldsymbol{0} & \boldsymbol{k}_{7bend}^{(i)} + \boldsymbol{k}_{7shear}^{(i)} & \boldsymbol{0} & \boldsymbol{k}_{8bend}^{(i)} + \boldsymbol{k}_{8shear} & \boldsymbol{0} \\
\boldsymbol{0} & \boldsymbol{k}_{9bend}^{(i)} & \boldsymbol{0} & \boldsymbol{0} & \boldsymbol{0} & \boldsymbol{k}_{10bend}^{(i)}
\end{bmatrix}^T \begin{bmatrix} \boldsymbol{p}_x \\ \boldsymbol{p}_y \\ \boldsymbol{p}_z \\ \boldsymbol{t}_x \\ \boldsymbol{t}_y \\ \boldsymbol{t}_z \end{bmatrix}
$$

Which can be simplified to:

$$
\boldsymbol{u}^{(i)} = \boldsymbol{K}^{(i)}(A, A_{sy}, A_{sz}, E, G, I_t, I_y, I_z, x_{Support1}, x_{Support2}, x_{DD1}, x_{DD2}, x_{DD3}, x_{DD4}, x_{(i)})\boldsymbol{p}
$$

Appendix III FE analysis main girder with variable cross section

Appendix III FE analysis main girder with variable cross section

SCIA ENGINEER	Project: Thesis Coen Stellinga	Auteur: Coen Stellinga	
	Onderdeel: Nonlinear main girder	Datum: 01. 06. 2022	

1. Layers

Naam	enkel Constructiemodel	Kleur
Hoofd	x	
DD	x	

2. Cross sections

Hoofd1_Dun1		
Type	Grafische doorsnede	
Onderdeelmateriaal	S355	
Bouwwijze	Algemeen	
Knik y-y, Knik z-z	d	d
A [mm^2]	70399,9999999999	
A_y [mm^2], A_z [mm^2]	34803,1997990195	32889,5812380470
I_y [mm^4], I_z [mm^4]	39532572666,6661758423	792541466,6666566133
$W_{el.y}$ [mm^3], $W_{el.z}$ [mm^3]	43016945,2303222045	3170165,8666666220
$W_{pl.y}$ [mm^3], $W_{pl.z}$ [mm^3]	48780000,0000001118	4895799,9999999823
I_w [mm^6], I_t [mm^4]	641249999999999,8750000000	21789866,6666704677
d_y [mm], d_z [mm]	0	0
$c_{Y.UCS}$ [mm], $c_{Z.UCS}$ [mm]	250	900
α [deg]	0,00	
$M_{pl.y.+}$ [Nmm], $M_{pl.y.-}$ [Nmm]	17316900000,0000419617	17316900000,0000495911
$M_{pl.z.+}$ [Nmm], $M_{pl.z.-}$ [Nmm]	1738008999,9999938011	1738008999,9999945164
A_L [mm^2/m], A_D [mm^2/m]	5640000,0000000009	5640000,0000000009

Picture

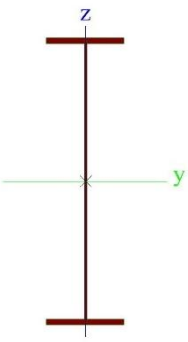

Hoofd2_Dun1		
Type	Grafische doorsnede	
Onderdeelmateriaal	S355	
Bouwwijze	Algemeen	
Knik y-y, Knik z-z	d	d
A [mm^2]	80228,0000000001	
A_y [mm^2], A_z [mm^2]	34870,4582185199	42946,6936845624
I_y [mm^4], I_z [mm^4]	71657451270,6669769287	792806822,6666648388
$W_{el.y}$ [mm^3], $W_{el.z}$ [mm^3]	60115311,4686802030	3171227,2906666561
$W_{pl.y}$ [mm^3], $W_{pl.z}$ [mm^3]	69340722,0000002086	4940025,9999999888
I_w [mm^6], I_t [mm^4]	1089277124999999,7500000000	22851290,6666716188
d_y [mm], d_z [mm]	0	0
$c_{Y.UCS}$ [mm], $c_{Z.UCS}$ [mm]	250	1173
α [deg]	0,00	
$M_{pl.y.+}$ [Nmm], $M_{pl.y.-}$ [Nmm]	24615956310,0000839233	24615956310,0000686646
$M_{pl.z.+}$ [Nmm], $M_{pl.z.-}$ [Nmm]	1753709230,0000090599	1753709229,9999959469
A_L [mm^2/m], A_D [mm^2/m]	6732000,0000000009	6732000,0000000009

Picture

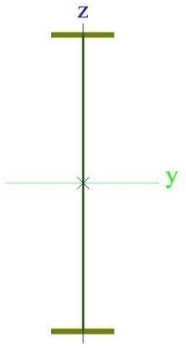

Hoofd3A_Dun1		
Type	Grafische doorsnede	
Onderdeelmateriaal	S355	
Bouwwijze	Algemeen	
Knik y-y, Knik z-z	d	d
A [mm^2]	97238,0000000002	
A_y [mm^2], A_z [mm^2]	34953,6570794996	59902,3570725706
I_y [mm^4], I_z [mm^4]	156361698923,1693115234	793266092,6666659117
$W_{el.y}$ [mm^3], $W_{el.z}$ [mm^3]	93939140,2362085432	3173064,3706666613
$W_{pl.y}$ [mm^3], $W_{pl.z}$ [mm^3]	111267064,4999998659	5016570,9999999953
I_w [mm^6], I_t [mm^4]	2143572281249998,7500000000	24688370,6666909680
d_y [mm], d_z [mm]	0	0
$c_{Y.UCS}$ [mm], $c_{Z.UCS}$ [mm]	250	1645
α [deg]	0,00	
$M_{pl.y.+}$ [Nmm], $M_{pl.y.-}$ [Nmm]	39499807897,4999465942	39499807897,4999542236
$M_{pl.z.+}$ [Nmm], $M_{pl.z.-}$ [Nmm]	1780882704,9999980927	1780882705,0000021458
A_L [mm^2/m], A_D [mm^2/m]	8622000,0000000000	8622000,0000000000

Picture

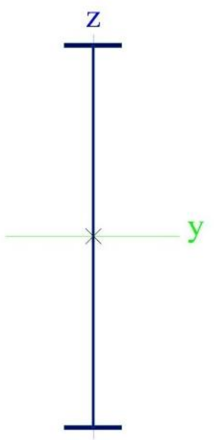

Hoofd3B_Dun1		
Type	Grafische doorsnede	
Onderdeelmateriaal	S355	
Bouwwijze	Algemeen	
Knik y-y, Knik z-z	d	d
A [mm^2]	136730,0000000002	
A_y [mm^2], A_z [mm^2]	39020,8452280028	97021,4671869126
I_y [mm^4], I_z [mm^4]	192005470094,1691894531	799071416,6666597128
$W_{el.y}$ [mm^3], $W_{el.z}$ [mm^3]	115353241,2701526433	3196285,6666666339
$W_{pl.y}$ [mm^3], $W_{pl.z}$ [mm^3]	143759107,4999998510	5490475,0000000196
I_w [mm^6], I_t [mm^4]	2143572281250000,0000000000	47909666,6666666642
d_y [mm], d_z [mm]	0	0
$c_{Y.UCS}$ [mm], $c_{Z.UCS}$ [mm]	250	1645
α [deg]	0,00	
$M_{pl.y.+}$ [Nmm], $M_{pl.y.-}$ [Nmm]	51034483162,5000000000	51034483162,4999465942
$M_{pl.z.+}$ [Nmm], $M_{pl.z.-}$ [Nmm]	1949118625,0000069141	1949118625,0000112057
A_L [mm^2/m], A_D [mm^2/m]	8597999,9999999981	8597999,9999999981

Picture

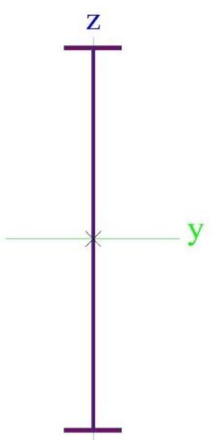

Hoofd4_Dun1		
Type	Grafische doorsnede	
Onderdeelmateriaal	S355	
Bouwwijze	Algemeen	
Knik y-y, Knik z-z	d	d
A [mm^2]	144230,0000000002	
A_y [mm^2], A_z [mm^2]	39111,1374229501	104020,3138113953
I_y [mm^4], I_z [mm^4]	230120715719,1678161621	799633916,6666741371
$W_{el.y}$ [mm^3], $W_{el.z}$ [mm^3]	128594979,4463076890	3198535,6666666949
$W_{pl.y}$ [mm^3], $W_{pl.z}$ [mm^3]	161319107,5000004470	5546725,0000000140
I_w [mm^6], I_t [mm^4]	2481613947916667,5000000000	50159666,6666442603
d_y [mm], d_z [mm]	0	0
$c_{Y.UCS}$ [mm], $c_{Z.UCS}$ [mm]	250	1771
α [deg]	0,00	
$M_{pl.y.+}$ [Nmm], $M_{pl.y.-}$ [Nmm]	57268283162,5001831055	57268283162,5001602173
$M_{pl.z.+}$ [Nmm], $M_{pl.z.-}$ [Nmm]	1969087375,0000050068	1969087375,0000059605
A_L [mm^2/m], A_D [mm^2/m]	9097999,9999999981	9097999,9999999981

Picture

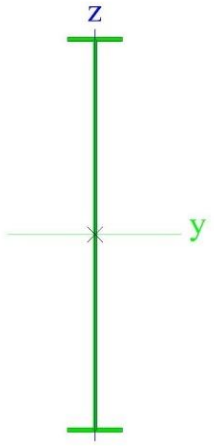

Hoofd5A_Dun1		
Type	Grafische doorsnede	
Onderdeelmateriaal	S355	
Bouwwijze	Algemeen	
Knik y-y, Knik z-z	d	d
A [mm^2]	129530,0000000003	
A_y [mm^2], A_z [mm^2]	38929,4161309355	90251,3340639735
I_y [mm^4], I_z [mm^4]	159437636294,1655273438	798531416,6666663885
$W_{el.y}$ [mm^3], $W_{el.z}$ [mm^3]	103229288,6333215237	3194125,6666666633
$W_{pl.y}$ [mm^3], $W_{pl.z}$ [mm^3]	127783507,5000007004	5436475,0000000075
I_w [mm^6], I_t [mm^4]	1842327281250000,5000000000	45749666,6666570157
d_y [mm], d_z [mm]	0	0
$c_{Y.UCS}$ [mm], $c_{Z.UCS}$ [mm]	250	1526
α [deg]	0,00	
$M_{pl.y.+}$ [Nmm], $M_{pl.y.-}$ [Nmm]	45363145162,5002441406	45363145162,5002441406
$M_{pl.z.+}$ [Nmm], $M_{pl.z.-}$ [Nmm]	1929948625,0000028610	1929948625,0000123978
A_L [mm^2/m], A_D [mm^2/m]	8118000,0000000000	8118000,0000000000

Picture

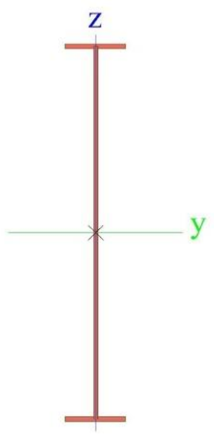

Hoofd5B_Dun1		
Type	Grafische doorsnede	
Onderdeelmateriaal	S355	
Bouwwijze	Algemeen	
Knik y-y, Knik z-z	d	d
A [mm^2]	92918,0000000002	
A_y [mm^2], A_z [mm^2]	34934,9392630844	55645,0228181110
I_y [mm^4], I_z [mm^4]	131037094643,1653442383	793149452,6666628122
$W_{el.y}$ [mm^3], $W_{el.z}$ [mm^3]	84841110,1606764346	3172597,8106666468
$W_{pl.y}$ [mm^3], $W_{pl.z}$ [mm^3]	99857704,5000007749	4997131,0000000130
I_w [mm^6], I_t [mm^4]	1842327281249999,7500000000	24221810,6666763239
d_y [mm], d_z [mm]	0	0
$c_{Y.UCS}$ [mm], $c_{Z.UCS}$ [mm]	250	1526
α [deg]	0,00	
$M_{pl.y.+}$ [Nmm], $M_{pl.y.-}$ [Nmm]	35449485097,5002746582	35449485097,5002746582
$M_{pl.z.+}$ [Nmm], $M_{pl.z.-}$ [Nmm]	1773981505,0000047684	1773981505,0000293255
A_L [mm^2/m], A_D [mm^2/m]	8142000,0000000009	8142000,0000000009

Picture

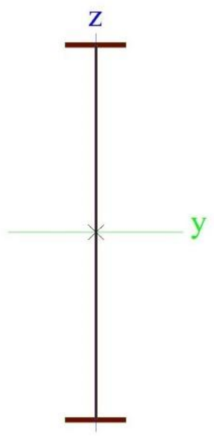

Hoofd6_Dun1		
Type	Grafische doorsnede	
Onderdeelmateriaal	S355	
Bouwwijze	Algemeen	
Knik y-y, Knik z-z	d	d
A [mm^2]	71984,0000000000	
A_y [mm^2], A_z [mm^2]	34815,6552461386	34524,8089067466
I_y [mm^4], I_z [mm^4]	43962529274,6667785645	792584234,6666626930
$W_{el.y}$ [mm^3], $W_{el.z}$ [mm^3]	45651639,9529249147	3170336,9386666482
$W_{pl.y}$ [mm^3], $W_{pl.z}$ [mm^3]	51912447,9999998957	4902927,9999999730
I_w [mm^6], I_t [mm^4]	705482666666666,7500000000	21960938,6666646749
d_y [mm], d_z [mm]	0	0
$c_{Y.UCS}$ [mm], $c_{Z.UCS}$ [mm]	250	944
α [deg]	0,00	
$M_{pl.y.+}$ [Nmm], $M_{pl.y.-}$ [Nmm]	18428919039,9999618530	18428919039,9999618530
$M_{pl.z.+}$ [Nmm], $M_{pl.z.-}$ [Nmm]	1740539439,9999921322	1740539439,9999904633
A_L [mm^2/m], A_D [mm^2/m]	5816000,0000000009	5816000,0000000009

Picture

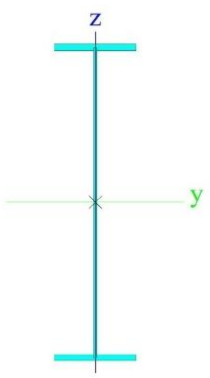

Hoofd7A_Dun1		
Type	Grafische doorsnede	
Onderdeelmateriaal	S355	
Bouwwijze	Algemeen	
Knik y-y, Knik z-z	d	d
A [mm^2]	70705,9999999999	
A_y [mm^2], A_z [mm^2]	34805,6675774186	33205,9202083336
I_y [mm^4], I_z [mm^4]	40366926436,1668853760	792549728,6666625738
$W_{el.y}$ [mm^3], $W_{el.z}$ [mm^3]	43522292,6535490379	3170198,9146666480
$W_{pl.y}$ [mm^3], $W_{pl.z}$ [mm^3]	49379700,4999997318	4897176,9999999609
I_w [mm^6], I_t [mm^4]	653419697916666,5000000000	21822914,6666685827
d_y [mm], d_z [mm]	0	0
$c_{Y.UCS}$ [mm], $c_{Z.UCS}$ [mm]	250	908
α [deg]	0,00	
$M_{pl.y.+}$ [Nmm], $M_{pl.y.-}$ [Nmm]	17529793677,4999046326	17529793677,4999046326
$M_{pl.z.+}$ [Nmm], $M_{pl.z.-}$ [Nmm]	1738497834,9999926090	1738497834,9999859333
A_L [mm^2/m], A_D [mm^2/m]	5673999,9999999991	5673999,9999999991

Picture

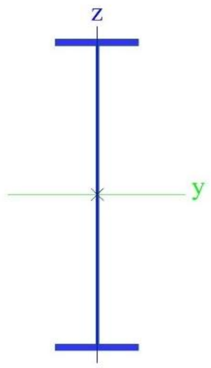

Hoofd7B_Dun1		
Type	Grafische doorsnede	
Onderdeelmateriaal	S355	
Bouwwijze	Algemeen	
Knik y-y, Knik z-z	d	d
A [mm^2]	57940,0000000000	
A_y [mm^2], A_z [mm^2]	22968,5963848621	33439,4666573654
I_y [mm^4], I_z [mm^4]	30124657583,3332290649	521722713,3333286643
$W_{el.y}$ [mm^3], $W_{el.z}$ [mm^3]	32479415,1841867678	2086890,8533333135
$W_{pl.y}$ [mm^3], $W_{pl.z}$ [mm^3]	37945050,0000000224	3273229,9999999874
I_w [mm^6], I_t [mm^4]	436054687500000,1250000000	8765853,3333314303
d_y [mm], d_z [mm]	0	0
$c_{Y.UCS}$ [mm], $c_{Z.UCS}$ [mm]	250	915
α [deg]	0,00	
$M_{pl.y.+}$ [Nmm], $M_{pl.y.-}$ [Nmm]	13470492750,0000114441	13470492750,0000076294
$M_{pl.z.+}$ [Nmm], $M_{pl.z.-}$ [Nmm]	1161996649,9999954700	1161996649,9999959469
A_L [mm^2/m], A_D [mm^2/m]	5674000,0000000009	5674000,0000000009

Picture

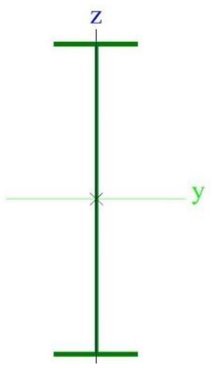

Hoofd8_Dun1		
Type	Grafische doorsnede	
Onderdeelmateriaal	S355	
Bouwwijze	Algemeen	
Knik y-y, Knik z-z	d	d
A [mm^2]	54862,0000000000	
A_y [mm^2], A_z [mm^2]	22952,7887683663	30355,0181640924
I_y [mm^4], I_z [mm^4]	24052109601,8331146240	521639607,3333311677
$W_{el.y}$ [mm^3], $W_{el.z}$ [mm^3]	28565450,8335310109	2086558,4293333234
$W_{pl.y}$ [mm^3], $W_{pl.z}$ [mm^3]	33122764,5000000075	3259378,9999999711
I_w [mm^6], I_t [mm^4]	358369921875000,1250000000	8433429,3333321847
d_y [mm], d_z [mm]	0	0
$c_{Y.UCS}$ [mm], $c_{Z.UCS}$ [mm]	250	830
α [deg]	0,00	
$M_{pl.y.+}$ [Nmm], $M_{pl.y.-}$ [Nmm]	11758581397,5000019073	11758581397,5000038147
$M_{pl.z.+}$ [Nmm], $M_{pl.z.-}$ [Nmm]	1157079544,9999971390	1157079544,9999897480
A_L [mm^2/m], A_D [mm^2/m]	5332000,0000000009	5332000,0000000009

Picture

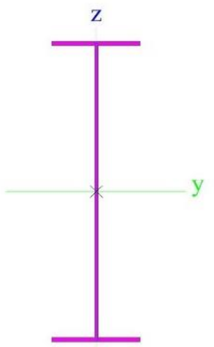

DD1&2_Dun1		
Type	Grafische doorsnede	
Onderdeelmateriaal	S355	
Bouwwijze	Algemeen	
Knik y-y, Knik z-z	d	d
A [mm^2]	47136,0000000000	
A_y [mm^2], A_z [mm^2]	20532,5610365557	22563,2392342305
I_y [mm^4], I_z [mm^4]	11953800323,6279792786	585914368,0000027418
$W_{el.y}$ [mm^3], $W_{el.z}$ [mm^3]	10482612,3003794141	2092551,3142857230
$W_{pl.y}$ [mm^3], $W_{pl.z}$ [mm^3]	19035664,0000000149	3234943,9999999898
I_w [mm^6], I_t [mm^4]	0,0000000000	14057472,0000000037
d_y [mm], d_z [mm]	0	-406
$c_{Y.UCS}$ [mm], $c_{Z.UCS}$ [mm]	280	406
α [deg]	0,00	
$M_{pl.y.+}$ [Nmm], $M_{pl.y.-}$ [Nmm]	6757660720,0000057220	6757660720,0000057220
$M_{pl.z.+}$ [Nmm], $M_{pl.z.-}$ [Nmm]	1148405119,9999964237	1148405120,0000021458
A_L [mm^2/m], A_D [mm^2/m]	4252000,0000000009	4252000,0000000009

Picture

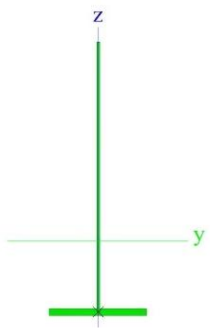

DD3_Dun1		
Type	Grafische doorsnede	
Onderdeelmateriaal	S355	
Bouwwijze	Algemeen	
Knik y-y, Knik z-z	d	d
A [mm^2]	45744,0000000000	
A_y [mm^2], A_z [mm^2]	20525,3065632881	21608,4645033836
I_y [mm^4], I_z [mm^4]	10227287957,1696472168	585884672,0000029802
$W_{el.y}$ [mm^3], $W_{el.z}$ [mm^3]	9411128,4942688867	2092445,2571428670
$W_{pl.y}$ [mm^3], $W_{pl.z}$ [mm^3]	17015524,0000000186	3229376,0000000000
I_w [mm^6], I_t [mm^4]	0,0000000000	13938688,0000000037
d_y [mm], d_z [mm]	0	-372
$c_{Y.UCS}$ [mm], $c_{Z.UCS}$ [mm]	280	372
α [deg]	0,00	
$M_{pl.y.+}$ [Nmm], $M_{pl.y.-}$ [Nmm]	6040511020,0000057220	6040511020,0000076294
$M_{pl.z.+}$ [Nmm], $M_{pl.z.-}$ [Nmm]	1146428480,0000000000	1146428480,0000028610
A_L [mm^2/m], A_D [mm^2/m]	4078000,0000000005	4078000,0000000005

Picture

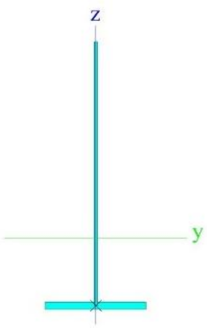

DD4_Dun1

Type	Grafische doorsnede	
Onderdeelmateriaal	S355	
Bouwwijze	Algemeen	
Knik y-y, Knik z-z	d	d
A [mm^2]	44368,0000000000	
A_y [mm^2], A_z [mm^2]	20517,5256550606	20476,4323104473
I_y [mm^4], I_z [mm^4]	8680996620,6712436676	585855317,3333420753
$W_{el.y}$ [mm^3], $W_{el.z}$ [mm^3]	8402925,8353073541	2092340,4190476472
$W_{pl.y}$ [mm^3], $W_{pl.z}$ [mm^3]	15095665,1172371134	3223871,9999999972
I_w [mm^6], I_t [mm^4]	0,0000000000	13821269,3333333377
d_y [mm], d_z [mm]	0	-340
$c_{Y.UCS}$ [mm], $c_{Z.UCS}$ [mm]	280	340
α [deg]	0,00	
$M_{pl.y.+}$ [Nmm], $M_{pl.y.-}$ [Nmm]	5358961116,6191749573	5358961116,6191749573
$M_{pl.z.+}$ [Nmm], $M_{pl.z.-}$ [Nmm]	1144474559,9999990463	1144474560,0000028610
A_L [mm^2/m], A_D [mm^2/m]	3906000,0000000005	3906000,0000000005

Picture

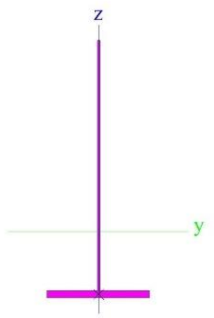

3. Materials

Staal	
S355	
Thermisch uitz. [m/mK]	0,00
Massa eenheid [kg/m^3]	7850,0
E-mod [MPa]	2,1000e+05
Poisson - nu	0.3
Onafhankelijke G-modulus	x
G-mod [MPa]	8,0769e+04
Log. decrement (niet-uniforme demping enkel)	0.025
Kleur	
Therm. exp. (brand) [m/mK]	0,00
Specifieke hitte [J/gK]	6,0000e-01
Thermische geleiding [W/mK]	4,5000e+01
Fu [N/mm^2]	510,0000000000
Fy [N/mm^2]	355,0000000000

4. Load cases

Naam	Actie type	Lastgroep	Belastingtype	Spec	Duur	'Master' belastingsgeval	Lastgroep
Fx_DD1	Variabel	LG1	Statisch	Standaard	Kort	Geen	LG1
Fx_DD2	Variabel	LG1	Statisch	Standaard	Kort	Geen	LG1
Fx_DD3	Variabel	LG1	Statisch	Standaard	Kort	Geen	LG1
Fx_DD4	Variabel	LG1	Statisch	Standaard	Kort	Geen	LG1
Fy_DD1	Variabel	LG1	Statisch	Standaard	Kort	Geen	LG1
Fy_DD2	Variabel	LG1	Statisch	Standaard	Kort	Geen	LG1
Fy_DD3	Variabel	LG1	Statisch	Standaard	Kort	Geen	LG1
Fy_DD4	Variabel	LG1	Statisch	Standaard	Kort	Geen	LG1
Fz_DD1	Variabel	LG1	Statisch	Standaard	Kort	Geen	LG1
Fz_DD2	Variabel	LG1	Statisch	Standaard	Kort	Geen	LG1
Fz_DD3	Variabel	LG1	Statisch	Standaard	Kort	Geen	LG1
Fz_DD4	Variabel	LG1	Statisch	Standaard	Kort	Geen	LG1
Mx_DD1	Variabel	LG1	Statisch	Standaard	Kort	Geen	LG1
Mx_DD2	Variabel	LG1	Statisch	Standaard	Kort	Geen	LG1
Mx_DD3	Variabel	LG1	Statisch	Standaard	Kort	Geen	LG1
Mx_DD4	Variabel	LG1	Statisch	Standaard	Kort	Geen	LG1
My_DD1	Variabel	LG1	Statisch	Standaard	Kort	Geen	LG1
My_DD2	Variabel	LG1	Statisch	Standaard	Kort	Geen	LG1
My_DD3	Variabel	LG1	Statisch	Standaard	Kort	Geen	LG1
My_DD4	Variabel	LG1	Statisch	Standaard	Kort	Geen	LG1
Mz_DD1	Variabel	LG1	Statisch	Standaard	Kort	Geen	LG1
Mz_DD2	Variabel	LG1	Statisch	Standaard	Kort	Geen	LG1
Mz_DD3	Variabel	LG1	Statisch	Standaard	Kort	Geen	LG1
Mz_DD4	Variabel	LG1	Statisch	Standaard	Kort	Geen	LG1

5. Load groups

Naam	Last	Relatie	Coëff.
LG1	Variabel	Exclusief	0.5

6. Settings net

Naam	NetInstelling1
Generatie van variabele excentriciteiten op elementen in plaats van constante excentriciteiten	✗
Generatie van knopen op staven	✗
Elastisch net	✓
Pas automatische netverfijning toe	✗
Constructie-entiteiten verbinden	✓
Verdeling op consoles en variabele staven	500
Verdeling voor integratiestrook en 2D-1D upgrade	50
Gemiddeld aantal 1D-netelementen op rechte 1D-elementen	100
Gemiddelde grootte van 2D-netelement [m]	1,000
Gemiddelde grootte van 1D-element op gebogen 1D-elementen [m]	0,100
Minimum lengte van staafelement [m]	0,001
Maximum lengte van staafelement [m]	1000,000
Gemiddelde grootte van voorspankabels, elementen op elastische bedding, niet-lineaire grondveer [m]	1,000
Maximale hoek uit het vlak van vierhoekig element [rad]	0,03000000000000000
Verh. voorgedefinieerd net	1.5
Minimumafstand tussen definitiepunt en -lijn [m]	0.001
Gemiddelde afmeting van paneelelement [m]	1,000
Netverfijning volgens het liggertype	Geen
Definitie van netelementen afmetingen voor panelen	Handmatig

7. Instellingen solver

Naam	SolverSetup1
Negeer dwarskrachtvervormingen (Ay, Az >> A)	x
Initiële spanning	x
Aantal diktes van plaatrib	20
Maximumaantal bodeminteractie-iteraties	10
Aantal sneden op gemiddelde staaf	5
Stap voor grond/waterdruk [m]	0,500
C1x [MN/m³]	1,0000e-01
C1y [MN/m³]	1,0000e-01
C1z [MN/m³]	1,0000e+01
C2x [MN/m]	5,0000e+00
C2y [MN/m]	5,0000e+00
Wapeningscoëfficiënt	1
Waarschuwing als de maximale translatie groter is dan [mm]	1000,0000000000000000
Waarschuwing als de maximale rotatie groter is dan [rad]	0,10000000000000001
Tolerantie van parallellisme [deg]	10,00
Verhouding tot helft - afstand tot aanliggende ligger beff,i/bi [-]	0,20
Verhouding tot effectieve overspanningslengte beff,i/l0 [-]	0,10
Maximale verhouding tot effectieve overspanningslengte beff,i/l0 [-]	0,20
Enkelvoudig opgelegde ligger [-]	1,00
Inwendige overspanning [-]	0,70
Eind overspanning [-]	0,85
Uitkraging, basisverhouding tot huidige overspanning [-]	1,00
Uitkraging, basisverhouding tot aangrenzende overspanning [-]	0,15
Uitkraging, maximale verhouding tot huidige overspanning [-]	1,50
Maximale aangrenzende overspanninglengteverhouding [-]	1,50
Maximale uitkragingslengteverhouding tot aangrenzende overspanning [-]	0,50
Overspanningslengteverhouding Le/beff,max (1 kant) [-]	8,00
Enkelvoudig opgelegde ligger [-]	1,00
Inwendige overspanning [-]	0,70
Eind overspanning [-]	0,85
Uitkraging [-]	2,00
Methode gebruikt voor niet-beton en niet-staal / staalbetonliggers	EN 1994-1-1
Grond combinatie	Geen
Buigtheorie van plaat/schaal berekening	Mindlin
Type solver	Direct

8. Nodes

Naam	Coördinaat X [m]	Coördinaat Y [m]	Coördinaat Z [m]
KStart	-8,050	0,000	-2,341
K1	-7,350	0,000	-2,341
K2	-4,787	0,000	-2,341
K3	-3,400	0,000	-2,341
K4	-2,950	0,000	-2,341
K8	4,550	0,000	-2,341
KEnd	10,850	0,000	-2,341
K7	2,401	0,000	-2,341
K5	-1,400	0,000	-2,341
DD1	0,750	0,000	-2,341
DD1_2	0,750	10,700	-2,341

Naam	Coördinaat X [m]	Coördinaat Y [m]	Coördinaat Z [m]
DD2	3,950	0,000	-2,341
DD2_2	3,950	10,700	-2,341
DD3	7,150	0,000	-2,341
DD3_2	7,150	10,700	-2,341
DD4	10,350	0,000	-2,341
DD4_2	10,350	10,700	-2,341
KSup1	-7,900	0,000	-2,341
KSup2	-2,400	0,000	-2,341
K6	0,000	0,000	-2,341
K9	10,810	0,000	-2,341

9. Elements

Naam	Doorsnede	Materiaal	Lengte [m]	Beginknoop	Eindknoop	Type	Laag
Main1	Hoofd1_Dun1 - Grafische doorsnede	S355	0,700	KStart	K1	Algemeen (0)	Hoofd
Main2	Hoofd1_Dun1 - Grafische doorsnede	S355	2,563	K1	K2	Algemeen (0)	Hoofd
Main3	Hoofd2_Dun1 - Grafische doorsnede	S355	1,387	K2	K3	Algemeen (0)	Hoofd
Main4	Hoofd3B_Dun1 - Grafische doorsnede	S355	0,450	K3	K4	Algemeen (0)	Hoofd
Main5	Hoofd4_Dun1 - Grafische doorsnede	S355	1,550	K4	K5	Algemeen (0)	Hoofd
Main6	Hoofd5B_Dun1 - Grafische doorsnede	S355	3,801	K5	K7	Algemeen (0)	Hoofd
Main7	Hoofd6_Dun1 - Grafische doorsnede	S355	2,149	K7	K8	Algemeen (0)	Hoofd
Main8	Hoofd7B_Dun1 - Grafische doorsnede	S355	6,300	K8	KEnd	Algemeen (0)	Hoofd
DD1	DD1&2_Dun1 - Grafische doorsnede	S355	10,700	DD1	DD1_2	Algemeen (0)	DD
DD2	DD1&2_Dun1 - Grafische doorsnede	S355	10,700	DD2	DD2_2	Algemeen (0)	DD
DD3	DD3_Dun1 - Grafische doorsnede	S355	10,700	DD3	DD3_2	Algemeen (0)	DD
DD4	DD4_Dun1 - Grafische doorsnede	S355	10,700	DD4	DD4_2	Algemeen (0)	DD

10. Variabel cross sections

Varia1-2			
Staaf	Main2		
Coör	Rela		
lengte 1, Css1(1), Css2(1)	1.000	Hoofd1_Dun1 - Grafische doorsnede	Hoofd2_Dun1 - Grafische doorsnede
Varia2-3A			
Staaf	Main3		
Coör	Rela		
lengte 1, Css1(1), Css2(1)	1.000	Hoofd2_Dun1 - Grafische doorsnede	Hoofd3A_Dun1 - Grafische doorsnede
Varia3B-4			
Staaf	Main4		
Coör	Rela		
lengte 1, Css1(1), Css2(1)	1.000	Hoofd3B_Dun1 - Grafische doorsnede	Hoofd4_Dun1 - Grafische doorsnede
Varia4-5A			
Staaf	Main5		
Coör	Rela		
lengte 1, Css1(1), Css2(1)	1.000	Hoofd4_Dun1 - Grafische doorsnede	Hoofd5A_Dun1 - Grafische doorsnede
Varia5B-6			
Staaf	Main6		
Coör	Rela		
lengte 1, Css1(1), Css2(1)	1.000	Hoofd5B_Dun1 - Grafische doorsnede	Hoofd6_Dun1 - Grafische doorsnede
Varia6-7A			
Staaf	Main7		
Coör	Rela		
lengte 1, Css1(1), Css2(1)	1.000	Hoofd6_Dun1 - Grafische doorsnede	Hoofd7A_Dun1 - Grafische doorsnede
Vari7B-8			
Staaf	Main8		
Coör	Rela		
lengte 1, Css1(1), Css2(1)	1.000	Hoofd7B_Dun1 - Grafische doorsnede	Hoofd8_Dun1 - Grafische doorsnede

11. Supports

Naam	Knoop	Systeem	Type	X	Y	Z	Rx	Ry	Rz
Support1	KSup1	GCS	Standaard	Vrij	Vrij	Vast	Vrij	Vrij	Vrij
Support2	KSup2	GCS	Standaard	Vast	Vast	Vast	Vast	Vrij	Vast

12. Overview, main girder + cross beams + supports

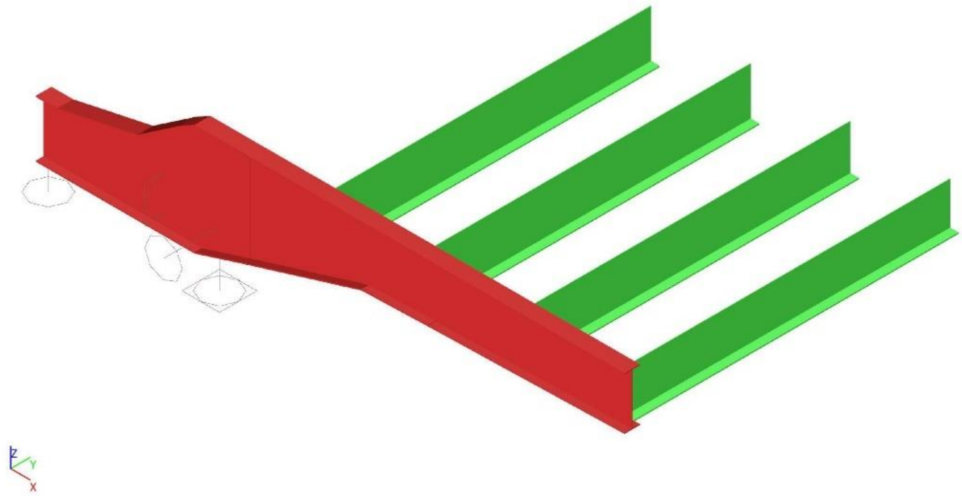

13. Pointload on element

Naam	Belastingsgeval	Systeem	Oors	Rich	Type	Pos x	Waarde - F [N]	Staaf
Fx_DD1	Fx_DD1	GCS	Vanaf begin	X	Kracht	0.000	1000,0000000000	DD1
Fx_DD2	Fx_DD2	GCS	Vanaf begin	X	Kracht	0.000	1000,0000000000	DD2
Fx_DD3	Fx_DD3	GCS	Vanaf begin	X	Kracht	0.000	1000,0000000000	DD3
Fx_DD4	Fx_DD4	GCS	Vanaf begin	X	Kracht	0.000	1000,0000000000	DD4
Fy_DD1	Fy_DD1	GCS	Vanaf begin	Y	Kracht	0.000	1000,0000000000	DD1
Fy_DD2	Fy_DD2	GCS	Vanaf begin	Y	Kracht	0.000	1000,0000000000	DD2
Fy_DD3	Fy_DD3	GCS	Vanaf begin	Y	Kracht	0.000	1000,0000000000	DD3
Fy_DD4	Fy_DD4	GCS	Vanaf begin	Y	Kracht	0.000	1000,0000000000	DD4
Fz_DD1	Fz_DD1	GCS	Vanaf begin	Z	Kracht	0.000	1000,0000000000	DD1
Fz_DD2	Fz_DD2	GCS	Vanaf begin	Z	Kracht	0.000	1000,0000000000	DD2
Fz_DD3	Fz_DD3	GCS	Vanaf begin	Z	Kracht	0.000	1000,0000000000	DD3
Fz_DD4	Fz_DD4	GCS	Vanaf begin	Z	Kracht	0.000	1000,0000000000	DD4

Verklaring van symbolen	
Staaf	(10,700 m)

14. Fx_DD1

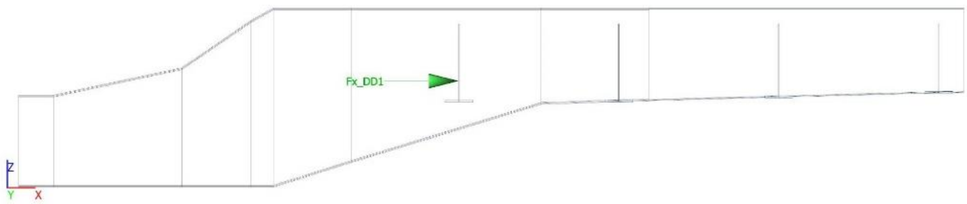

15. Fx_DD2

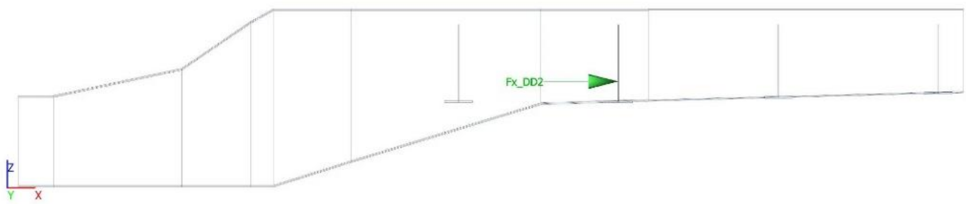

16. Fx_DD3

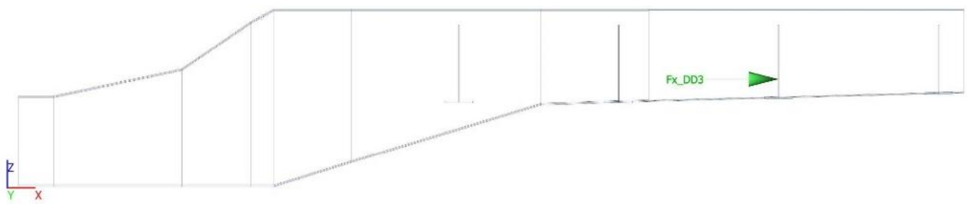

17. Fx_DD4

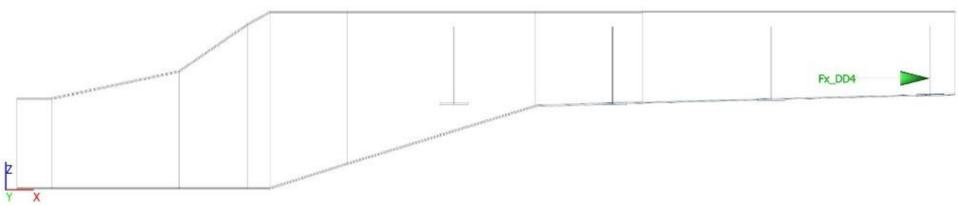

18. Fy_DD1

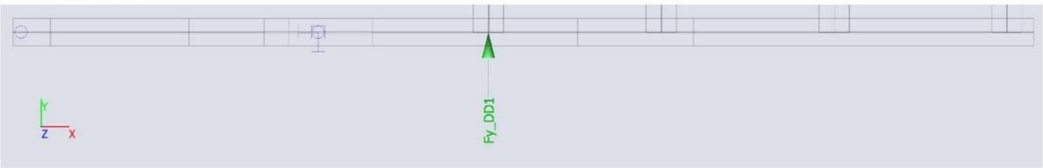

19. Fy_DD2

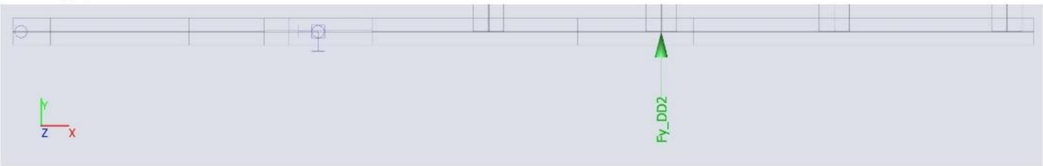

20. Fy_DD3

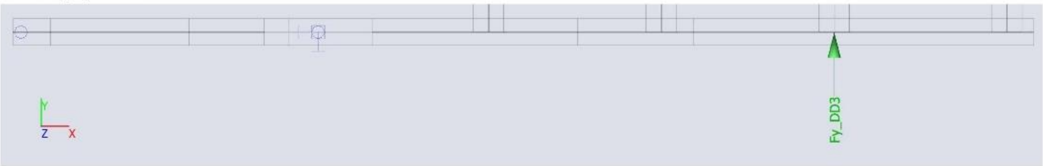

21. Fy_DD4

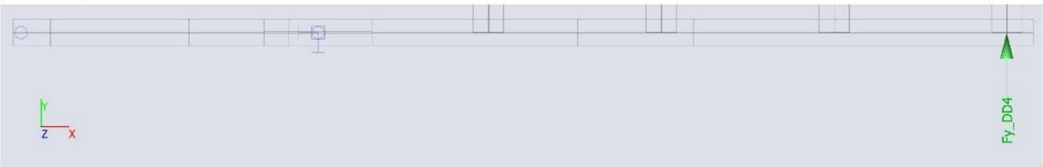

22. Fz_DD1

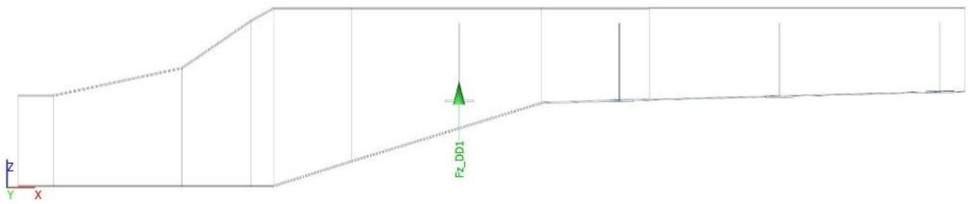

23. Fz_DD2

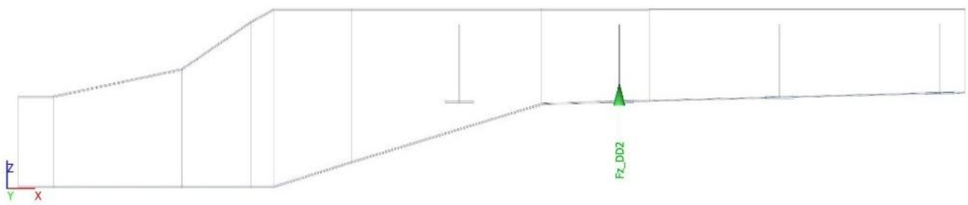

24. Fz_DD3

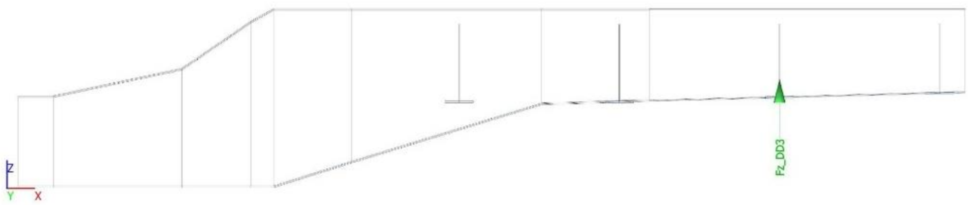

25. Fz_DD4

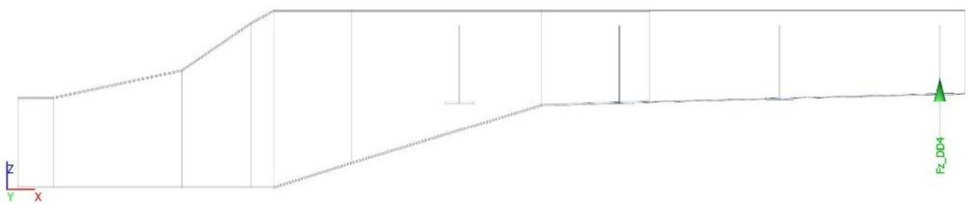

26. Moment on element

Naam	Staaf	Systeem	Waarde - M [Nmm]	Pos x	Coör	Herh (n)	Staaf
	Belastingsgeval	Rich	Type		Oors	dx	
Mx_DD1	DD1	GCS	1000000,0000000000	0.000	Rela	1	DD1
	Mx_DD1	Mx	Moment		Vanaf begin		
Mx_DD2	DD2	GCS	1000000,0000000000	0.000	Rela	1	DD2
	Mx_DD2	Mx	Moment		Vanaf begin		
Mx_DD3	DD3	GCS	1000000,0000000000	0.000	Rela	1	DD3
	Mx_DD3	Mx	Moment		Vanaf begin		
Mx_DD4	DD4	GCS	1000000,0000000000	0.000	Rela	1	DD4
	Mx_DD4	Mx	Moment		Vanaf begin		
My_DD1	DD1	GCS	1000000,0000000000	0.000	Rela	1	DD1
	My_DD1	My	Moment		Vanaf begin		
My_DD2	DD2	GCS	1000000,0000000000	0.000	Rela	1	DD2
	My_DD2	My	Moment		Vanaf begin		
My_DD3	DD3	GCS	1000000,0000000000	0.000	Rela	1	DD3
	My_DD3	My	Moment		Vanaf begin		
My_DD4	DD4	GCS	1000000,0000000000	0.000	Rela	1	DD4
	My_DD4	My	Moment		Vanaf begin		
Mz_DD1	DD1	GCS	1000000,0000000000	0.000	Rela	1	DD1
	Mz_DD1	Mz	Moment		Vanaf begin		
Mz_DD2	DD2	GCS	1000000,0000000000	0.000	Rela	1	DD2
	Mz_DD2	Mz	Moment		Vanaf begin		
Mz_DD3	DD3	GCS	1000000,0000000000	0.000	Rela	1	DD3
	Mz_DD3	Mz	Moment		Vanaf begin		
Mz_DD4	DD4	GCS	1000000,0000000000	0.000	Rela	1	DD4
	Mz_DD4	Mz	Moment		Vanaf begin		

27. Mx_DD1

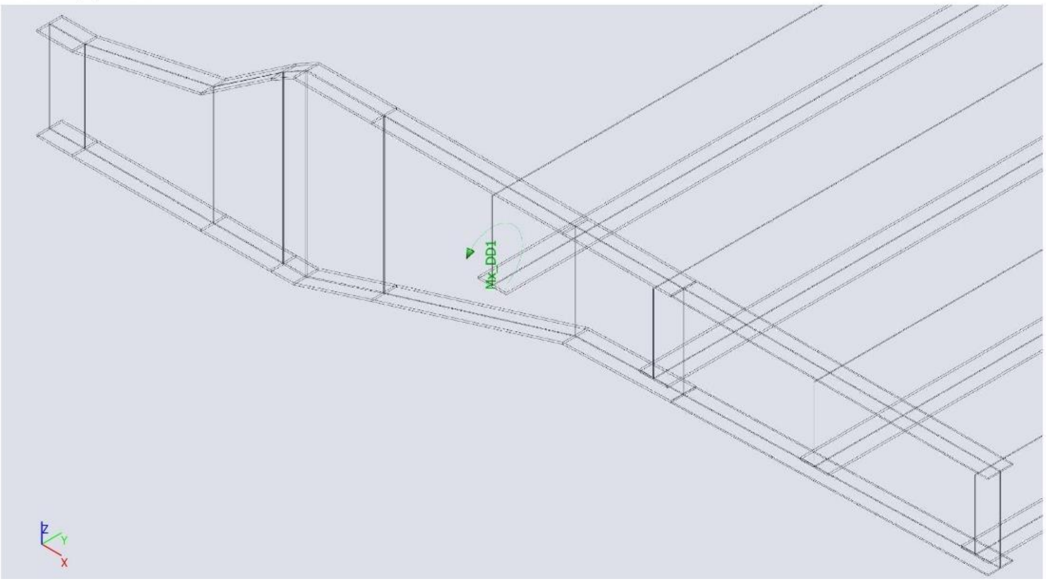

28. Mx_DD2

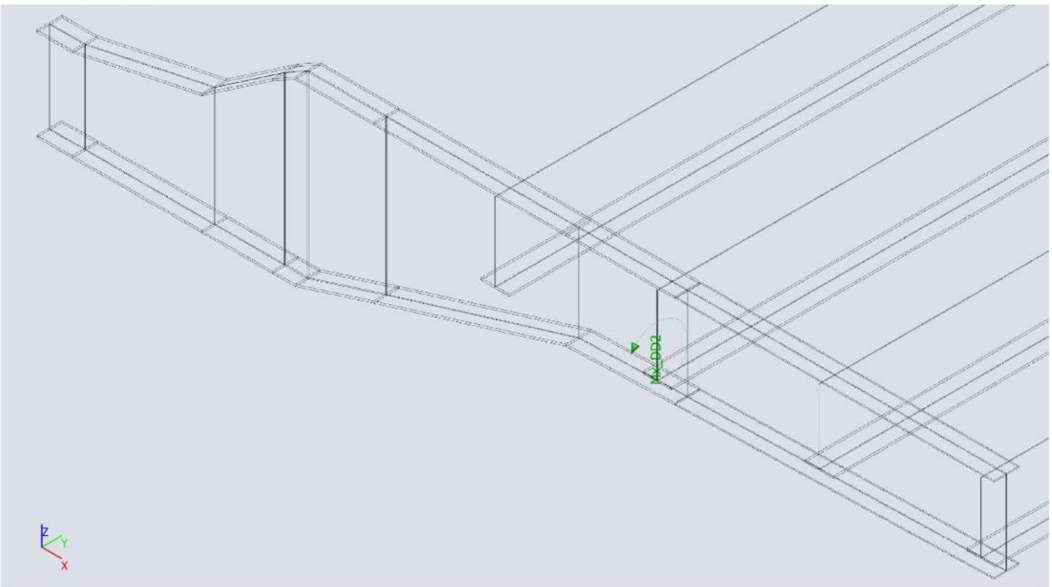

29. Mx_DD3

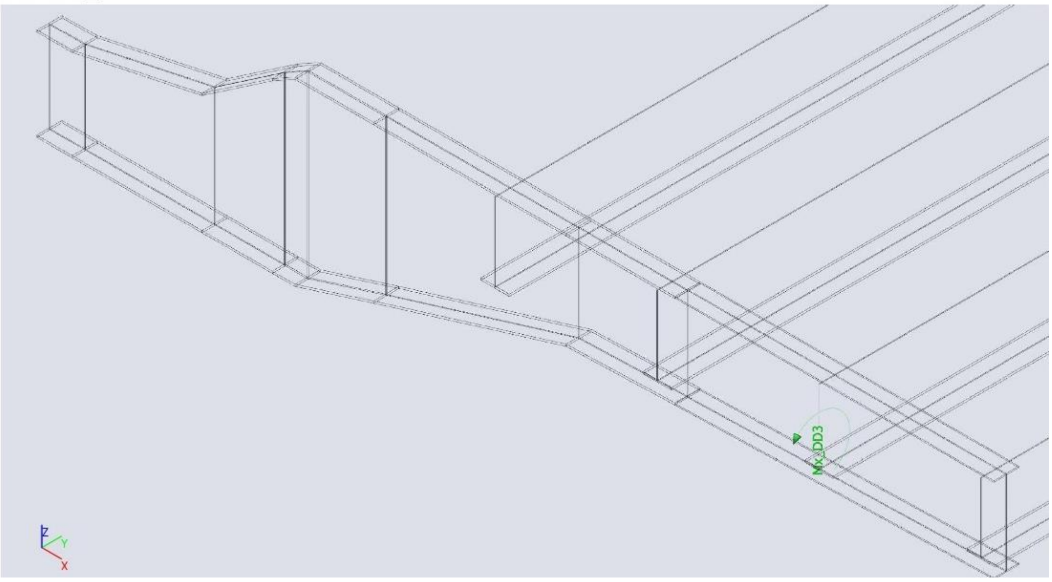

30. Mx_DD4

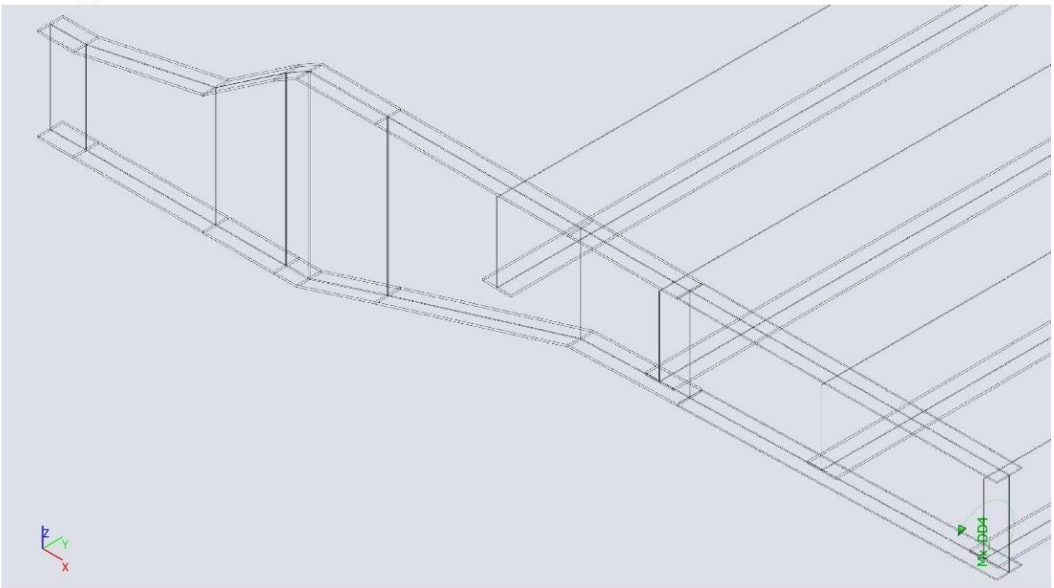

31. My_DD1

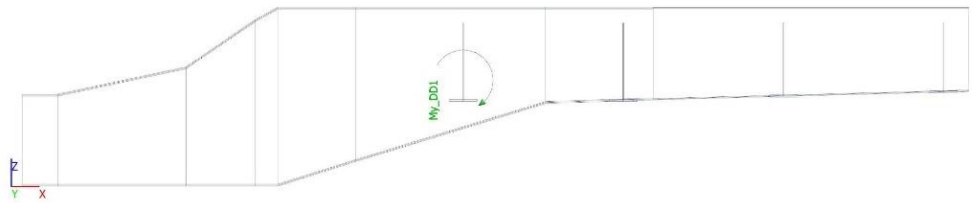

32. My_DD2

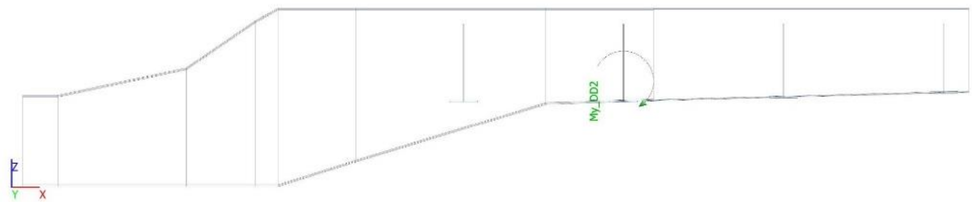

33. My_DD3

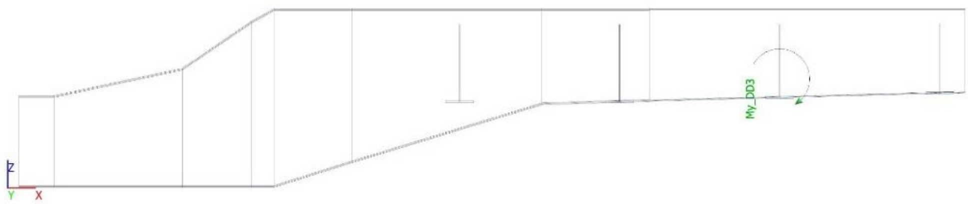

34. My_DD4

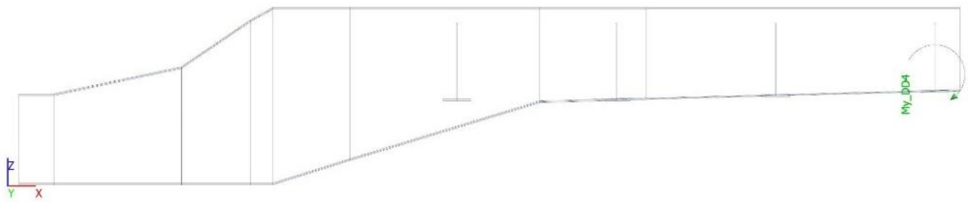

35. Mz_DD1

36. Mz_DD2

37. Mz_DD3

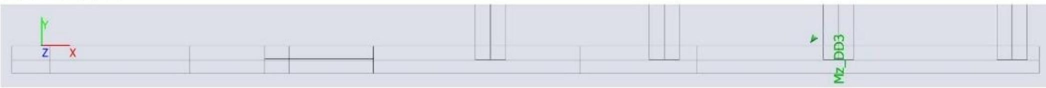

38. Mz_DD4

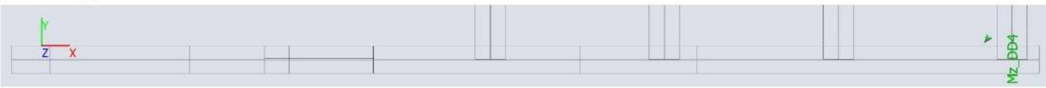

39. 1D-vervormingen

Lineaire berekening
Klasse: Alle indiv belastingen
Assenstelsel: Globaal
Extreme 1D: Nee
Selectie: DD1..DD4
Filter: Laag = DD
Geselecteerde doorsnedes: Ingevoerd
Vervormingen

Naam	dx [m]	Belasting	Doorsnede	u_x [mm]	u_y [mm]	u_z [mm]	φ_x [rad]	φ_y [rad]	φ_z [rad]
DD1	0,000	Fx_DD1	DD1&2_Dun1 - Grafische doorsnede	0,00033399999210815	0,00000000000000000	-0,00047599999675185	0,00000000000000000	0,0000014299999407	0,00000000000000000
DD1	0,000	Fx_DD2	DD1&2_Dun1 - Grafische doorsnede	0,00033399999210815	0,00000000000000000	-0,00047599999675185	0,00000000000000000	0,0000014299999407	0,00000000000000000
DD1	0,000	Fx_DD3	DD1&2_Dun1 - Grafische doorsnede	0,00034199999277007	0,00000000000000000	-0,00050599999212864	0,00000000000000000	0,0000015700000233	0,00000000000000000
DD1	0,000	Fx_DD4	DD1&2_Dun1 - Grafische doorsnede	0,00034999999343199	0,00000000000000000	-0,00053600001592713	0,00000000000000000	0,0000017000000696	0,00000000000000000
DD1	0,000	Fy_DD1	DD1&2_Dun1 - Grafische doorsnede	0,00000000000000000	0,08842800161801279	0,00000000000000000	0,00004831999831367	0,00000000000000000	0,00002967299951706
DD1	0,000	Fy_DD2	DD1&2_Dun1 - Grafische doorsnede	0,00000000000000000	0,18338300287723541	0,00000000000000000	0,00004831999831367	0,00000000000000000	0,00009006199979922
DD1	0,000	Fy_DD3	DD1&2_Dun1 - Grafische doorsnede	0,00000000000000000	0,27574700652621686	0,00000000000000000	-0,00002629899972817	0,00000000000000000	0,00015045100008138
DD1	0,000	Fy_DD4	DD1&2_Dun1 - Grafische doorsnede	0,00000000000000000	0,36811101017519832	0,00000000000000000	-0,00010093000310007	0,00000000000000000	0,00021083900355734
DD1	0,000	Fz_DD1	DD1&2_Dun1 - Grafische doorsnede	-0,00047599999675185	0,00000000000000000	0,00221899995267449	0,00000000000000000	-0,0000055999998949	0,00000000000000000
DD1	0,000	Fz_DD2	DD1&2_Dun1 - Grafische doorsnede	-0,00093400001333066	0,00000000000000000	0,00401199986299616	0,00000000000000000	-0,0000137200004247	0,00000000000000000
DD1	0,000	Fz_DD3	DD1&2_Dun1 - Grafische doorsnede	-0,00139099995521974	0,00000000000000000	0,00580500000069151	0,00000000000000000	-0,0000218400009544	0,00000000000000000
DD1	0,000	Fz_DD4	DD1&2_Dun1 - Grafische doorsnede	-0,00184900000022026	0,00000000000000000	0,00759900012781145	0,00000000000000000	-0,0000299599992104	0,00000000000000000
DD1	0,000	Mx_DD1	DD1&2_Dun1 - Grafische doorsnede	0,00000000000000000	0,04831999831367284	0,00000000000000000	0,00139157299418002	0,00000000000000000	0,00000000000000000
DD1	0,000	Mx_DD2	DD1&2_Dun1 - Grafische doorsnede	0,00000000000000000	0,04831999831367284	0,00000000000000000	0,00139157497324049	0,00000000000000000	0,00000000000000000
DD1	0,000	Mx_DD3	DD1&2_Dun1 - Grafische doorsnede	0,00000000000000000	0,04831999831367284	0,00000000000000000	0,00139157602097839	0,00000000000000000	0,00000000000000000
DD1	0,000	Mx_DD4	DD1&2_Dun1 - Grafische doorsnede	0,00000000000000000	0,04831999831367284	0,00000000000000000	0,00139157602097839	0,00000000000000000	0,00000000000000000
DD1	0,000	My_DD1	DD1&2_Dun1 - Grafische doorsnede	0,00014299999406830	0,00000000000000000	-0,00055999998949119	0,00000000000000000	0,0000025400001391	0,00000000000000000
DD1	0,000	My_DD2	DD1&2_Dun1 - Grafische doorsnede	0,00014299999406830	0,00000000000000000	-0,00055999998949119	0,00000000000000000	0,0000025400001391	0,00000000000000000
DD1	0,000	My_DD3	DD1&2_Dun1 - Grafische doorsnede	0,00014299999406830	0,00000000000000000	-0,00055999998949119	0,00000000000000000	0,0000025400001391	0,00000000000000000
DD1	0,000	My_DD4	DD1&2_Dun1 - Grafische doorsnede	0,00014299999406830	0,00000000000000000	-0,00055999998949119	0,00000000000000000	0,0000025400001391	0,00000000000000000
DD1	0,000	Mz_DD1	DD1&2_Dun1	0,00000000000000000	0,02967299951706082	0,00000000000000000	0,00000000000000000	0,00000000000000000	0,0000188710000 6570

Naam	dx [m]	Belasting	Doorsnede	u_x [mm]	u_y [mm]	u_z [mm]	φ_x [rad]	φ_y [rad]	φ_z [rad]
			- Grafische doorsnede						
DD1	0,000	Mz_DD2	DD1&2_Dun1 - Grafische doorsnede	0,00000000000000000	0,02967299951706082	0,00000000000000000	0,00000000000000000	0,00000000000000000	0,0000188710006570
DD1	0,000	Mz_DD3	DD1&2_Dun1 - Grafische doorsnede	0,00000000000000000	0,02967299951706082	0,00000000000000000	0,00000000000000000	0,00000000000000000	0,0000188710006570
DD1	0,000	Mz_DD4	DD1&2_Dun1 - Grafische doorsnede	0,00000000000000000	0,02967299951706082	0,00000000000000000	0,00000000000000000	0,00000000000000000	0,0000188710006570
DD2	0,000	Fx_DD1	DD1&2_Dun1 - Grafische doorsnede	0,00033399999210815	0,00000000000000000	-0,00093400001333066	0,00000000000000000	0,0000014299999407	0,00000000000000000
DD2	0,000	Fx_DD2	DD1&2_Dun1 - Grafische doorsnede	0,00060600001461353	0,00000000000000000	-0,00075100001595274	0,00000000000000000	0,0000000300000003	0,00000000000000000
DD2	0,000	Fx_DD3	DD1&2_Dun1 - Grafische doorsnede	0,00060600001461353	0,00000000000000000	-0,00084900000274502	0,00000000000000000	0,0000003299999918	0,00000000000000000
DD2	0,000	Fx_DD4	DD1&2_Dun1 - Grafische doorsnede	0,00060600001461353	0,00000000000000000	-0,00094600000011269	0,00000000000000000	0,0000006300000166	0,00000000000000000
DD2	0,000	Fy_DD1	DD1&2_Dun1 - Grafische doorsnede	0,00000000000000000	0,18338300287723541	0,00000000000000000	0,00004831999831367	0,00000000000000000	0,00002967299951706
DD2	0,000	Fy_DD2	DD1&2_Dun1 - Grafische doorsnede	0,00000000000000000	0,89543301146477461	0,00000000000000000	0,00083175697363913	0,00000000000000000	0,00012081900058547
DD2	0,000	Fy_DD3	DD1&2_Dun1 - Grafische doorsnede	0,00000000000000000	1,23745400924235582	0,00000000000000000	0,00066137698013335	0,00000000000000000	0,00024272600421682
DD2	0,000	Fy_DD4	DD1&2_Dun1 - Grafische doorsnede	0,00000000000000000	1,57946802210062742	0,00000000000000000	0,00049096997827291	0,00000000000000000	0,00036463298602030
DD2	0,000	Fz_DD1	DD1&2_Dun1 - Grafische doorsnede	-0,00047599999675185	0,00000000000000000	0,00401199986299616	0,00000000000000000	-0,0000055999998949	0,00000000000000000
DD2	0,000	Fz_DD2	DD1&2_Dun1 - Grafische doorsnede	-0,00075100001595274	0,00000000000000000	0,01038499976857565	0,00000000000000000	-0,0000182099995527	0,00000000000000000
DD2	0,000	Fz_DD3	DD1&2_Dun1 - Grafische doorsnede	-0,00075899998819295	0,00000000000000000	0,01621199953660835	0,00000000000000000	-0,0000362600007975	0,00000000000000000
DD2	0,000	Fz_DD4	DD1&2_Dun1 - Grafische doorsnede	-0,00076700001727659	0,00000000000000000	0,02203899930464104	0,00000000000000000	-0,0000543099986317	0,00000000000000000
DD2	0,000	Mx_DD1	DD1&2_Dun1 - Grafische doorsnede	0,00000000000000000	0,04831999831367284	0,00000000000000000	0,00139157194644213	0,00000000000000000	0,00000000000000000
DD2	0,000	Mx_DD2	DD1&2_Dun1 - Grafische doorsnede	0,00000000000000000	0,83175697363913059	0,00000000000000000	0,00317740091122687	0,00000000000000000	0,00000000000000000
DD2	0,000	Mx_DD3	DD1&2_Dun1 - Grafische doorsnede	0,00000000000000000	0,83175697363913059	0,00000000000000000	0,00317740300670266	0,00000000000000000	0,00000000000000000
DD2	0,000	Mx_DD4	DD1&2_Dun1 - Grafische doorsnede	0,00000000000000000	0,83175802137702703	0,00000000000000000	0,00317740510217845	0,00000000000000000	0,00000000000000000
DD2	0,000	My_DD1	DD1&2_Dun1 - Grafische doorsnede	0,00014299999406830	0,00000000000000000	-0,00137200004246552	0,00000000000000000	0,0000025400001391	0,00000000000000000
DD2	0,000	My_DD2	DD1&2_Dun1 - Grafische doorsnede	0,00000300000002618	0,00000000000000000	-0,00182099995527096	0,00000000000000000	0,0000056400000403	0,00000000000000000
DD2	0,000	My_DD3	DD1&2_Dun1 - Grafische doorsnede	0,00000300000002618	0,00000000000000000	-0,00182099995527096	0,00000000000000000	0,0000056400000403	0,00000000000000000
DD2	0,000	My_DD4	DD1&2_Dun1 - Grafische doorsnede	0,00000300000002618	0,00000000000000000	-0,00182099995527096	0,00000000000000000	0,0000056400000403	0,00000000000000000
DD2	0,000	Mz_DD1	DD1&2_Dun1	0,00000000000000000	0,09006199979921803	0,00000000000000000	0,00000000000000000	0,00000000000000000	0,0000188710006570

SCIAENGINEER	Project	Thesis Coen Stellinga	Auteur	Coen Stellinga
	Onderdeel	Nonlinear main girder	Datum	01. 06. 2022

Naam	dx [m]	Belasting	Doorsnede	u_x [mm]	u_y [mm]	u_z [mm]	φ_x [rad]	φ_y [rad]	φ_z [rad]
			- Grafische doorsnede						
DD2	0,000	Mz_DD2	DD1&2_Dun1 - Grafische doorsnede	0,00000000000000000	0,12081900058547035	0,00000000000000000	0,00000000000000000	0,00000000000000000	0,00003809600093518
DD2	0,000	Mz_DD3	DD1&2_Dun1 - Grafische doorsnede	0,00000000000000000	0,12081900058547035	0,00000000000000000	0,00000000000000000	0,00000000000000000	0,00003809600093518
DD2	0,000	Mz_DD4	DD1&2_Dun1 - Grafische doorsnede	0,00000000000000000	0,12081900058547035	0,00000000000000000	0,00000000000000000	0,00000000000000000	0,00003809600093518
DD3	0,000	Fx_DD1	DD3_Dun1 - Grafische doorsnede	0,00034199999277007	0,00000000000000000	-0,00139099995521974	0,00000000000000000	0,00000014299999407	0,00000000000000000
DD3	0,000	Fx_DD2	DD3_Dun1 - Grafische doorsnede	0,00060600001461353	0,00000000000000000	-0,00075899998819295	0,00000000000000000	0,00000000300000003	0,00000000000000000
DD3	0,000	Fx_DD3	DD3_Dun1 - Grafische doorsnede	0,00098600003184401	0,00000000000000000	-0,00058799997759706	0,00000000000000000	-0,00000021399999639	0,00000000000000000
DD3	0,000	Fx_DD4	DD3_Dun1 - Grafische doorsnede	0,00097400004506198	0,00000000000000000	-0,00082299999348834	0,00000000000000000	-0,00000015700000233	0,00000000000000000
DD3	0,000	Fy_DD1	DD3_Dun1 - Grafische doorsnede	0,00000000000000000	0,27574799605645239	0,00000000000000000	0,00004831999831367	0,00000000000000000	0,00002967299951706
DD3	0,000	Fy_DD2	DD3_Dun1 - Grafische doorsnede	0,00000000000000000	1,23745400924235582	0,00000000000000000	0,00083175697363913	0,00000000000000000	0,00012081900058547
DD3	0,000	Fy_DD3	DD3_Dun1 - Grafische doorsnede	0,00000000000000000	3,05103906430304050	0,00000000000000000	0,00265783607028425	0,00000000000000000	0,00028403199394234
DD3	0,000	Fy_DD4	DD3_Dun1 - Grafische doorsnede	0,00000000000000000	3,81739810109138489	0,00000000000000000	0,00227068900130689	0,00000000000000000	0,00049341598059982
DD3	0,000	Fz_DD1	DD3_Dun1 - Grafische doorsnede	-0,00050599999212864	0,00000000000000000	0,00580500000069151	0,00000000000000000	-0,00000055999998949	0,00000000000000000
DD3	0,000	Fz_DD2	DD3_Dun1 - Grafische doorsnede	-0,00084900000274502	0,00000000000000000	0,01621199953660835	0,00000000000000000	-0,00000182099995527	0,00000000000000000
DD3	0,000	Fz_DD3	DD3_Dun1 - Grafische doorsnede	-0,00058799997759706	0,00000000000000000	0,03055499837500975	0,00000000000000000	-0,00000437900007455	0,00000000000000000
DD3	0,000	Fz_DD4	DD3_Dun1 - Grafische doorsnede	0,00009600000083765	0,00000000000000000	0,04456800161278807	0,00000000000000000	-0,00000778400044510	0,00000000000000000
DD3	0,000	Mx_DD1	DD3_Dun1 - Grafische doorsnede	0,00000000000000000	-0,02630000017234124	0,00000000000000000	0,00139157299418002	0,00000000000000000	0,00000000000000000
DD3	0,000	Mx_DD2	DD3_Dun1 - Grafische doorsnede	0,00000000000000000	0,66137500107288361	0,00000000000000000	0,00317739788442850	0,00000000000000000	0,00000000000000000
DD3	0,000	Mx_DD3	DD3_Dun1 - Grafische doorsnede	0,00000000000000000	2,65783607028424740	0,00000000000000000	0,00721876509487629	0,00000000000000000	0,00000000000000000
DD3	0,000	Mx_DD4	DD3_Dun1 - Grafische doorsnede	0,00000000000000000	2,65784189105033875	0,00000000000000000	0,00721877720206976	0,00000000000000000	0,00000000000000000
DD3	0,000	My_DD1	DD3_Dun1 - Grafische doorsnede	0,00015700000233210	0,00000000000000000	-0,00218400009543984	0,00000000000000000	0,00000025400001391	0,00000000000000000
DD3	0,000	My_DD2	DD3_Dun1 - Grafische doorsnede	0,00003299999917772	0,00000000000000000	-0,00362600007974834	0,00000000000000000	0,00000056400000403	0,00000000000000000
DD3	0,000	My_DD3	DD3_Dun1 - Grafische doorsnede	-0,00021399999639016	0,00000000000000000	-0,00437900007455028	0,00000000000000000	0,00000106400000277	0,00000000000000000
DD3	0,000	My_DD4	DD3_Dun1 - Grafische doorsnede	-0,00021399999639016	0,00000000000000000	-0,00437900007455028	0,00000000000000000	0,00000106400000277	0,00000000000000000
DD3	0,000	Mz_DD1	DD3_Dun1 -	0,00000000000000000	0,15045100008137524	0,00000000000000000	0,00000000000000000	0,00000000000000000	0,00001887100006570

SCIA ENGINEER

Project	Thesis Coen Stellinga	Auteur	Coen Stellinga
Onderdeel	Nonlinear main girder	Datum	01. 06. 2022

Naam	dx [m]	Belasting	Doorsnede	u_x [mm]	u_y [mm]	u_z [mm]	φ_x [rad]	φ_y [rad]	φ_z [rad]
			Grafische doorsnede						
DD3	0,000	Mz_DD2	DD3_Dun1 - Grafische doorsnede	0,00000000000000000	0,24272600421682000	0,00000000000000000	0,00000000000000000	0,00000000000000000	0,00003809600093518
DD3	0,000	Mz_DD3	DD3_Dun1 - Grafische doorsnede	0,00000000000000000	0,28403199394233525	0,00000000000000000	0,00000000000000000	0,00000000000000000	0,00006543299969053
DD3	0,000	Mz_DD4	DD3_Dun1 - Grafische doorsnede	0,00000000000000000	0,28403199394233525	0,00000000000000000	0,00000000000000000	0,00000000000000000	0,00006543299969053
DD4	0,000	Fx_DD1	DD4_Dun1 - Grafische doorsnede	0,00034999999343199	0,00000000000000000	-0,00184900000022026	0,00000000000000000	0,00000014299999407	0,00000000000000000
DD4	0,000	Fx_DD2	DD4_Dun1 - Grafische doorsnede	0,00060600001461353	0,00000000000000000	-0,00076700001727659	0,00000000000000000	0,00000000300000003	0,00000000000000000
DD4	0,000	Fx_DD3	DD4_Dun1 - Grafische doorsnede	0,00097400004506198	0,00000000000000000	0,00009600000083765	0,00000000000000000	-0,00000021399999639	0,00000000000000000
DD4	0,000	Fx_DD4	DD4_Dun1 - Grafische doorsnede	0,00137500001073931	0,00000000000000000	0,00011600000249246	0,00000000000000000	-0,00000043899999014	0,00000000000000000
DD4	0,000	Fy_DD1	DD4_Dun1 - Grafische doorsnede	0,00000000000000000	0,36811101017519832	0,00000000000000000	0,00004832099875784	0,00000000000000000	0,00002967299951706
DD4	0,000	Fy_DD2	DD4_Dun1 - Grafische doorsnede	0,00000000000000000	1,57946895342320204	0,00000000000000000	0,00083175802137703	0,00000000000000000	0,00012081900058547
DD4	0,000	Fy_DD3	DD4_Dun1 - Grafische doorsnede	0,00000000000000000	3,81739903241395950	0,00000000000000000	0,00265783909708261	0,00000000000000000	0,00028403199394234
DD4	0,000	Fy_DD4	DD4_Dun1 - Grafische doorsnede	0,00000000000000000	6,45250082015991211	0,00000000000000000	0,00450418516993523	0,00000000000000000	0,00054015201749280
DD4	0,000	Fz_DD1	DD4_Dun1 - Grafische doorsnede	-0,00053600001592713	0,00000000000000000	0,00759900012781145	0,00000000000000000	-0,00000055999998949	0,00000000000000000
DD4	0,000	Fz_DD2	DD4_Dun1 - Grafische doorsnede	-0,00094600000011269	0,00000000000000000	0,02203899930464104	0,00000000000000000	-0,00000182099995527	0,00000000000000000
DD4	0,000	Fz_DD3	DD4_Dun1 - Grafische doorsnede	-0,00082299999348834	0,00000000000000000	0,04456800161278807	0,00000000000000000	-0,00000437900007455	0,00000000000000000
DD4	0,000	Fz_DD4	DD4_Dun1 - Grafische doorsnede	0,00011600000249246	0,00000000000000000	0,07268400077009574	0,00000000000000000	-0,00000870500025485	0,00000000000000000
DD4	0,000	Mx_DD1	DD4_Dun1 - Grafische doorsnede	0,00000000000000000	-0,10093000310007483	0,00000000000000000	0,00139157404191792	0,00000000000000000	0,00000000000000000
DD4	0,000	Mx_DD2	DD4_Dun1 - Grafische doorsnede	0,00000000000000000	0,49096898874267936	0,00000000000000000	0,00317739904858172	0,00000000000000000	0,00000000000000000
DD4	0,000	Mx_DD3	DD4_Dun1 - Grafische doorsnede	0,00000000000000000	2,27068993262946606	0,00000000000000000	0,00721876788884401	0,00000000000000000	0,00000000000000000
DD4	0,000	Mx_DD4	DD4_Dun1 - Grafische doorsnede	0,00000000000000000	4,50419122353196144	0,00000000000000000	0,01185583043843508	0,00000000000000000	0,00000000000000000
DD4	0,000	My_DD1	DD4_Dun1 - Grafische doorsnede	0,00017000000696044	0,00000000000000000	-0,00299599992104049	0,00000000000000000	0,00000025400001391	0,00000000000000000
DD4	0,000	My_DD2	DD4_Dun1 - Grafische doorsnede	0,00006300000165993	0,00000000000000000	-0,00543099986316520	0,00000000000000000	0,00000056400000403	0,00000000000000000
DD4	0,000	My_DD3	DD4_Dun1 - Grafische doorsnede	-0,00015700000233210	0,00000000000000000	-0,00778400044509908	0,00000000000000000	0,00000106400000277	0,00000000000000000
DD4	0,000	My_DD4	DD4_Dun1 - Grafische doorsnede	-0,00043899999013775	0,00000000000000000	-0,00870500025484944	0,00000000000000000	0,00000165100004779	0,00000000000000000
DD4	0,000	Mz_DD1	DD4_Dun1 -	0,00000000000000000	0,21083900355733931	0,00000000000000000	0,00000000000000000	0,00000000000000000	0,00001887100006570

SCIA ENGINEER

Project	Thesis Coen Stellinga	Auteur	Coen Stellinga
Onderdeel	Nonlinear main girder	Datum	01. 06. 2022

Naam	dx [m]	Belasting	Doorsnede	u_x [mm]	u_y [mm]	u_z [mm]	φ_x [rad]	φ_y [rad]	φ_z [rad]
			Grafische doorsnede						
DD4	0,000	Mz_DD2	DD4_Dun1 - Grafische doorsnede	0,00000000000000000	0,36463298602029681	0,00000000000000000	0,00000000000000000	0,00000000000000000	0,00003809600093518
DD4	0,000	Mz_DD3	DD4_Dun1 - Grafische doorsnede	0,00000000000000000	0,49341598059982061	0,00000000000000000	0,00000000000000000	0,00000000000000000	0,00006543299969053
DD4	0,000	Mz_DD4	DD4_Dun1 - Grafische doorsnede	0,00000000000000000	0,54015201749280095	0,00000000000000000	0,00000000000000000	0,00000000000000000	0,00009464300092077

Appendix IV Uninterpreted results mesh independend 1D elements model

Appendix IV Uninterpreted results mesh independent 1D elements model

As mentioned before (Paragraph 4.5) the proposed mesh independent 1D model has no connections between the webs of the troughs and the deck plate strip. Thus, no relevant stress values at these locations can be found at the locations of the theoretical connections between the trough webs and the deck plate strip. However, it does have relevant stress values at either side of the neutral axis of a trough. One approach could be to state that the value of the maximum stress interval directly next to the neutral axis of a trough is a measure of the maximum stress interval of the trough web at the same side of the neutral axis. If this is assumed, the following results are obtained:

Stress interval [Mpa]	Stress	Point where stress is determined: trough	Leg	x coord	y coord	Centre of left wheel of applied axle [Wheel, x-coord, y-coord]
280,4893082	-280,4893082	tr[2]	R	151	850	[Axis_B, 151, 1150]
271,0309648	-271,0309648	tr[2]	R	1600	850	[Axis_B, 1600, 1150]
278,3255714	-278,3255714	tr[2]	R	3049	850	[Axis_B, 3049, 1150]
278,2957596	-278,2957596	tr[2]	R	3351	850	[Axis_B, 3351, 1150]
270,3969914	-270,3969914	tr[2]	R	4800	850	[Axis_B, 4800, 1150]
279,4819173	-279,4819173	tr[2]	R	6249	850	[Axis_B, 6249, 1150]
279,8706442	-279,8706442	tr[2]	R	6551	850	[Axis_B, 6551, 1150]
273,1989814	-273,1989814	tr[2]	R	8000	850	[Axis_B, 8000, 1150]
277,1518001	-277,1518001	tr[2]	R	8750	850	[Axis_B, 8750, 1150]
284,0933084	-284,0933084	tr[2]	R	9449	850	[Axis_B, 9449, 1150]
243,1230758	-243,1230758	tr[3]	L	151	1450	[Axis_B, 151, 1150]
232,4977666	-232,4977666	tr[3]	L	1600	1450	[Axis_B, 1600, 1150]
245,0072591	-245,0072591	tr[3]	L	3049	1450	[Axis_B, 3049, 1150]
245,0500086	-245,0500086	tr[3]	L	3351	1450	[Axis_B, 3351, 1150]
233,1827234	-233,1827234	tr[3]	L	4800	1450	[Axis_B, 4800, 1150]
244,0233144	-244,0233144	tr[3]	L	6249	1450	[Axis_B, 6249, 1150]
243,7016722	-243,7016722	tr[3]	L	6551	1450	[Axis_B, 6551, 1150]
230,8849852	-230,8849852	tr[3]	L	8000	1450	[Axis_B, 8000, 1150]
235,8208832	-235,8208832	tr[3]	L	8750	1450	[Axis_B, 8750, 1150]
239,9827454	-239,9827454	tr[3]	L	9449	1450	[Axis_B, 9449, 1150]
282,192865	-282,192865	tr[3]	R	151	1450	[Axis_B, 151, 1750]
271,8655259	-271,8655259	tr[3]	R	1600	1450	[Axis_B, 1600, 1750]
279,7683947	-279,7683947	tr[3]	R	3049	1450	[Axis_B, 3049, 1750]
279,6713044	-279,6713044	tr[3]	R	3351	1450	[Axis_B, 3351, 1750]
271,0575351	-271,0575351	tr[3]	R	4800	1450	[Axis_B, 4800, 1750]
280,9888793	-280,9888793	tr[3]	R	6249	1450	[Axis_B, 6249, 1750]
281,3053101	-281,3053101	tr[3]	R	6551	1450	[Axis_B, 6551, 1750]
273,3977431	-273,3977431	tr[3]	R	8000	1450	[Axis_B, 8000, 1750]
277,9996047	-277,9996047	tr[3]	R	8750	1450	[Axis_B, 8750, 1750]
286,3019213	-286,3019213	tr[3]	R	9449	1450	[Axis_B, 9449, 1750]
244,2078735	-244,2078735	tr[4]	L	6551	2050	[Axis_B, 6551, 1750]
232,701379	-232,701379	tr[4]	L	8000	2050	[Axis_B, 8000, 1750]
236,9852397	-236,9852397	tr[4]	L	8750	2050	[Axis_B, 8750, 1750]
240,1918223	-240,1918223	tr[4]	L	9449	2050	[Axis_B, 9449, 1750]
281,0978011	-281,0978011	tr[4]	R	6551	2050	[Axis_B, 6551, 2350]
272,1070046	-272,1070046	tr[4]	R	8000	2050	[Axis_B, 8000, 2350]
277,2308537	-277,2308537	tr[4]	R	8750	2050	[Axis_B, 8750, 2350]
286,4165306	-286,4165306	tr[4]	R	9449	2050	[Axis_B, 9449, 2350]
246,2483158	-246,2483158	tr[5]	L	6551	2650	[Axis_B, 6551, 2350]
235,6017974	-235,6017974	tr[5]	L	8000	2650	[Axis_B, 8000, 2350]
239,5223444	-239,5223444	tr[5]	L	8750	2650	[Axis_B, 8750, 2350]
242,4274904	-242,4274904	tr[5]	L	9449	2650	[Axis_B, 9449, 2350]
280,8492775	-280,8492775	tr[5]	R	151	2650	[Axis_B, 151, 2950]

Stress interval [Mpa]	Stress	Point where stress is determined: trough	Leg	x coord	y coord	Centre of left wheel of applied axle [Wheel, x-coord, y-coord]
269,2044547	-269,2044547	tr[5]	R	1600	2650	[Axis_B, 1600, 2950]
278,419456	-278,419456	tr[5]	R	3049	2650	[Axis_B, 3049, 2950]
278,2888892	-278,2888892	tr[5]	R	3351	2650	[Axis_B, 3351, 2950]
268,6838276	-268,6838276	tr[5]	R	4800	2650	[Axis_B, 4800, 2950]
279,5261476	-279,5261476	tr[5]	R	6249	2650	[Axis_B, 6249, 2950]
279,7188651	-279,7188651	tr[5]	R	6551	2650	[Axis_B, 6551, 2950]
270,2821666	-270,2821666	tr[5]	R	8000	2650	[Axis_B, 8000, 2950]
275,6042738	-275,6042738	tr[5]	R	8750	2650	[Axis_B, 8750, 2950]
284,9213281	-284,9213281	tr[5]	R	9449	2650	[Axis_B, 9449, 2950]
254,4271077	-254,4271077	tr[6]	L	151	3250	[Axis_B, 151, 1070]
248,3122349	-248,3122349	tr[6]	L	1600	3250	[Axis_B, 1600, 1070]
255,3381456	-255,3381456	tr[6]	L	3049	3250	[Axis_B, 3049, 1070]
255,3925989	-255,3925989	tr[6]	L	3351	3250	[Axis_B, 3351, 1070]
247,9966791	-247,9966791	tr[6]	L	4800	3250	[Axis_B, 4800, 1070]
255,1791304	-255,1791304	tr[6]	L	6249	3250	[Axis_B, 6249, 1070]
255,1884119	-255,1884119	tr[6]	L	6551	3250	[Axis_B, 6551, 1070]
248,7965639	-248,7965639	tr[6]	L	8000	3250	[Axis_B, 8000, 1070]
251,6951056	-251,6951056	tr[6]	L	8750	3250	[Axis_B, 8750, 1070]
253,4575064	-253,4575064	tr[6]	L	9449	3250	[Axis_B, 9449, 1070]
274,6837446	-274,6837446	tr[7]	R	6551	3850	[Axis_B, 6551, 4150]
265,9337719	-265,9337719	tr[7]	R	8000	3850	[Axis_B, 8000, 4150]
270,7833317	-270,7833317	tr[7]	R	8750	3850	[Axis_B, 8750, 4150]
278,5356986	-278,5356986	tr[7]	R	9449	3850	[Axis_B, 9449, 4150]
264,000809	-264,000809	tr[9]	L	151	5050	[Axis_B, 151, 2870]
257,380657	-257,380657	tr[9]	L	1600	5050	[Axis_B, 1600, 2870]
263,9034887	-263,9034887	tr[9]	L	3049	5050	[Axis_B, 3049, 2870]
263,8774286	-263,8774286	tr[9]	L	3351	5050	[Axis_B, 3351, 2870]
256,4261635	-256,4261635	tr[9]	L	4800	5050	[Axis_B, 4800, 2870]
264,2239525	-264,2239525	tr[9]	L	6249	5050	[Axis_B, 6249, 2870]
264,3423337	-264,3423337	tr[9]	L	6551	5050	[Axis_B, 6551, 2870]
258,0024064	-258,0024064	tr[9]	L	8000	5050	[Axis_B, 8000, 2870]
261,2234172	-261,2234172	tr[9]	L	8750	5050	[Axis_B, 8750, 2870]
264,7884156	-264,7884156	tr[9]	L	9449	5050	[Axis_B, 9449, 2870]
267,9732279	-267,9732279	tr[9]	R	151	5050	[Axis_B, 151, 5350]
260,0913499	-260,0913499	tr[9]	R	1600	5050	[Axis_B, 1600, 5350]
267,3161257	-267,3161257	tr[9]	R	3049	5050	[Axis_B, 3049, 5350]
267,2623943	-267,2623943	tr[9]	R	3351	5050	[Axis_B, 3351, 5350]
259,2528558	-259,2528558	tr[9]	R	4800	5050	[Axis_B, 4800, 5350]
267,8183111	-267,8183111	tr[9]	R	6249	5050	[Axis_B, 6249, 5350]
267,9443965	-267,9443965	tr[9]	R	6551	5050	[Axis_B, 6551, 5350]
260,8118573	-260,8118573	tr[9]	R	8000	5050	[Axis_B, 8000, 5350]
264,5753265	-264,5753265	tr[9]	R	8750	5050	[Axis_B, 8750, 5350]
269,5547171	-269,5547171	tr[9]	R	9449	5050	[Axis_B, 9449, 5350]

These are the results obtained in the points in which the 1D model was applied (Figure 34). To get the results in the remaining points cubic interpolation is applied. Thereby the results presented in Figure 53 are found.

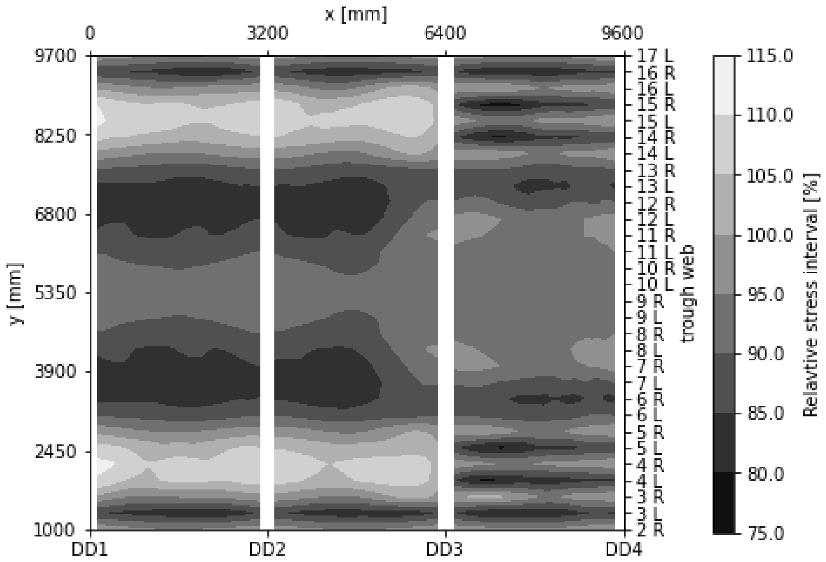

Figure 53: Contour plot obtained without interpretation method

These results show a significant difference between the result obtained between the first and second as well as the second and third cross beam in comparison with the results obtained between the third and fourth cross beam. To investigate this the results of 3 cross sections was taken a closer look at. The following plot of the results in these cross sections were obtained.

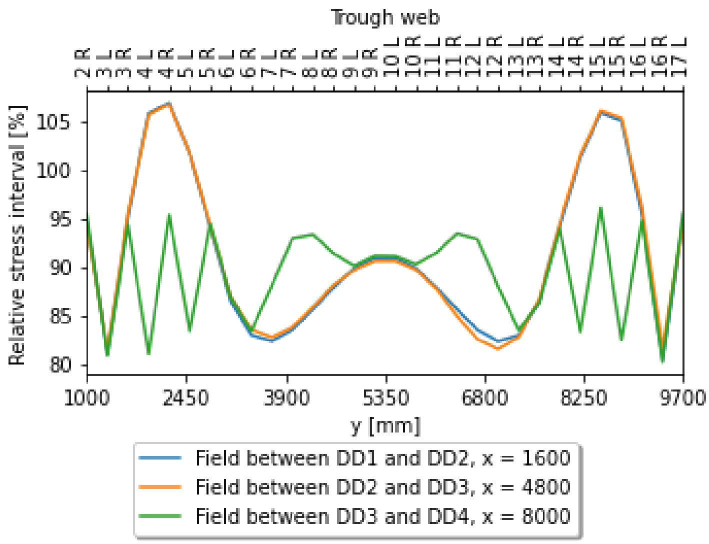

Figure 54: Results obtained between different cross beams without interpretation

It can be noted that the behaviour predicted on the areas where points are interpolated is very different from the behaviour of the areas in which points are located for which the model was used. This would suggest that the chosen interpolation algorithm (the use of cubic splines) cannot be used to predict values at unknown points. This seems logical since cubic splines assume that the closest points to an unknown point give the most information of the predicted value at the unknown point. However, for in this case there is a big difference between the left and right webs of the troughs. Therefore, not the closest point, but the closes point on the same sided trough leg gives the most information. There either an alternative interpolation method, or an alternative interpretation method should be used. In this report it was decided to research different interpretation of the obtained data.

Appendix V Shortlist of potential critical points

Based on intuition of structural engineers

Appendix V Shortlist of potential critical points

All structural engineers within Antea Group, who have experience in regards fatigue calculations of steel orthotropic bridge decks, identify 18 potential points which are considered more likely to be exposed to the highest stress interval. When asked why these points the structural engineers give a reasoning stated below.

It seems likely that the deformations in the deck plate are governed by bending. Therefore, it is assumed that the strains are mainly governed by bending. Which results in the stresses being mainly governed by bending (Appendix I Derivation system of differential equations of a Timoshenko beam element [4, 21, 22]). In most cases bending is the result of internal moments therefore, it is assumed that the highest stress interval will be found at the location of the highest internal moment. These can often be determined by applying basic equilibrium equations as explained in [37]. In the determination of the short list the crossbeams are simplified to all have the same stiffness. Since local effects are considered to have a bigger influence on the stresses than the global effects only one field is considered at a time. Thus, the following symmetrical load cases were considered of interest (Figure 55).

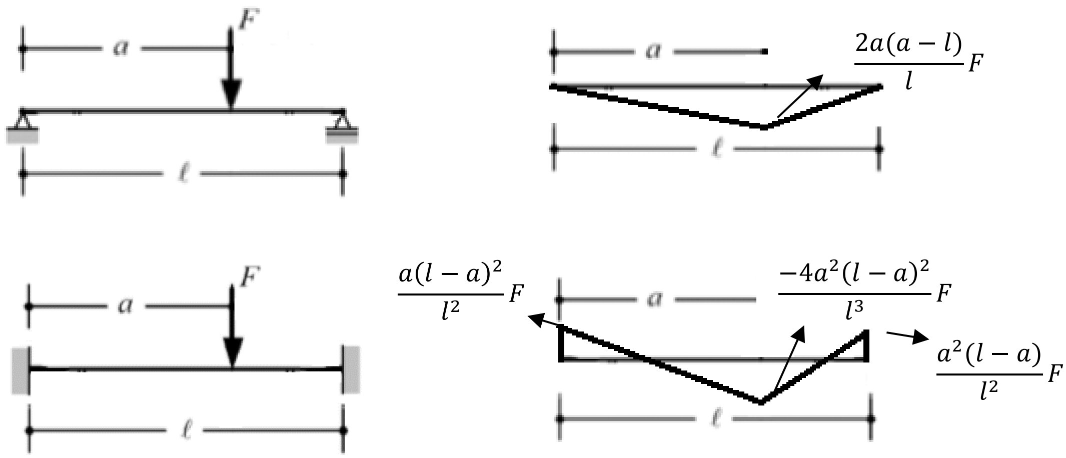

Figure 55: Moment lines of basic load case situations[13]

In both these load cases the maximum or minimum moment is found at either a support or in at the location of the load. The internal moments obtain the biggest value when $a = \frac{l}{2}$ thus maximum or minimum internal moment is found either at the support or in the middle of the considered field. As a result of this the structural engineers expect the maximum and minimum stress intervals either close to the main girders and cross beams or in the middle of the field between the main girders and the cross beams. This leads to the short list of points as in Figure 56.

[13] These moment lines found when the Euler-Bernoulli beam theory is applied. Since this is the first theory most structural engineers will learn usually this is where their intuition is based on.

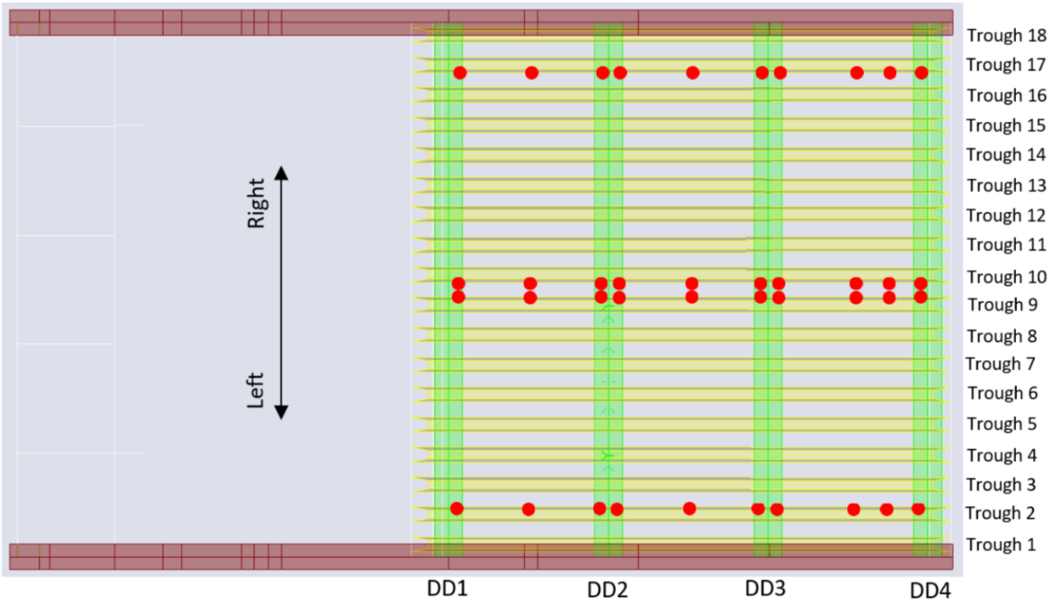

Figure 56: Short list of potential points

Some structural engineers hesitate to mitigate the list even further. Stating that this specific bridge is supported at one side only. Therefore, it is expected that the first field is the stiffest and the last field is the least stiff. As a result of this they omit all points in between cross beam 2 and cross beam 3. However, these structural engineers state that they are not entirely sure if this method is valid. Therefore, it was decided to keep these points on the short list.

Appendix VI Results mesh independend 1D element model interpretated via method 2

Appendix VI Results mesh independent 1D element model interpretated via method 2

Stress interval [Mpa]	Stress	Point where stress is determined trough	x coord	y coord
262,6579704	-262,6579704	tr[3]	151	1450
252,1816463	-252,1816463	tr[3]	1600	1450
262,3878269	-262,3878269	tr[3]	3049	1450
262,3606565	-262,3606565	tr[3]	3351	1450
252,1201293	-252,1201293	tr[3]	4800	1450
262,5060969	-262,5060969	tr[3]	6249	1450
262,5034912	-262,5034912	tr[3]	6551	1450
252,1413642	-252,1413642	tr[3]	8000	1450
256,910244	-256,910244	tr[3]	8750	1450
263,1423334	-263,1423334	tr[3]	9449	1450
262,6528373	-262,6528373	tr[4]	6551	2050
252,4041918	-252,4041918	tr[4]	8000	2050
257,1080467	-257,1080467	tr[4]	8750	2050
263,3041765	-263,3041765	tr[4]	9449	2050
262,9835905	-262,9835905	tr[5]	6551	2650
252,941982	-252,941982	tr[5]	8000	2650
257,5633091	-257,5633091	tr[5]	8750	2650
263,6744093	-263,6744093	tr[5]	9449	2650
265,9870185	-265,9870185	tr[9]	151	5050
258,7360035	-258,7360035	tr[9]	1600	5050
265,6098072	-265,6098072	tr[9]	3049	5050
265,5699115	-265,5699115	tr[9]	3351	5050
257,8395097	-257,8395097	tr[9]	4800	5050
266,0211318	-266,0211318	tr[9]	6249	5050
266,1433651	-266,1433651	tr[9]	6551	5050
259,4071319	-259,4071319	tr[9]	8000	5050
262,8993719	-262,8993719	tr[9]	8750	5050
267,1715664	-267,1715664	tr[9]	9449	5050

Appendix VII Elaboration calculating maximum stress interval 2D FE model

Appendix VII Elaboration calculating maximum stress interval 2D FE model

Determination of dimension of weld details in 2D FE model.
The weld dimension, in the FE model, can be determined using article 00912, figure F00912-1 F) in combination with the figure in article 00915, table T00915 of the ROK. These are shown in Figure 57.

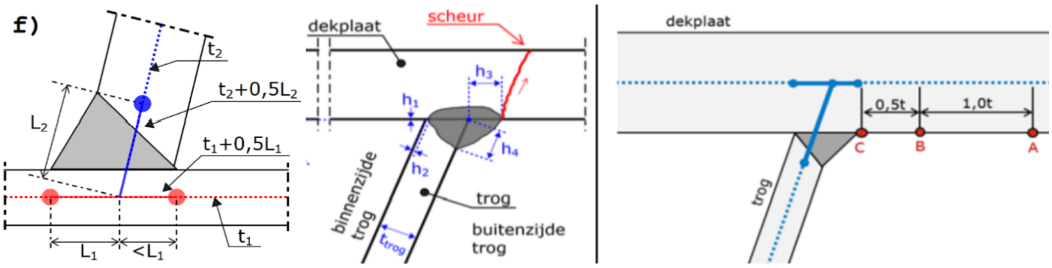

Figure 57: Sketches provided by ROK [3] to model weld details [3]

The thickness of the trough and the deck plate is known. These can be inserted in Figure 57. h_3 and h_4 are given in in the regulations (ROK [3], table T00915) and therefore known. The updated sketches are shown in Figure 58.

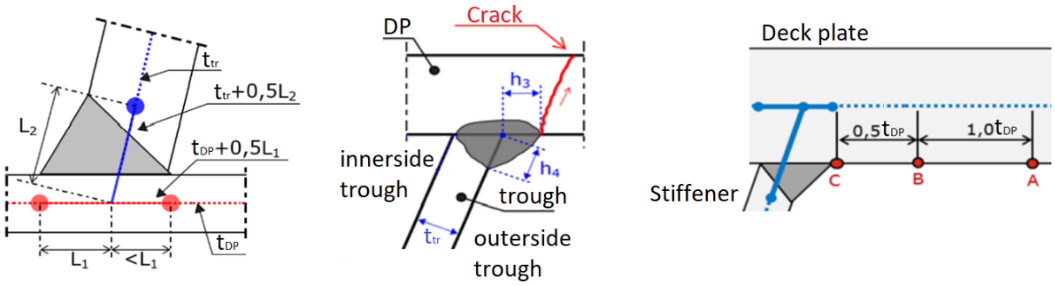

Figure 58: ROK sketches of weld details updated for Goereese bridge [3]

The unknowns that still need to be determined are: L_1, $<L_1$ and L_2. These are dependent on the geometrical properties of the bridge. Therefore, they can be expressed in terms of the geometrical properties of the bridge. To be able to this some geometrically quantities will be determined in intermediate steps. In this document they are determined step by step clarified by addition sketches.

α

α is the angle between the trough web and the deck plate. This angle can be determined using the geometry of a trough. To demonstrate this a sketch is made (Figure 59).

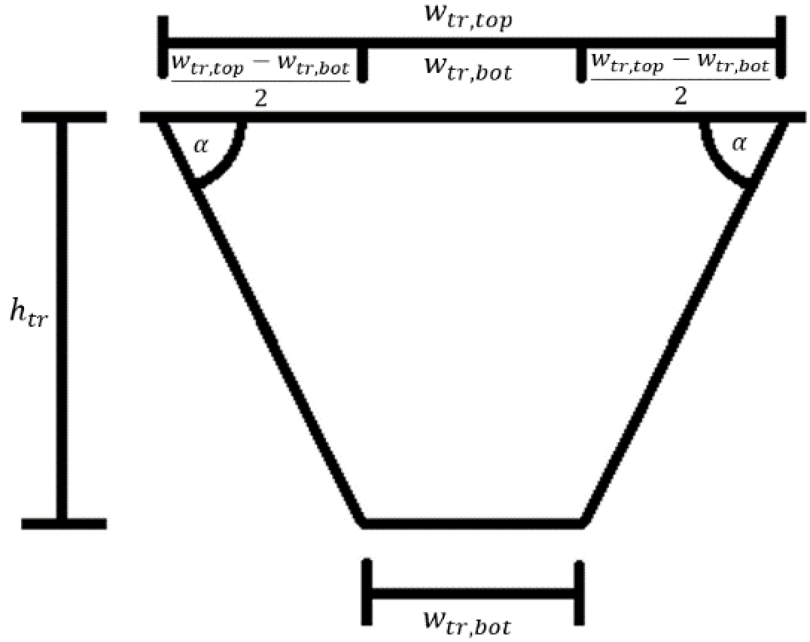

Figure 59: Sketch clarifying angle α

Using basic geometrical definitions, it can be found that:

$$\alpha = \arctan\left(\frac{2h_{tr}}{w_{tr,top} - w_{tr,bot}}\right) \tag{16}$$

a

a is the length of the contact line between the trough web and the deck plate ().

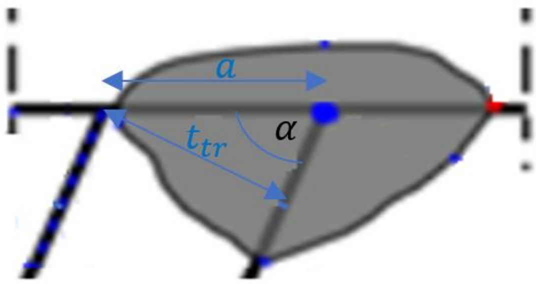

Figure 60: Sketch clarifying length a [3]

Using basic geometrical definitions, it can be found that:

$$a = \frac{t_{tr}}{\sin(\alpha)} \tag{17}$$

Substitution of α (16) in the definition of a (17) leads to:

$$a = \frac{t_{tr}}{\sin\left(\arctan\left(\frac{2h_{tr}}{w_{tr,top} - w_{tr,bot}}\right)\right)}$$

b

b is the horizontal difference between the contact point of the deck plate with the trough web and the intersection point of the neutral axis of the deck plate and the neutral axis of the trough web (Figure 61):

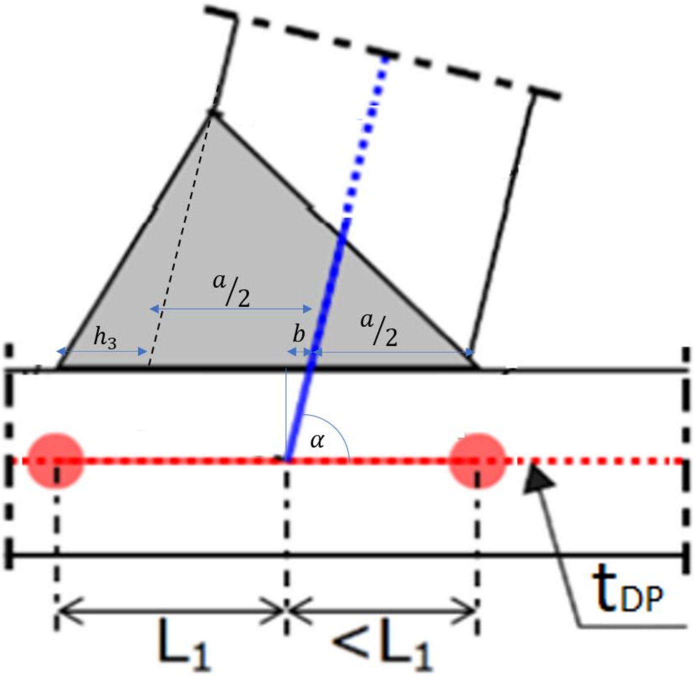

Figure 61: Sketch clarifying length b [3]

Using basic geometrical definitions, it can be found that:

$$b = \frac{t_{DP}}{2\tan(\alpha)} \; ; < L_1 = \frac{a}{2} + b = \frac{1}{2}\left(a + \frac{t_{DP}}{\tan(\alpha)}\right) \; ; L_1 = \frac{a}{2} - b + h_3 \qquad (18)$$

Substitution of α (16) in the definitions of b, <L_1 and L_1 (18) leads to:

$$b = \frac{t_{DP}(w_{tr,top} - w_{tr,bot})}{4h_{tr}} \qquad (19)$$

$$< L_1 = \frac{w_{tr,top} - w_{tr,bot}}{2}\left(t_{tr}\sqrt{\frac{1}{(w_{tr,top} - w_{tr,bot})^2} + \frac{1}{4h_{tr}^2}} + \frac{t_{DP}}{2h_{tr}}\right) \qquad (20)$$

$$L_1 = \frac{w_{tr,top} - w_{tr,bot}}{2}\left(t_{tr}\sqrt{\frac{1}{(w_{tr,top} - w_{tr,bot})^2} + \frac{1}{4h_{tr}^2}} - \frac{t_{DP}}{2h_{tr}}\right) + h_3 \qquad (21)$$

c and d
Lengths c and d are clarified in Figure 62.

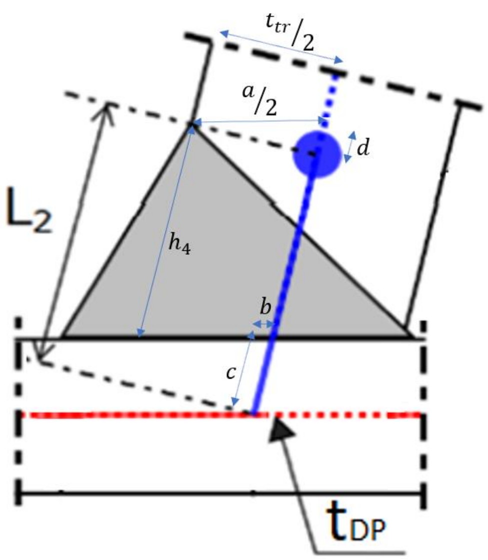

Figure 62: Sketch clarifying length c and d [3]

Using basic geometrical definitions, it can be found that:

$$c = \sqrt{b^2 + \left(\frac{t_{DP}}{2}\right)^2} \; ; d = \sqrt{\left(\frac{a}{2}\right)^2 - \left(\frac{t_{tr}}{2}\right)^2} \; ; \; L_2 = h_4 + c - d \tag{22}$$

Substitution of the expression found for a (17) and b (19) into the definitions found for c, d and L_2 (22) leads to:

$$c = \frac{t_{DP}}{2}\sqrt{\frac{\left(w_{tr,top} - w_{tr,bot}\right)^2}{4h_{tr}^2} + 1} \; ; \; d = \frac{t_{tr}\left(w_{tr,top} - w_{tr,bot}\right)}{4h_{tr}}$$

$$L_2 = h_4 + \frac{t_{DP}}{2}\sqrt{\frac{\left(w_{tr,top} - w_{tr,bot}\right)^2}{4h_{tr}^2} + 1} - \frac{t_{tr}\left(w_{tr,top} - w_{tr,bot}\right)}{4h_{tr}} \tag{23}$$

All remaining expression are based on the dimension of the bridge:

$$h_{tr} = 350mm \, ; t_{DP} = 20mm \, ; t_{tr} = 6mm \, ; w_{tr,bot} = 170mm \, ; w_{tr,top} = 300mm \tag{24}$$

Substitution of the dimensions of the bridge (24) into the expression for <L_1 (20) , L_1 (21) and L_2 (23) leads to:

$$< L_1 = \frac{3\sqrt{5069} + 130}{70} \approx 4.9mm \, ; \; L_1 = \frac{3\sqrt{5069} - 130}{70} + h_3 \approx 1.1942 + h_3 \, mm \tag{25}$$

$$L_2 = h_4 + \frac{10\sqrt{5069} - 39}{70} \approx h_4 + 9.6138 \, mm \tag{26}$$

It can be noted that L1 and L2 are dependent on the quality of the weld. To ensure the bridge remains safe it is assumed that the smallest weld dimensions are used. The values can be found in the regulations (ROK [3], table T00915). In this table all dimensions are given in tents of millimetres. To ensure the bridges is not undersized the determined weld sizes ware rounded down. Substitution of these into the expression for <L_1, L_1 (25) and L_2 (26) leads to:

$$< L_1 \approx 4.9mm\ ;\ L_1 = \frac{3\sqrt{5069}+220}{70} \approx 6.1mm\ ;\ L_2 = \frac{311+10\sqrt{5069}}{70} \approx 14.6\ mm$$
$$t_{DP} + \frac{L_1}{2} = \frac{3020+3\sqrt{5069}}{140} \approx 23.0mm\ ;\ t_{tr} + \frac{L_2}{2} = \frac{1151+10\sqrt{5069}}{140} \approx 13.3mm$$

Which are the values given in the report (Figure 44). This results in a weld detail in the FE model as shown in Figure 63:

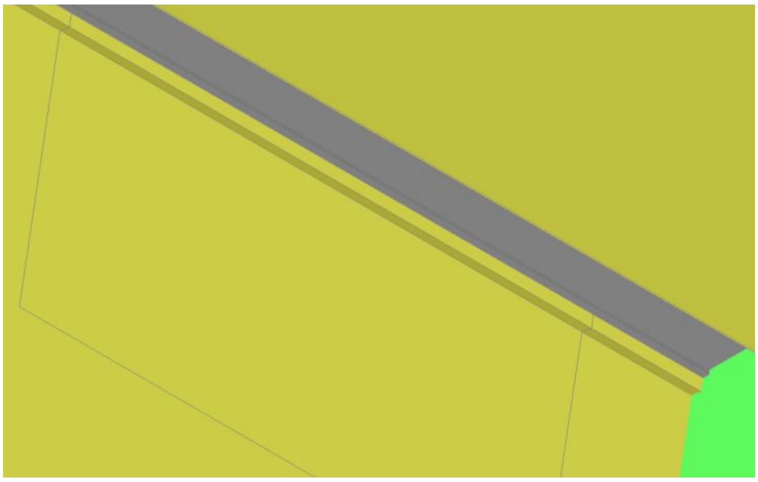

Figure 63: Weld detail in 2D FE model at a connection of a trough (yellow), the deck plate (grey) and a cross beam (green)

Mesh refinement

To be able to use the FE model mesh settings need to be applied. To acquire sufficient accuracy a fine mesh needs to be applied, however this rapidly increases the time needed to compute the results [29]. As a result of this structural engineers tend to apply a fine mesh locally at the location where the results are of most interest, while remaining a course mesh at less relevant locations. The regulations (ROK [3], table T00915) provide a maximum allowable mesh size adapted at the analysed weld. It states that the maximum allowable mesh size equals half the deck plate thickness (in the considered case 10mm). This results in the mesh shown in Figure 64.

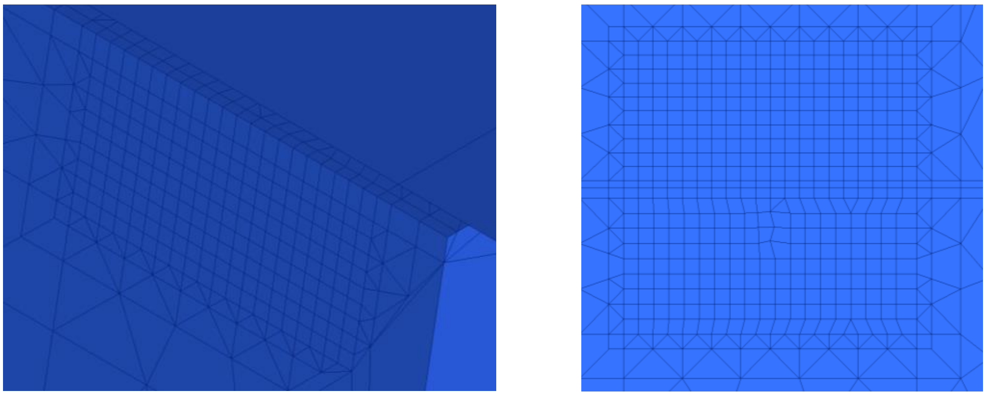

(A) (B)

Figure 64: Mesh refinements in the 2D FE in (A) the trough web and (B) the deck plate

Load cases

To get the relevant results not only the bridge should be modelled properly but also the right load cases should be applied. In this case the goal of the FE model is to find the maximum stress interval in the considered point. In Chapter 3.6 it is shown that the maximum stress interval occurs when the load is applied next to the considered point. Therefore, only trucks at the location of the considered point have to be considered. It is assumed that the maximum stress interval due to load cases considering single axles is found in the same point as the maximum stress interval due to trucks. As a result of this only the effect of a single axle is studied. The ROK [3] mentions to locations of wheel spreads which have to be accounted for in Figure 65.

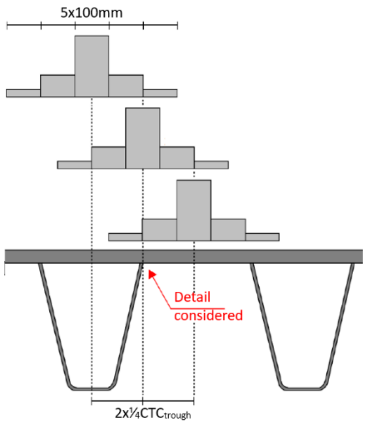

Figure 65: Wheel track spread positions having to be considered according ROK [3]

This leads to a total of 15 maximum possible wheel positions. However, depending on the centre-to-centre distance of the trough some the load cases resulting from the different spread positions are not unique. This is the case for the considered bridge (Goereese bridge). In this case the total number of unique wheel positions is 13. The regulations do not specify which wheel of a truck is positioned at this wheel track position. Therefore, both options are considered if possible[14]. This leads to a total of 26 axle configurations. For all these configuration 3 types of axles are considered. The definition of the axles in given in [17] and updated by ROK [3]. The later states that the length of a wheel should be equal to 220mm. The axles are presented in Figure 66.

[14] If the considered point is part of trough 2 or 4 only one wheel configuration can be used. Since the other configuration results in a wheel placed outside of the bridge. If the considered point is part of trough 9 both configurations are analysed.

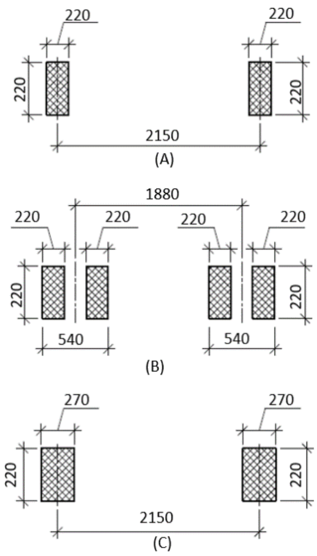

Figure 66: Truck axle definitions according to regulations [17] and [3], given in mm

Now the locations of all loads are defined. However, the size of loads still needs to be set. To determine the fatigue damage a model is used to represent the entire stress history. In this case the model is used to determine the maximum stress interval. Therefore, only the maximally loaded axles need to be used. These can be found in the Dutch annex of Eurocode 1 table NB.6 4.7 [16]. The maximum load on an axle type A is 70kN, the maximum load on an axle type B is 150kN and the maximum load on an axle type C is 90kN. Together with 26 axle configurations this results in 78 load cases.

Stress determination

To determine the stresses at a weld toe is not allowed to use the stresses found at this location directly. Instead, the stress values have to be linearly interpolated to this point from two different points [3]. The interpolation happens from point A and B to point C (Figure 58). The stresses values at point A and point B will be different for each applied load case. In this example the stress at point will be given as σ_A and at point B as σ_B. Linear interpolation from the stresses at A and B means that the stress in point C can be expressed in the stresses at point A and B.

$$\sigma_C = \frac{3\sigma_B - \sigma_A}{2}$$

Stress interval determination

To determine the occurring stress interval the difference between two different load cases is determined. In a formula this means that:

$$\Delta\sigma_{LC1;LC2} = abs\left(\sigma_{C;L1} - \sigma_{C;L2}\right)$$

The stress interval can be determined for all load cases in spread of the traffic wheel position. Each spread location has a total of 120 combinations. This means a total possible maximum of 360 load combination could exist. However, in the considered bridge the spreads of two locations partly overlap (Figure 65) resulting in a reduced number of load combinations. In the considered load cases in the case is study is 339. From these the highest is the highest expected stress interval. To determine the resulting fatigue damage this has to be multiplied with a dynamic amplification factor of 1.15 [3]. This factor has to be applied if a considered point is withing 6m of expansion joint. Since the considered bridge is only 10.8 meters long all points have the dynamic amplification factor applied to them.